TECHNISCHE UNIVERSITÄT DARMSTADT

Modulation of autophagy impacts the fate of senescent skin fibroblasts

Vom Fachbereich Chemie

der Technischen Universität Darmstadt

zur Erlangung des Grades eines

Doctor rerum naturalium

(Dr. rer. nat.)

Dissertation

vorgelegt von

Gregory Som

Referent: Prof. Dr. Harald Kolmar

Korreferent: Prof. Dr. Jörg von Hagen

Tag der Einreichung: 03.07.2020

Tag der mündlichen Prüfung: 07.09.2020

Darmstadt 2020

Die vorliegende Arbeit wurde unter der Leitung von Herrn Prof. Dr. Harald Kolmar am Clemens-Schöpf- Institut für Organische Chemie und Biochemie der Technischen Universität Darmstadt sowie bei Merck KGaA in Darmstadt von Mai 2017 bis Juli 2020 angefertigt.

Gregory Som, Modulation of autophagy impacts the fate of senescent skin fibroblasts
Technische Universität Darmstadt, 2021
urn:nbn:de:tuda-tuprints-178616
07.09.2020

Publication or patents derived from the presented work

Two publications and two patents are currently being written, reviewed or already published.

Contribution to conferences

Part of this work was presented (poster) at the International Federation of Societies od Cosmetic Chemists (IFSCC) in 2018 and 2019.

Table of contents

1. Abstract

1.1. Zusammenfassung

Hautalterung geht mit der Akkumulation von seneszenten Zellen einher, welche eine chronische Entzündung und den Abbau der Extrazellulären Matrix fördern. Autophagie ist ein speziesübergreifend konservierter Prozess, der durch den Abbau von alten oder beschädigten Proteinen und Organellen zur Instandhaltung zellulärer Homöostase beiträgt. Da dieser Prozess im Zuge des Alterns beeinträchtigt ist, wird angenommen, dass Autophagie eine Rolle bei der Entwicklung von Seneszenz spielt. Der Zusammenhang von Autophagie undzellulärer Seneszenz ist derzeit unzureichend verstanden und scheint vom Zelltyp, Gewebetyp und der Art und Weise, wie Seneszenz in Modellsystemen initiiert wird, abzuhängen. Warum beschädigte Zellen Seneszenz anstelle von Apoptose einleiten bleibt eine der Hauptfragestellungen in der Erforschung von altersbedingten Krankheiten.

In dieser Arbeit wurden mittels 2D-LC-MS/MS *labeling-assisted proteomics* 230 hochregulierte Proteine und 228 herunterregulierte Proteine in seneszenten normalen humanen dermalen Fibroblasten (NHDF) identifiziert. Unter den hochregulierten Proteinen wurden mittels *gene set enrichment analysis* (GSEA) 27 biologische Prozesse identifiziert, die möglicherweise im direkten Zusammenhang mit Autophagie stehen. Unter anderem waren die Lysosomen Biogenese, mTOR Signalwege und Makroautophagie erhöht. Dies zeigt, dass Stress-induzierte Seneszenz (SIPS) zu einer Erhöhung des Autophagie Flux in NHDF führt.

Zur Untersuchung der Frage, ob die Erhöhung des Autophagie Flux eine Rolle in der Entwicklung von Seneszenz spielt oder eine Folge dieser ist, wurden mehrere Experimente durchgeführt. Die Stimulierung des Autophagie-Flux in humanen WS1 Fibroblasten mittels Rapamycin vor der Induktion von SIPS konnte diese verzögern, wohingegen die Blockierung des Autophagie Flux keinen Effekt zeigte. Die Erhöhung des Autophagie-Flux nach der Induktion von SIPS verzögerte ihre Ausbildung, wobei die Blockierung zum Absterben der Zellen führte. Es wurde gezeigt, dass dies spezifisch seneszente Zellen betrifft, was auf eine Autophagie-bedingte Reprogrammierung zur Apoptose hindeutet. Erste Daten belegen, dass die Anzahl an Mitochondrien und oder Calcium Signalwege eine Rolle spielen. Der genaue molekulare Mechanismus muss allerdings noch aufgeklärt werden. Die in dieser Arbeit erhobenen Daten weisen auf eine duale gegenläufige Rolle der Autophagie bei der Entwicklung von Seneszenz in Hautfibroblasten hin. Siezeigt, dass die Modulation von Autophagie einen potenziellen Angriffspunkt zur Bekämpfung von altersbedingten Krankheiten ist.

In dieser Arbeit wurden außerdem mehrere Kohlenhydrate und deren Derivate auf die Fähigkeit getestet Autophagie zu beeinflussen. Raffinose, Sucrose, Isomaltulose, Sorbitol und Methyl-a-glucopyranosid wurden als neue mTOR-unabhängige Aktivatoren des Autophagie-Flux identifiziert, wohingegen Trehalose einen inhibierenden Effekt zeigte.

Neben Autophagie wurden mittels GSEA ca. 40 weitere biologische Prozesse identifiziert, die in seneszenten NHDF signifikant verstärkt reguliert werden. siRNA vermitteltes *Silencing* von vier hochregulierten Proteinen führte zum Zelltod. Damit konnte gezeigt werden, dass (I) der Alkohol Metabolismus (APOL2), (II) der

Fettsäuremetabolismus (CES2), (III) Sauerstoffmangel (MGARP) und die Regulierung des Apoptose Signalwegs (PTTG1IP) eine direkte Rolle bei der Entwicklung von Seneszenz spielen.

Das Verständnis der molekularen Zusammenhänge von Seneszenz, Autophagie und Apoptose werden immer wichtiger in der Alters- und Krebsforschung. Ein Verständnis, wie diese Prozesse sich gegenseitig regulieren, könnte dazu beitragen neue Therapien zur spezifischen Eliminierung von seneszenten Hautfibroblasten zu entwickeln. Derzeit gibt es keine robusten spezifischen biologischen Marker zur Identifizierung von seneszenten Zellen in vitro und in vivo. Die Identifizierung von neuen Seneszenzmarkern hätte großes diagnostisches und therapeutisches Potential.

1.2. Abstract

Skin aging is accompanied by an accumulation of senescent cells, which promote a low chronic inflammation and degradation of the extracellular matrix. Autophagy is a conserved biological process involved in cellular homeostasis through the recycling of long-lived or damaged proteins and organelles. Impaired during aging, it has been speculated that autophagy could be involved in senescence. The role of autophagy in the context of cellular senescence remains elusive and is not understood yet, seemingly dependent on the cell type, tissue, and manner in which senescence is induced. Why damaged cells resort to senescence instead of apoptosis remains a key question in the understanding of aging and age-related pathologies.

In this work, 2D-LC-MS/MS labeling-assisted proteomics identified 230 upregulated and 228 downregulated proteins in senescent normal human dermal fibroblasts (NHDF). When upregulated proteins were subjected to agenesetenrichmentanalysis(GSEA), 27autophagy-relatedbiologicalprocesseswerefoundenriched, showing that stress-induced premature senescence (SIPS) leads to an increased autophagic activity in senescent NHDF. This included biological processes such as lysosome biogenesis, mTOR signaling and macroautophagy.
Although autophagy is increased in SIPS, whether it is involved in senescence development or a consequence remained to be clarified. In WS1 human fibroblasts, rapamycin-mediated stimulation of autophagic flux *prior* to SIPS induction delayed the onset of senescence, whereas its inhibition through chloroquine showed no effect. *After* SIPS induction, stimulation of autophagy delayed the onset of senescence, whereas its inhibition changed the cell fate from senescence to cell death. The latter observation was further shown to be specific to senescent WS1, suggesting the existence of an autophagy-mediated "apoptotic switch". Although the exact molecular mechanism of this switch remains to be determined, this work implicates mitochondrial abundance and/or mass as well as calcium signaling as part of the process. These data highlighted a dual beneficial/detrimental role of autophagy in skin fibroblasts senescence and thus its modulation is a potential target for age-related pathologies. In this regard, carbohydrates and derivatives have been tested for the ability to modulate autophagy. Whereas raffinose, sucrose, isomaltulose, sorbitol and methyl-α-glucopyranoside could be use as novel mTOR-independent activators of autophagy, trehalose could have an inhibitory effect.
Aside from autophagy, GSEA allowed the identification of approximately 40 other biological processes significantly enriched in senescent NHDF, some of which could directly be involved in senescent fibroblasts immortality. Selection of four upregulated candidates involved in (I) alcohol metabolism (APOL2), (II) fatty acid metabolism (CES2), (III) response to hypoxia (MGARP) and (IV) regulation of apoptotic signaling (PTTG1IP) allowed to validate their role in senescent cell immortality, as the siRNA-mediated silencing of these 4 proteins led to cell death.

The understanding of molecular mechanisms involved in cellular senescence, autophagy and apoptosis becomes increasingly important in aging and cancer research. Sufficient understanding how they regulate each other could provide novel therapeutic opportunities for the specific elimination of senescent skin fibroblasts. Current biological markers used to detect senescent cells *in vitro* and *in vivo* are limited and lack specificity. Thus, identification of novels senescent markers would have diagnostic and therapeutic potential.

2. Introduction

2.1. Skin

The human skin is a large and complex organ whose primary function is to protect the organism against external threats. This includes protection from bacteria, viruses and fungi, mechanical impacts and pressure, radiations, chemicals, temperature variations and dehydration[1-5]. The skin is also the place where physiological processes are regulated, such as body temperature (perspiration, hairs and vascular system) and vitamin D_3 synthesis[6,7]. Finally, it is composed of mechano- and thermo-receptors, providing tactical and thermal sensitivity to the organism[8,9].

2.1.1. Structure, composition and functions of the skin

The skin is divided into three distinct layers; the epidermis, the dermis and the hypodermis (or subcutaneous tissue)[10]. Outermost layer of the skin, the function of the epidermis is to form a barrier with the exterior environment, avoiding water loss and entry of potential pathogens[11]. The epidermis is mostly made of keratinocytes which differentiate from the basal lamina to the top, where terminally differentiated keratinocytes form the stratum corneum, melanocytes and immune cells [Fig. 1].

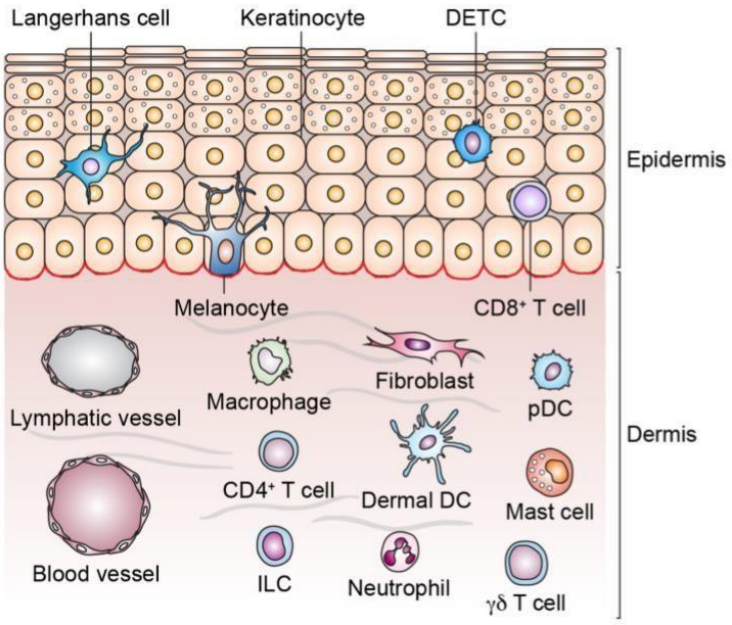

Figure 1: Structure and cell populations of the skin. The epidermis mostly comprises keratinocytes at various stages of differentiation, melanocytes and immunes cells, forming the barrier of the skin. Below the epidermis, the dermis has a relatively poor cell density and is mostly composed of fibroblasts and immune cells. The dermis is the layer where blood and lymphatic vessels are found, involved in nutrients supply and immune response. Highly abundant in the dermis, collagen and elastin fibers, involved in skin elasticity and turgor. The list of cell types is non-exhaustive. DETC: dendritic epidermal T cells, DC: dendritic cells, ILC: innate lymphoid cell and pDC: plasmacytoid dendritic cell. Figure from A. Pfalzgraff *et al.*[12].

The dermis is a layer located deep to the epidermis and superficial to the hypodermis[13]. With a relatively low cell density, it is mainly composed of extracellular matrix (ECM), made of collagen and elastin fibers surroundedby glycoproteins, proteoglycans and glycosaminoglycans[14]. Fibroblasts are the most abundant cell type and are responsible for the synthesis of collagen and elastin fibers and ECM material, building a network of connective tissue which provides skin elasticity, turgor and mechanical resistance[15]. The dermis hosts blood & lymphatic vessels, hair follicles and sebaceous glands, supported in their respective function by macrophages, mast cells and adipocytes. Mast cells are inflammatory cells, involved in inflammatory response, wound healing and collagen remodeling[16]. Dermal adipocytes provide thermal protection, energy storage and are described to playa role in wound healing[17].

Also known as the subcutaneous layer, the hypodermis is the innermost and thickest layer of the skin. Made of a population of adipocytes, fibroblasts and macrophages, it is involved in fat storage and thermoregulation, hormone production and immune surveillance while providing attachment support for the upper layers to underlying tissues[18].

2.2. Skin aging and hallmarks of aging

Because of its direct contact with the external environment, skin aging is impacted by internal *and* external factors which impairs cellular metabolism and induce structural and functional changes in the extracellular matrix.

Intrinsic aging is an inevitable and genetically determined process partially due to free radical accumulation, hormonal shift and reduced cellular efficiency to repair internal damages. Other intrinsic factors, as oxidative stress, chronic inflammation and glycation have been shown to have a significant contribution to internal aging of the skin[19]. Upon natural aging, the population of fibroblasts and mast cells decreases in the dermis, reducing the production of collagen and elastin fibers. In parallel, the abundance of oligosaccharides decreases, limiting skin ability to bind and retain water.

Extrinsic factors impacting the aging of the skin mostly depend on lifestyle and the environment, factors suchas sun light, smoke, pollution and sleep. Skin exposition to UV radiations is the major extrinsic factor of aging and is responsible for about 80% of facial aging (referred as photoaging)[20].

Aging does not only involve skin, as a time-dependent progressive accumulation of damages and a loss of physiological integrity lead to an impairment of the function of many other organs and tissues. The accumulation of cellular damages overtime is considered as the main cause of aging and increases the risk factor of age-related pathologies such as cancer, diabetes and neurodegenerative diseases[21-23]. Intrinsic and extrinsic factors of aging induce cellular and molecular changes classified in 9 hallmarks of aging [Fig. 2][24].

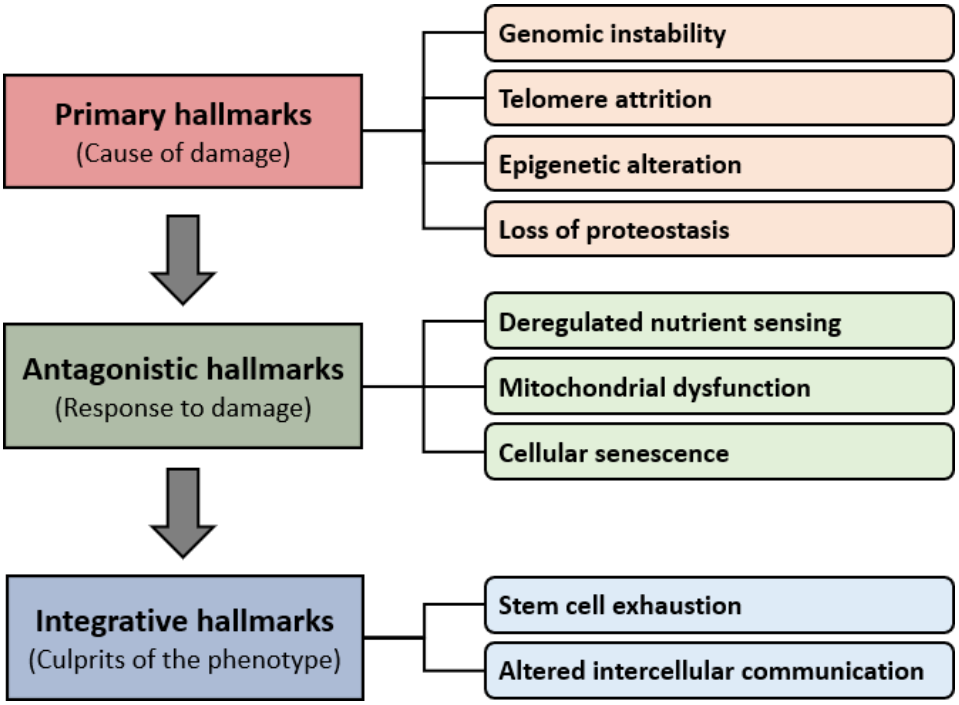

Figure 2: Hallmarks of aging and their functional interconnections. The figure lists the 9 hallmarks of aging, classified in three groups: causes of damages (primary hallmarks), response to damages (antagonistic hallmarks) and response to the phenotypes (integrative hallmarks). Adapted from C. Lopez-Otín *et al*.[24].

2.2.1. Primary hallmarks of aging

Genomic instability refers to the accumulation of unrepaired genetic damages upon aging[25]. Throughout lifetime, the integrity of the genetic material is constantly challenged by intrinsic factors (error in DNAreplication, reactive oxygen species and viral-induced genome modifications) and extrinsic factors (chemical agents, pollution and UV), affecting nuclear and mitochondrial DNA[26-28].

During DNA replication, the ability of telomerase to completely replicate the end of the chromosomes (telomeres) is limited, leading to a loss in their integrity after each replication[29]. Sensed as DNA damage, this triggers a DNA Damage Response (DDR), involved in many aspects of aging[30].

Epigenetic alterations, including histone modifications, DNA methylation and chromatin remodeling play a role in organism longevity and aging[31-33].

Proteostasis englobes all biological pathways in the cell that mediate protein biogenesis, folding, trafficking and degradation[34]. Endogenous and exogenous cellular stresses cause the unfolding of proteins. Unfolded proteins are normally refolded by heat shock proteins (HSPs, which also control protein quality after translation)[35], or targeted for degradation by the ubiquitin-proteasome system or by the lysosomal pathway (autophagy)[34-37]. Impaired protein proteostasis has been shown to play a role in aging and age-related pathologies[34].

2.2.2. Antagonistic hallmark of aging

The Insulin and IGF-1 signaling (IIS) pathway is an extraordinary conserved regulator of aging in evolution, influencing invertebrate and vertebrate longevity[38,39]. Downstream targets of the IIS include the FOXO proteins family and the mTOR complexes, both directly involved in aging processes[40], and mutations among members of the IIS have been linked to longevity[41].

Mitochondria are the organelles responsible for cellular energy production. As cell age, the efficiency of the respiratory chain (responsible for the production of ATP) decreases, while the production of ROS increases[42]. This phenomenon, known as the "free radical theory", generates cellular damages. Contribution of dysfunctional mitochondria additionally occur through ROS-independent mechanisms, as deficient mitochondria are more sensitive to permeabilization and subsequent inflammation and/or apoptosis[42].

2.3. Cellular senescence, a hallmark of aging

Skin fibroblasts have a finite lifespan in culture, known as the "Hayflick limit". Observed for the first time by Leonard Hayflick in 1962, cells can divide approximatively 50-60 times before entering a non-proliferating state later known as cellular senescence[43,44]. Senescence is characterized by the irreversible cell cycle arrest and was first shown to be a consequence of the telomeres shortening, which occurs after each cell division (called replicative senescence)[45-47].

Not only restricted to telomeres shortening, senescence is triggered by various stresses, leading to stress- induced premature senescence (SIPS). These include oncogene hyperactivation (oncogene-induced senescence, OIS)[48-50], oxidative stress[51-53], mitochondrial dysfunction[54,55], tumor suppression loss[56,57], certain cytokines[58,59] and other stresses inducing DNA/chromatin damages, such as UV, gamma irradiations and chemotherapeutic drugs[60-63].

2.3.1. Pathways involved in cellular senescence

Molecular mechanisms underlying cellular senescence are complex and involve numerous pathways. The cell cycle arrest occurs mostly in the G_1 phase and is mediated by the activation of the $p16^{INK4a}$/Rb and/or the $p53/p21^{CIP1}$ tumor suppressor pathways, which regulate cell cycle progression through cyclin-dependent kinase (CDK) inhibitors[64-66] [Fig. 3].

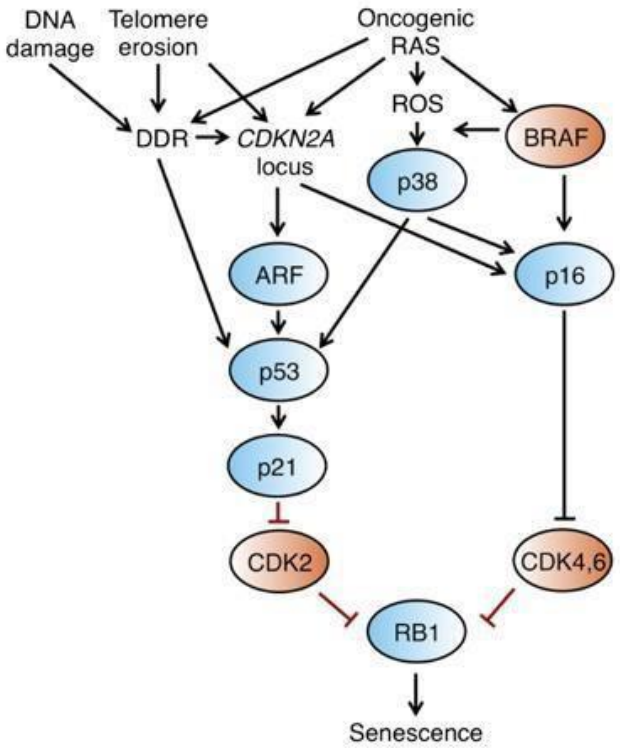

Figure 3: Stressors and pathways involved in cell cycle arrest. The senescence cell cycle arrest is mediated through two major pathways: $p16^{INK4a}$/Rb and the $p53/p21^{CIP1}$, which result in the repression of the Cyclin-Dependent Kinases 2, 4 & 6 (CDK4/6), the subsequent inhibition of retinoblastoma and of cell cycle. The DNA Damage Response (DDR) activates the p53 and the p16 pathways and is a common feature of almost all type of senescence. DDR-independent mechanisms also exist and converge in the p53 and p16 pathways. ROS: reactive oxygen species, CDK: cyclin-dependent kinase, DDR: DNA damage response. Figure adapted from Lujambio *et al.*[67].

The DNA Damage Response (DDR) is a network of cellular pathways involved in the detection and the repair of DNA damages through the regulation of the $p53/p21^{CIP1}$ pathway. In the context of cellular senescence, the role of p53 varies according to the cellular stress; whereas persistent activation of DDR leads to cell cycle arrest through p53 activation, transient stress induces p53 to initiate a quiescence program and DNA repair process[68]. During senescence, exit from the cell cycle is often the consequence of a persistent DDR[69], either caused by internal (telomeres shortening, oxidative stress) or external (UV, irradiation or chemotherapeutic drugs) stimuli. DNA damages and ROS (generated by OIS, dysfunctional mitochondria or senescence-associated secretory phenotype (SAPS)) activate p53 via the p38MAPK-ATM signaling pathway. Activated by the persistent DDR, the $p53/p21^{CIP1}$ pathway drives the cell growth arrest through activation of the cyclin- dependent kinase inhibitor $p21^{CIP1}$, which in turn blocks CDK2 activity and hypophosphorylates Rb[70-72]. In senescence, CDK inhibitors maintain Rb in a hypophosphorylated (active) form, which then inhibits E2F and promote senescence[73]. Accordingly, impairment of the $p53/p21^{CIP1}$ pathway impairs the senescence program[74, 75].

Persistent stress activates $p16^{INK4a}$/Rb pathway, involved in the long-lasting arrest of the cell cycle through induction of INK4/ARF locus[76]. This locus, which encodes for CDKN2A, CDKN2B and $p14^{ARF}$ is repressed in

proliferating cells[77]. $p14^{ARF}$ is involved in the cell cycle arrest by stabilizing p53 via inhibition of HMDM2 ubiquitin ligase. In senescent cells, CDKN2A (p16) is increased and contributes to the induction of premature senescence[78], whereas CDKN2B (p15) is detected in SASP-mediated, DNA-damage, OIS- and developmentally programmed senescence[79-81]. It has been hypothesized that the $p53/p21^{CIP1}$ pathway triggers the onset of senescence, whereas $p16^{INK4a}$/Rb pathway maintains a durable cell cycle arrest[82].

2.3.2. The Senescence-Associated Secretory phenotype (SASP)

Although blocked in G_1 phase, senescent cells remain metabolically active and secrete a cocktail of growth factors, inflammatory cytokines, chemokines and matrix metalloproteases (MMP), called the senescence - associated secretory phenotype (SASP)[83-86]. Activation of the SASP is triggered by the DDR, via activation of NF- κB and C/EBP transcription factors and on the MAPK pathway[87].

The specific composition of the SASP depends on the cell type and the senescence inducer, which can have beneficial *and* detrimental effects on surrounding cells and tissue[84] [Fig. 4].

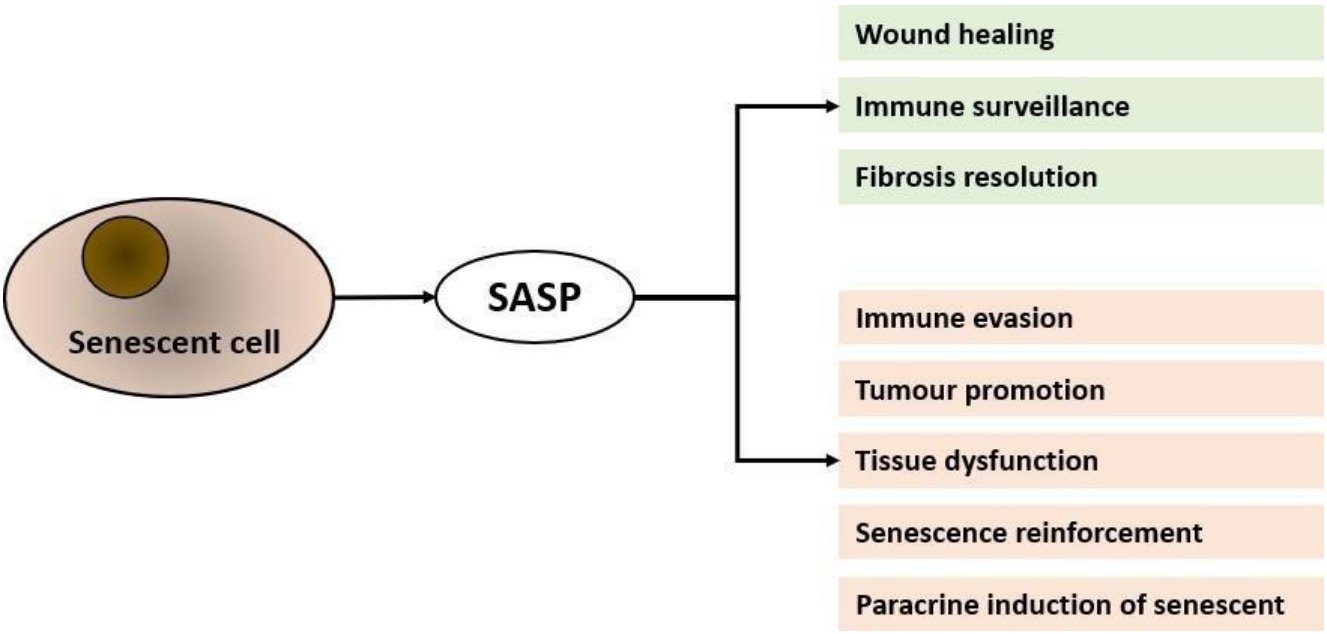

Figure 4: Influence of the Senescence-Associated Secretory Phenotype (SASP) on surrounding cells and tissue. The SASP has both beneficial (green) and detrimental (red) effects. It accelerates would healing and plays a role in immune surveillance, favorizes tumor progression, induces senescence in nearby proliferating cells and promotes a chronic level of inflammation. Figure modified from N. Herranz et *al.*[88].

Through a positive gene expression feedback loop, the SASP reinforces itself in an intra-, auto- and paracrine manner[89]. Moreover, the SASP has been shown to induce senescence in nearby proliferating cells in a paracrine manner[90,91].

While SASP-mediated induction of senescence in surrounding cells has a protective effect on tumor expansion, it also promotes malignant cell proliferation and vascularization increase, generating a pro-tumorigenic environment[92,93].

The role played by the SASP in the immune response is pleiotropic: The SASP stimulates the immune system and helps for the elimination of cancer and senescent cells[94] and has immunosuppressive properties[95].

The SASP is linked to aging and age-related pathologies. The release of pro-inflammatory cytokines by senescent cells generates a low, chronic inflammation state referred as inflammaging[96]. Indeed, targeted elimination of senescence cells decreases the levels of proinflammatory cytokines and delays age-associated disorders[97].

2.3.3. Senescence and skin

Senescent cells are reported apoptotic resistant[98]. Surprisingly, senescent fibroblasts upregulate pro-apoptotic initiators and downregulate the anti-apoptotic BCL-2 proteins, suggesting that the apoptotic program is initiated in senescent cells, but somehow restricted[99]. In the skin, senescent cells have been shown to accumulateupon aging in the dermis and epidermis[100,101]. In young tissue, the SASP adopted by senescent cells recruits macrophages and T cells, which target and eliminate senescent cells, allowing theclearance and the regeneration of the tissue. In aged tissues, ability of the immune system to target senescent cells decreases, leading to their accumulation[102] [Fig. 5].

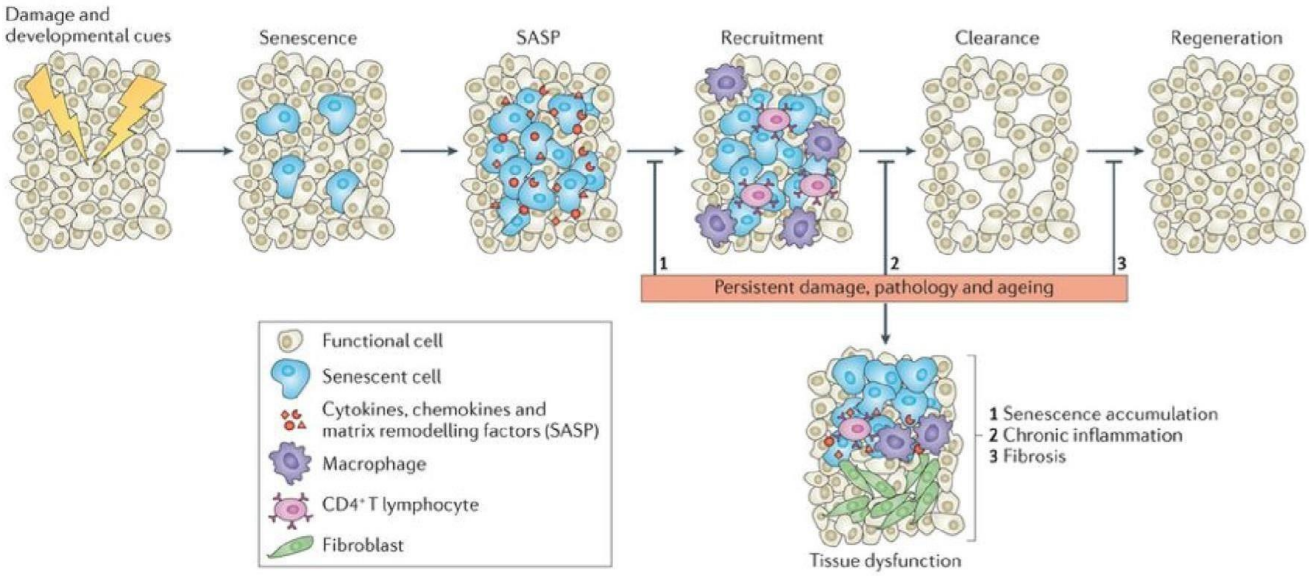

Figure 5: Senescent cells accumulate in aged tissue. Upon exposure to extrinsic and/or intrinsic stresses, a cell can turn senescent. In young tissue, the SASP mediates the recruitment of macrophages, which target and eliminate senescent cells, allowing the clearance and regeneration of the tissue. In aged tissue, senescent cells accumulate, which leads to a state of chronic inflammation and fibrosis, impairing tissue function. Figure obtained from Munoz-Espin *et al.*[86], reproduced with permission and used under the conditions of Springer Nature (terms and conditions for copyright).

2.4. Markers of senescence

Involved in aging, age-related pathologies and cancer, identification and targeting senescent cells has animportant therapeutic potential. Although considerable progresses have been done, the molecular mechanisms underlying cellular senescence remains partially understood and lack specific markers.

Senescent cells undergo profound structural changes, notably at the level of chromatin. During the development of senescence, chromatin condensates and form foci, known as senescence-associated heterochromatin foci (SAHF), which are visible under microscopy[103]. SAHF silences E2F-regulated genes and triggers $p16^{INK4a}$/Rb and $p53/p21^{CIP1}$ pathways[104].

As $p16^{INK4a}$/Rb and $p53/p21^{CIP1}$ are critical pathways of senescence, respective expression of p16, p21 and p53 are used as senescence markers[105,106]. In parallel, markers like p15, ARF, IL-6 and IL-8 (SASP component) may also be used[107,108].

The DNA damage response leads to the recruitment of several protein complexes, including the phosphorylated form of the histone H2AX (γH2AX) which forms foci at the lesion site. γH2AX foci increases *in vitro* and *invivo* during aging, making it a reliable senescence marker[109].

The current standard for the detection of senescent cells *in vitro* relies on the activity at pH 6.0 of a specific enzyme, the senescence-associated β-galactosidase (SA-β-Gal)[110]. The SA-β-Gal is a lysosomal enzyme which activity is thought to be a consequence of the enlargement of lysosomes observed in senescent cells, and might have no impact on senescence development nor maintenance[111]. The activity of the SA-β-Gal increases with aging in human skin[100]. Weather SA-β-Gal activity is a suitable marker for the identification of senescent cells remains debated for several reasons; First, high cell confluence and certain chemical treatments stimulates the SA-β-Gal activity[112]. Second, lysosomes are directly involved in the autophagic process, whose exact role is strongly debated in the context of senescence. This rends the activity of this enzyme in the context of senescenceambiguous and might lead to false positive results.

Markers currently used to detect senescent cells are involved in several biological processes which are not *per se* linked to senescence. Thus, none of the one described above are reliable for the detection and the targeting of senescence, which urges for the identification of novels markers.

2.5. Loss of proteostasis

Accumulation of misfolded proteins upon aging has deleterious effects on cellular metabolism. Two major pathways are responsible for the elimination of these proteins: The ubiquitin-proteasome system (UPS) and autophagy.

Autophagy is an evolutionary conserved mechanism maintaining cellular homeostasis through degradation and recycling of misfolded proteins and misfunctioning organelles. Not directly considered as a hallmark of aging *perse,* autophagytakespartwiththeubiquitin-proteasomesysteminthehallmark "loss ofproteostasis"[24]. During life span, the efficiency of the autophagy-lysosome system and the ubiquitin-proteasome system declines, leadingto theaccumulation of misfolded proteins (aggregates) and dysfunctional organelles, such as mitochondria [113,114] [Fig. 6].

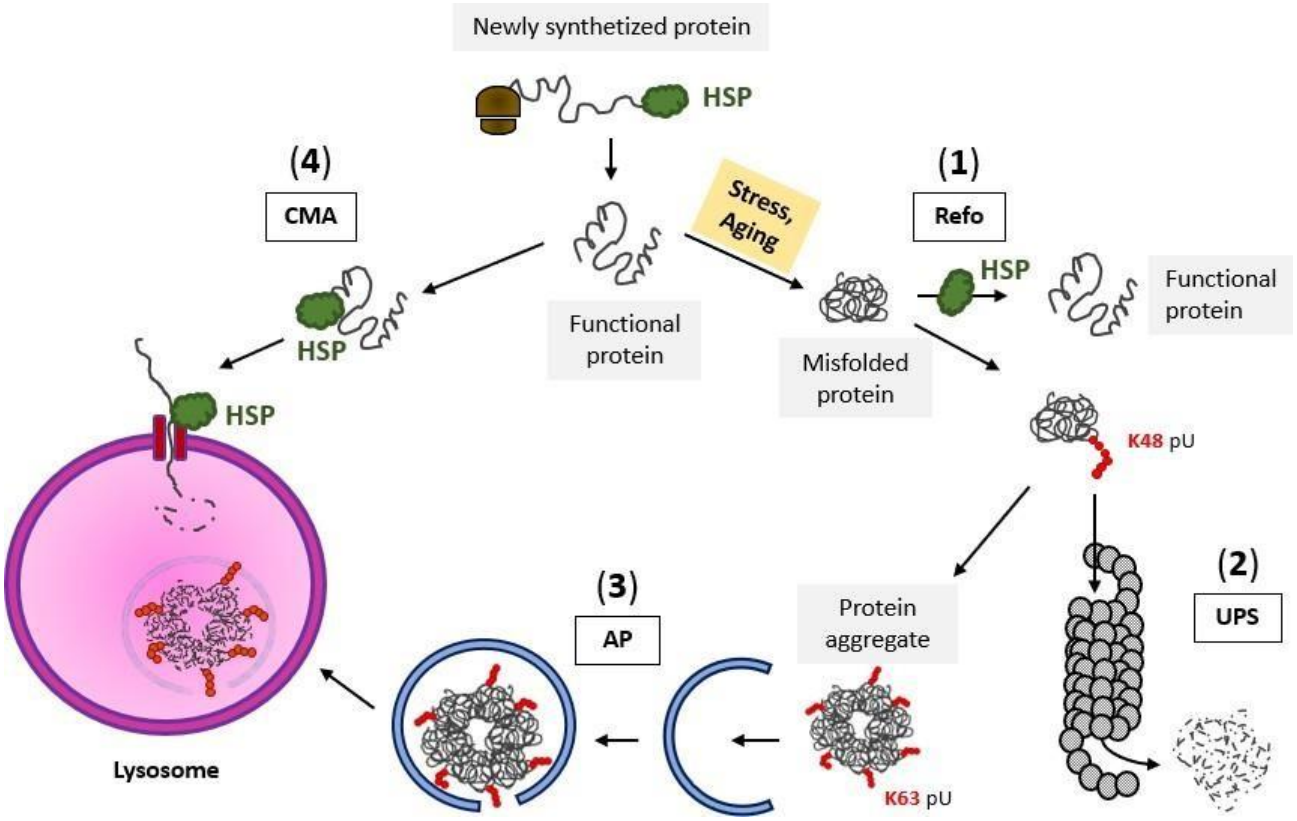

Figure 6: Protein quality control systems. During and after translation, Heat Shock Proteins (**HSPs**) help with the formation of functional proteins by ensuring correct folding. With aging and stresses, misfolded proteins accumulate, impairing cellular functions. (**1**) The HSPs represent the first line of defense by refolding (**Refo**) misfolded proteins. (**2**) When HSPs are unable to refold proteins, chaperones proteins direct misfolded proteins for degradation via the Ubiquitin-Proteasome System (**UPS**). This requires previous poly- ubiquitination (**pU**) of the misfolded proteins, most commonly on lysine residue 48 (**K48**). The ubiquitinated protein is then recognized and degraded by the proteasome. (**3**) When HSP refolding and UPS are overloaded, misfolded proteins aggregate in the cytosol and are poly-ubiquitinated on lysine residue 63 (**K63**). K63 poly- ubiquitination induces degradation by autophagy (**AP**). This includes sequestration of protein aggregates in a double-membrane vesicle, called autophagosome, which subsequently fuses with lysosome. Lysosomal enzymesdegrade autophagosome content. (**4**) HSPs are involved in protein quality control by targeting misfolded proteins for lysosomal degradation. This specific form of autophagy, called Chaperone-Mediated Autophagy (**CMA**), allows to degrade proteins in a very precise and selective way. Adapted from K-L. Lim *et al.*[115].

Autophagy occurs in different programs; microautophagy, chaperone-mediated autophagy (CMA) and macroautophagy (hereinafter referred to as autophagy) [Fig. 7], which all deliver cytoplasmic components to the lysosome[116]. Autophagy delivers cellular materials to the lysosome by first engulfing it in a double membrane structure (phagophore), which matures in a LC-3 containing vacuole (autophagosome). At the end of the maturation, the autophagosome fuse with the lysosome (forming an autolysosome) where its content is degraded and recycled. By contrast, CMA and microautophagy delivers their content directly to the lysosome.

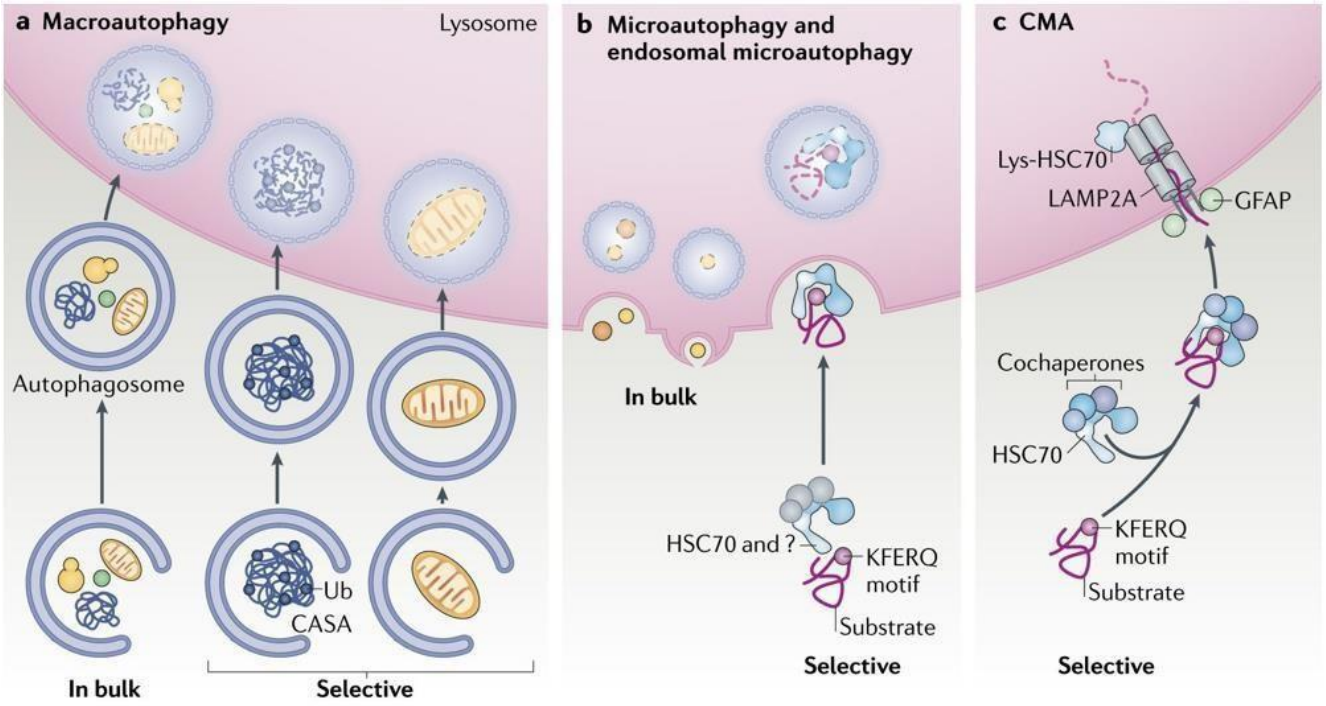

Figure 7: Autophagic pathways. Autophagy occurs in 3 different programs. (**a**) Macroautophagy engulfs cytosolic cargo in double membrane vesicles called autophagosomes. After a maturation process, autophagosomes fuse with lysosomes where their content is degraded by lysosomal enzymes. Macroautophagy can be in bulk, when nutrients are limited, or selective. (**b**) Microautophagy entraps cytosolic cargo by lysosomemembrane invagination. Microautophagy can be in bulk or selective (mediated by HSP HSC70). (**c**) Chaperone- mediated autophagy (CMA) degrades proteins bearing KFERQ motif by delivering them to lysosomes via HSPs(HSC70) and LAMP2A receptors. Figure from S. Kaushik *et al.*[117], reproduced with permission and used under the conditions of Springer Nature (terms and conditions for copyright).

First described as a non-selective degradative pathway activated by poor nutrient containing culture medium, it is now known that autophagy plays a rolein several pathologies including cancer, neurodegenerative diseases, immune response and aging [118,119]. Autophagy is activated upon starvation or deprivation of growth factors to ensure the energy balance of the cell, or upon various stresses including low oxygen levels, high oxidative stress or exposition to cytotoxic agent[120].

Under normal condition (nutrient-rich environment), a basal level of autophagy ensures that protein aggregates, as well as damaged and redundant organelles are selectively eliminated. This selectivity requires the cell to distinguish between normal and abnormal content and is mediated by the binding on the target of ubiquitin, a small regulatory protein (called ubiquitination)[121].

Ubiquitin is involved in two degradation processes: (**1**) the ubiquitin-proteasome system (UPS) and (**2**) the selective autophagy system, both activated after accumulation of damages. What directs an ubiquitinated product to be degraded by the UPS or the autophagic machinery is not fully understood and seems the depend on how ubiquitinis attached toits substrate (mono *vs* polyubiquitination) and on which of the 7 lysine residues[122]. Increasing evidences suggest that the two processes are strongly interconnected[123]. However, whether they act independently or in accordance remains unclear. Upon proteasome dysfunction, a compensatory autophagic

pathway for the elimination of proteins aggregates has been shown to be settled by p62, suggesting that theUPS and autophagic machinery work together for the elimination of misfolded proteins[124].

2.5.1. Pathways involved in autophagy

Autophagy is activated upon starvation or deprivation of growth factors to ensure the energy balance of the cell or upon various stresses including low oxygen levels, high oxidative stress or exposition to cytotoxic agent[120]. The autophagy machinery is regulated by several autophagy-related proteins (ATG) and is divided into 5 sequential steps: (**1**) initiation, (**2**) membrane nucleation and formation of the phagophore, (**3**) expansion, (**4**) fusion and (**5**) degradation [Fig. 8].

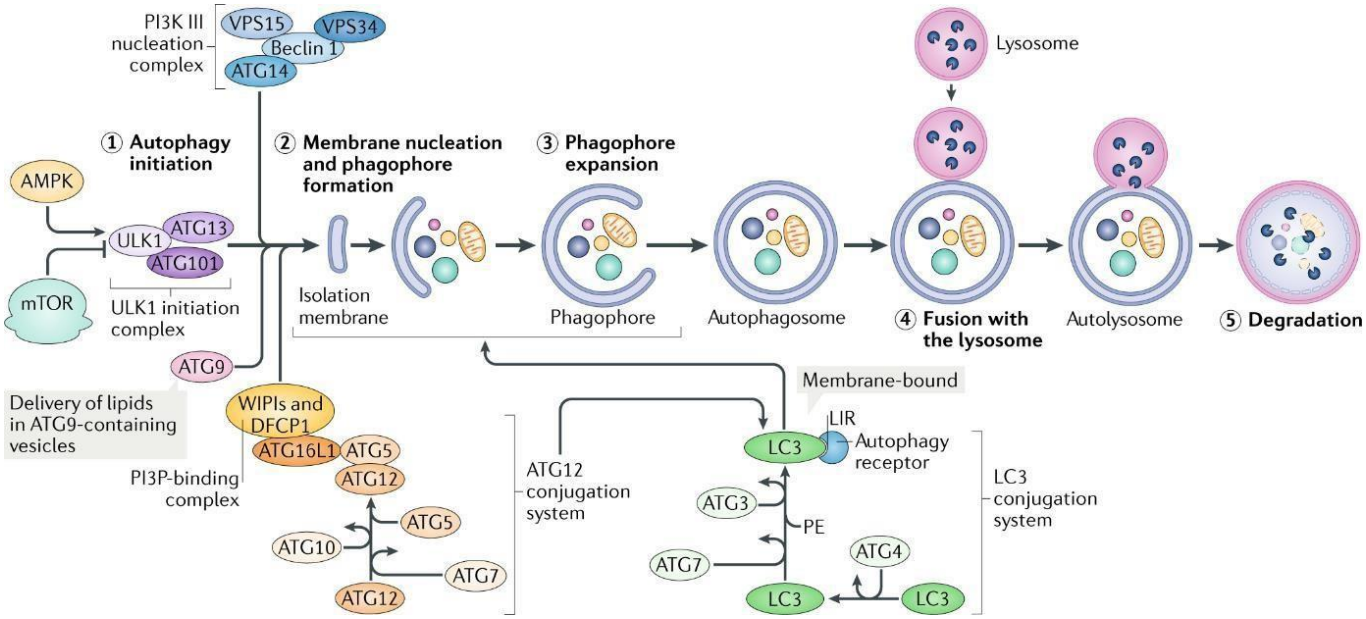

Figure 8: Schematic depiction of the macroautophagy process. mTOR and AMPK signaling are regulators of autophagy. Upon autophagy initiation, a double membrane forms and englobes the cytoplasmic component to be recycled (phagophore). Nucleation, maturation and expansion of the phagophore rely on the activity of the PI3KIII complex, ATG and LC3 proteins and leads to the formation of the autophagosome. Following autophagosome maturation, its fusion with lysosome (autolysosome) degrades its content by the activity of lysosomal hydrolases. Figure obtained from M. Hansen *et al.*[125], reproduced with permission and used under the conditions of Springer Nature (terms and conditions for copyright).

Autophagy is tightly regulated by two upstream regulators, AMPK and mTOR [Fig. 8]. mTOR comprises two distinct complexes, mTORC1 and mTORC2. The mammalian target of rapamycin complex 1 (mTORC1) is a master regulator of cell growth and metabolism[126], whose activity is impaired upon cellular stress signals including amino acids starvation, growth factor deprivation, hypoxia and ROS accumulation. Inhibition of mTORC1 leads to ULK1 dephosphorylation, which subsequently activates the autophagy machinery[127,128]. Components of the mTORC1 are mTOR, rapamycin-associated protein of TOR (Raptor) and mLST8[129].

Inhibition of mTORC2 activates autophagy through impaired inhibition of FoxO3, a transcription factor involved in the regulation of several autophagy-related genes[130,131]. The core components of the mTORC2 are mTOR, rapamycin-insensitive companion of TOR (Rictor), SIN1 and mLST8[129]. During starvation, adenosine mono-phosphate-activated protein kinase (AMPK) senses decreases cellular ATP levels and activates autophagydirectly through ULK1 phosphorylation.

When the autophagic machinery is activated, the nucleation of the autophagosome membrane is regulated by the PI3K complex, including Atg5, Atg7 and Atg12. Maturation of the autophagosome include the binding of LC3 to the phagophore membrane, which is responsible for the specific recognition of cargo through the use of protein adaptor, such as p62. Mature autophagosome fuses with lysosomes, which induces the degradation of the autophagosome content.

2.5.2. Carbohydrates as modulators of autophagy

During aging, a decline in autophagic activity has been reported in a variety of tissues, and its genetic/pharmacological inhibition leads to premature aging[132]. Consistently, stimulation of autophagy delay aging and has beneficial effects on organism's longevity[132]. In contrast, the increased autophagic activity observed in cancer cells contributes to their survival[133]. Therefore, context-dependent modulation of autophagy is the core of several therapeutic approaches for the treatment of aging and age-related pathologies.

Carbohydrates, commonly termed "sugars", are a large class of molecules consisting of carbon, hydrogen and oxygen. Carbohydrates are classified in four groups: (**1**) The monosaccharides, built of a single unit of carbohydrate with the chemical structure $C_6H_{12}O_6$, such as glucose. (**2**) The disaccharides, made of two monosaccharides, such as trehalose. (**3**) The oligosaccharides, containing three to ten monosaccharides, such as raffinose. (**4**) The polysaccharides, polymers of long monosaccharides chains connected through glycosidic bonds, such as cellulose. Based on their capability to act as reducing agent, sugars are further classified into *reducing* and *non-reducing* sugars. Reducingsugarshaveafree aldehyde orketonegroup, abletocedean electronto oxidizing agents. Reducing sugars include *all* monosaccharides, along with some di-, oligo- and poly- saccharides. Non-reducing sugars, such as sucrose, are carbohydrates that cannot be oxidized in aqueous solution, thus unable to generate aldehyde/ketone groups-containing compounds.

Sugars gained attention for their potential ability to modulate autophagy. For instance, trehalose has been reported to increase autophagic activity, providing neuroprotection in Huntington disease and contracting prion infection[134,135]. First thought to modulate autophagy through regulation of mTOR activity, Chen *et al*. reported an mTOR-*independent* activation of autophagy by trehalose, sucrose and raffinose[136]. Although sugars are widely considered as autophagy inducers, recent report from *Yoon et al*. showed that trehalose could be in fact a potent inhibitor.

Although the exact mechanisms by which carbohydrates modulate autophagy are poorly understood, their careful use as autophagy modulators may have beneficial effects in the context of aged-related pathologies.

2.6. Senescence and autophagy

In the context of senescence, the role of autophagy remains poorly understood. Senescence and autophagy share similarities, as they both have cytoprotective and cytotoxic effects[137,138]. While autophagy promotes cell survival by ensuring proteins and organelles quality control, it is also involved in the apoptotic program[139]. Similarly, while senescence prevents the multiplication of damaged cells, its associated secretory phenotype (SASP) promotes inflammation and a favorizes a tumorigenic environment[140].

The role of autophagy in senescence is perceived as a "double edge sword", as it can promote *and* prevent senescence [Fig. 9].

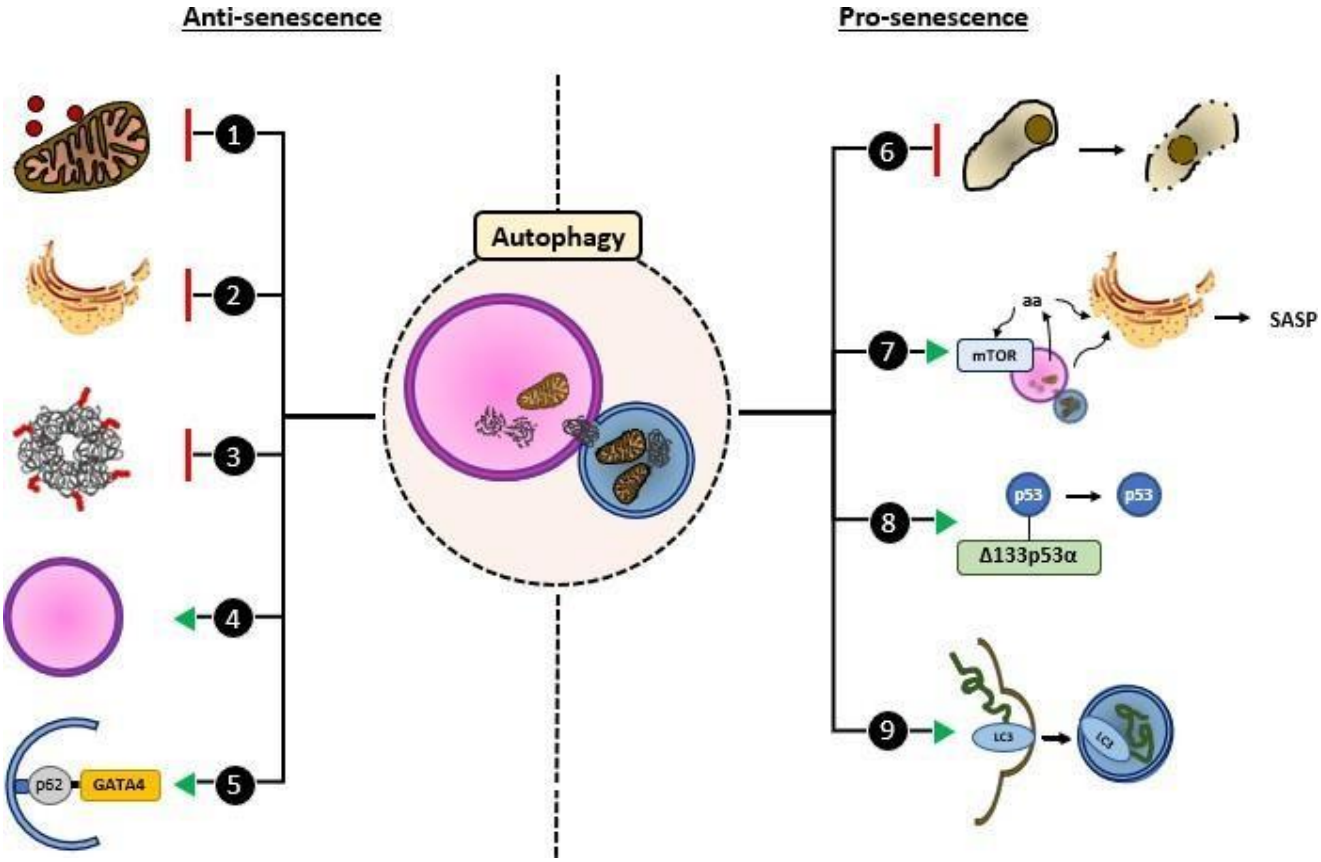

Figure 9: Pro- and anti-senescence role of autophagy. In the context of senescence, autophagy is a double-edge sword and has anti-senescence properties (**1-5**, left panel) and pro-senescence properties (**6-9**, right panel). (**1-3**) Autophagy mitigates stressors that cause cellular senescence, such as dysfunctional mitochondria & ROS, ER stress and protein aggregates. (**4**) Autophagy maintains lysosomal membrane integrity. (**5**) p62-dependent autophagy degrades GATA4, a main regulator of the SASP. (**6**) By dealing with the accumulation of cellular stresses in senescent cells that should normally lead to cell death, autophagy promotes senescent cell longevity. (7) Through the TASCC, autophagy provides required building blocks for the synthesis of SASP components. (8) Autophagy degrades Δ133p53α, which releases p53 and triggers cell cycle arrest. (**9**) Autophagy degrades nuclear lamin B, which induces senescence. Figure adapted from Kwon *et al.*[141].

Under normal conditions, autophagy acts as an anti-senescence mechanism [Fig. 9, left panel]. Autophagy mitigates stressors that cause senescence, such as dysfunctional mitochondria and ROS, ER stress, misfolded proteins and protein aggregates. Autophagy also regulates lysosomal integrity, as permeable lysosomes are extensively ubiquitinated and targeted for autophagic degradation, preventing the onset of senescence[142]. Through ubiquitination and p62-mediated elimination of GATA4, autophagy inhibits the production of the SASP[143].

Autophagy can also act as a pro-senescence mechanism [Fig. 9, right panel]. Autophagy promotes senescent cell survival by modulating the accumulation of cellular damages that should normally trigger a death programin senescent cells. The SASP requires a constant production of different factors and it has been shown that autophagy sustains this production by recycling amino acids used in their production[144]. As a consequence of oncogene-induced senescence, lysosomes and mTOR accumulate in a distinct cellular compartment, known as the "TOR-autophagy spatial coupling compartment (TASCC)". At the TASCC, autophagy recycles amino acids which in turn stimulate the production of IL-6 and IL-8 (2 components of the SASP)[145]. Horikawa et al. demonstrated that autophagy is involved in the ubiquitin-mediated degradation of Δ133p53α, a p53 isoform that inhibits p53 full-length[146]. Subsequent activation of p53 full length drives the cell cycle arrest and triggers senescence. Study of Dou *et al*. highlighted the presence the presence in the nucleus of LC3B, a ubiquitin-like protein associated with autophagosomal membrane. LC3B interacts with nuclear component lamin B and drive its degradation via autophagy during oncogene-induced senescence[147].

Current hypothesis proposes that the pro- and anti-senescent role of autophagy depends on different factors[148]. More specifically, Kwon *et al*. recently proposed a toolkit for the understanding of the complex relationship between autophagy and senescence, based on (**1**) the type of autophagy (selective *vs* bulk), (**2**) the timing (early *vs* late autophagy) and (**3**) the location (lamina degradation (nucleus) *vs* SAPS production (TASCC))[141].

Whether autophagy triggers and/or sustains a senescence phenotype in senescent skin fibroblasts remains poorly understood and could lead to therapeutic approaches for the elimination of senescent cells.

3. Aims of the study

Aging is accompanied by multiple cellular changes which alter organ homeostasis and function, promoting the onset of various aged-related pathologies. During lifespan, cells are exposed to various intrinsic and extrinsic stresses which trigger the senescence program. Apoptosis-resistant, senescent fibroblasts accumulate in the skin, where they promote a chronic inflammation state, favorize a tumorigenic environment and impact its overall appearance.

Current markers allowing the identification of senescent cells are ambiguous and lack specificity. Thus, the identification of novel targets for the removal of senescent cells are of therapeutic interest in the context of aging and age-related pathologies.

Autophagy is a degradative mechanism involved in organism longevity, whose function decreases upon aging. Although the implication of autophagy in the context of senescence is not questioned, their exact relationship remains poorly understood and debated.

Thus, the aims of this work were as follows:

- Analyze and compare the proteome of senescent and proliferating skin fibroblasts
- Identify novel and relevant markers of senescence in skin fibroblasts
- Evaluate the role of these markers in senescent skin fibroblasts viability
- Understand the role of autophagy in the initiation, development and sustainability of doxorubicin-induced premature senescence in skin fibroblasts
- Evaluate autophagy as a target for the elimination of senescent cells
- Evaluate the ability of different carbohydrates to modulate autophagy in human skin fibroblasts

4. Materials and Methods

4.1. Cell culture

Juvenile foreskin fibroblasts (NHDF) were cultured in corresponding fibroblast growth medium (both PromoCell, Germany). WS1 fibroblasts (ATCC® CRL-1502™, Germany) were cultured in Minimum Essential Medium (gibco® by Life Technologies™, ThermoFisher Scientific, USA) supplemented with 10 % fetal bovineserum (Biochrom GmbH, Merck KGaA, Germany) and 1 % UltraGlutamine™ I (Lonza, Belgium). All cells werecultured under standard cell culture conditions (37°C and 5 % CO_2).

4.2. Induction of premature senescence

Senescence was induced in WS1 and NHDF using 0.5 μM doxorubicin (Sigma-Aldrich, USA) in corresponding culture medium for 24 hours, under standard cell culture conditions (37°C and 5 % CO_2). After doxorubicin treatment, cells were washed 3 times in phosphate-buffered saline (PBS) (VWR, Germany) and allowed to recover for 14 days in corresponding culture media and under standard cell culture conditions (37°C and 5 % CO_2). Senescence was induced when cell reached 70% confluency. Despite Doxorubicin treatment, it happened that fibroblasts were still proliferating 48 hours after the treatment. In this case, a second treatment with 0.3 μM doxorubicin for 24 hours was applied.

4.3. Detection of cellular senescence

4.3.1. Cellular senescence activity assay

NHDF and WS1 were cultured in 96-well plates (VWR, Germany) and treated with doxorubicin as previously explained. Senescence was assessed in doxorubicin-treated WS1 and NHDF using the Cellular Senescence Activity Assay (SA-β-gal Activity, Fluorometric Format) (ENZO, USA). Briefly, culture medium was removed, and cell were washed 1x with 200 µL/well cold PBS (VWR, Germany). Cells were further lysed with 100 µL/well cold lysis buffer and incubated for 5 minutes at 4°C. Whole cell lysates were transferred to microcentrifuge tubes and centrifuged for 10 minutes at 4°C. Supernatants were collected and protein concentration determined by Bradford assay (see below). 50 µL of lysates at a concentration of 50 mg/mL were used in triplicate in another 96-well plate. Lysates were incubated with 50 µL freshly prepared 2x Assay Buffer for 2.5 hours at 37 °C (w/o CO_2), protected from light. 50 µL of the reaction mixture were removed, and 200µL stop solution added. Fluorescence intensity was detected using a Spark® 20M multiplate reader (TECAN, Switzerland). Excitation 360 nm, Emission 465 nm.

4.3.2. SA-β-Gal staining

NHDF and WS1 were cultured in 6-well plates (VWR, Germany) and treated with doxorubicin as previously explained. Senescence was assessed in WS1 and NHDF using a senescence β-galactosidase staining kit (Cell Signaling, Germany). Briefly, culture medium was removed, and cell were washed 1x with 2 mL/well cold PBS. Cells were further fixed at room temperature with 1mL 1X fixative solution (Cell Signaling, Germany). After

15 minutes, cells were washed 3x with 2 mL/well cold PBS. Cells were further stained with 930 µL/well staining solution (equilibrated at pH 6) for 12 hours at 37 °C (w/o CO_2). Staining solution was removed, cells were washed 3x in cold PBS and 500 µL/well culture medium added. Imaging was performed with a Primovert light microscope using an Axiocam 105 color (Carl Zeiss Microscopy GmbH, Germany).

4.4. Protein concentration

Protein concentration was determined using the Quick Start™ Bradford protein assay (Bio-Rad, USA). Briefly, cells were washed 1x in cold PBS and lysed on ice for 15 minutes in CellLytic M (Sigma Aldrich, USA) containing protease inhibitor cocktail cOmplete Mini and phosphatase inhibitor PhosSTOP (both from Roche Diagnostic GmbH, Germany). Subsequently, cell lysates were stocked at -80°C four 1 hour. Prior to Bradford assay, cell lysates were centrifuged at 1300G for 3 minutes and supernatant collected for Bradford assay. Bradford assay was performed according to manufacturer´s protocol.

4.5. Samples preparation for 2D-LC-MS/MS analysis

For each condition (proliferating and senescent), 3 donors of Normal human Dermal Fibroblast (NHDF) were used. NHDF were harvested, homogenized and lysed using Cell Lytic M and protease/phosphatase inhibitors (Roche). Subsequently, total protein amount was measured with the Pierce™ Rapid Gold BCA Protein Assay Kit (Thermo Fisher, Germany). Cells were lysed as previously explained. 10 µg of each sample were reduced, alkylated, digested and purified using EasyPrep Mini MS sample Prep Kit (Thermo Fisher, Germany). After a drying step, samples were resuspended in 100 mM TEAB solution and labeled with TMT6plex™ Isobaric Label Reagent Set according to manufacturer's protocol (Thermo Fisher, Germany). Finally, samples were merged and cleaned up using Pierce™ Peptide Desalting Spin Columns (Thermo Fisher, Germany).

4.6. 2D-LC-MS/MS analysis

Mass spectrometry analysis of proteome was carried out using 2D-LC-MS/MS system and a TMT6plex label quantification approach. Mixture containing 3 biological replicates for each condition (normal and senescent) were first separated sequentially using multidimensional chromatographic techniques. The first eight fractions were generated by the ion-exchange chromatography and were further separated by reversed-phase chromatography. MS/MS analysis was performed using a and a Q-Exactive™ Hybrid QuadrupoleOrbitrap™ mass spectrometer (ThermoFisher) equipped with a nano-electrospray ion source. LC-MS/MS analysis was performed in 2 technical replicates.

4.7. Protein identification and quantification

Proteins were identified and quantified using Proteome Discoverer search engine (version 2.3.0.523). MS/MS spectra were searched against the UniProtKB database (06.05.2019). Search parameters were as follows: Enzyme Name: Trypsin / Max. Missed Cleavage Sites: 3 / Precursor Mass Tolerance: 12ppm / Fragment Masse Tolerance: 0.04Da / Dynamic Modifications: Carbamidomethyl (+57.021Da, C), TMT6plex

(+229.163Da, K), Oxidation (+15.995Da, M), phosphorylation (+79.996Da, C,S,T and Y) and deamination (+0.984Da, N, Q and R). The false discovery rate was set to 1% ($p \leq 0.01$). A minimum of 2 unique peptides were required and only proteins found in all samples were retained for quantification. Then, protein abundance was compared across samples by taking the protein abundance ratio senescent/proliferating.

4.8. Gene set enrichment analysis

Functional enrichment analysis was performed using g:Profiler (version e98_eg45_p14_ce5b097), mining Gene Ontology Biological Processes (GO:BP) and Reactome (REAC) databases. Multiple testing correction was performed using Benjamini-Hochberg FDR multiple testing correction method with a significance threshold set to 0.05. To avoid limited interpretative value of large pathways and statistical power decrease due to small pathways, the size of functional category was set between 5 (min) and 350 (max) genes, as previously described (J. Reimand *et al.*, Nature protocols 2019). Resulting enrichment analysis data were exported in Cytoscape (version 3.7.1) and visualized using EnrichmentMap application with a node cutoff Q-value of 0.04 and an edge cutoff (similarity) of 0.5. Nodes were manually grouped into cluster of similar biological functions.

4.9. Modulation of autophagy

4.9.1. Chemicals-mediated modulation of autophagy

To stimulated autophagy, WS1 and NHDF were treated with 0.5 µM rapamycin (Novex® by Life Technologies™, ThermoFisher Scientific, USA) for 24 hours in corresponding culture media and under standard cell culture conditions (37°C and 5 % CO_2). After rapamycin treatment, cells were washed 1x in cold PBS. To inhibit autophagy, WS1 and NHDF were treated with 10 μM chloroquine (provided in CYTO-ID® Autophagy Detection Kit 2.0, Enzo, USA), or 16.5 μM wortmannin (InvivoGen, Germany) for 24 hours in corresponding culture media and under standard cell culture conditions (37°C and 5 % CO_2). After treatment, cells were washed 1x in cold PBS and cultured under standard cell culture conditions (37°C and 5 % CO_2).

4.9.2. siRNA-mediated inhibition of autophagy

Autophagy was inhibited in NHDF using siRNA. All siRNA (Silencer® Select) were purchased from ThermoFisher. Scramble siRNA (cat. no. 4390844), siRNA targeting GAPDH (cat. no. 4390850), Atg5 (cat. no. 4393421), and Atg7 (cat. no. 4393420), were used at a concentration of 20 nM in culture medium for 72 hours, and under standard cell culture conditions (37°C and 5 % CO_2). Briefly, 10^4 NHDF/well were seeded in a 96- well plate. The next day, NHDF were transfected with 20 nM siRNA using Lipofectamine® 3000 reagent (Thermo Fisher, Germany), according to manufacturer's protocol.

4.9.3. Carbohydrates-mediated inhibition of autophagy

Autophagy was modulated in NHDF using different carbohydrates (sugars). Glucose, maltose, sorbitol, raffinose, trehalose, sucrose, methyl-α-glucopyranoside and gluconic acid (all from Sigma-Aldrich, USA) were used at a concentration of 50, 100 and 200 mM in culture medium for 24 hours. Isomaltulose (USP, USA) and

meglumine (Merck KGaA, Germany) were used at a concentration of 50, 100 and 200 mM for 24 hours. After treatment, cells were washed 1x in cold PBS and cultured under standard cell culture conditions (37°C and 5 % CO_2).

4.10. Detection of autophagic activity

The level of autophagic vesicles in WS1 fibroblasts at a given timepoint was assessed using the CYTO-ID® Autophagy Detection Kit 2.0 (Enzo, USA) according to the manufacturer's instructions for fluorescence microplate applications. Briefly, WS1 were seeded at a density of 10^4 cell/well in a 96-well plate. After modulation of autophagy, cells were washed 1x in 100 µL/well 1X assay buffer. Right after, 100 µL microplate dual detection reagents were added to each well for an incubation time of 60 minutes (instead of 30) at 37°C, protected from light. Cells were further washed twice with 200 µL/well assay buffer and 100 µL/well of assay buffer added to each well. Fluorescence intensities were detected using a Spark® 20M multiplate reader (TECAN, Switzerland) (CYTO-ID® Excitation 485 nm, Emission 535 nm. Hoechst 33342 Excitation 320 nm, Emission 465 nm).

4.11. Western Blot analysis

Protein extracts were obtained by lysing WS1 fibroblasts in CellLytic M (Sigma-Aldrich, USA) complemented with protease inhibitor cOmplete Mini and phosphatase inhibitor PhosSTOP (Roche Diagnostics, Germany) for 15 minutes on ice, and subsequently frozen 1 hour at -80°C. Total protein concentration was determined by Bradford assay (Bio-Rad, USA). Indicated protein amounts were separated on 8-16% Midi Criterion™ TGX Stain-Free™ precast polyacrylamide gels (LC3) or on 4-15% Midi Criterion™ TGX Stain-Free™ precast polyacrylamide gels (all other target) (Bio-Rad, USA) at 100 Volts. Proteins were transferred onto PVDF membranes (Bio-Rad, USA) using Trans-Blot® Turbo™ Transfer System (Bio-Rad, USA) at 2.4 A and 25 V for 7 minutes. Membranes were blocked in TBS (Bio-Rad, USA) supplemented with 5% Tween20 (Merck, Germany) and 5% BSA (Sigma-Aldrich, USA) for 1 hour at RT. Membranes were incubated with primary antibodies (anti-LC3A/B (D3U4C) XP®, anti-ß-actin (D6A8), anti mTOR (7C10), anti-Phospho-mTOR (Ser2481), anti-Rictor (53A2), anti-Phospho-Rictor (Thr1135) (D30A3), anti-Raptor (24C12), anti-Phospho- Raptor (Ser792), all from Cell Signaling Technology, (USA) diluted 1:1000 in 5 % BSA in TBS-T (0.1 %). Anti- APOL2 (rabbit polyclonal, ab196771, Abcam) was diluted 1:1000, anti-CES2 (rabbit polyclonal, ab126970, Abcam) was diluted 1:1000, anti-MGARP (mouse monoclonal, MA5-27537, Thermo Fisher) was diluted 1:2000and anti-PTTG1IP (mouse polyclonal, ab68208, Abcam) was diluted 1:500 in 5% BSA in TBS-T (o.1%). Prior to secondary antibody incubation, membranes were washed 3 times in TBS-T (0.1%) for 5 min. Membranes were incubated with secondary antibody (anti-rabbit-IgG, HRP-conjugated, Cell Signaling, USA) diluted 1:2000in TBS-T (0.1%) and 5% BSA at RT for 2 hours. Protein bands were visualized by adding AceGlowTM chemiluminescence substrate solutions A and B (1:1) (VWR International, USA) and chemiluminescence was captured with the imaging system Fusion FX (Vilber Lourmat, Germany). Band intensities were quantified with the BIO-1D software, version 15.07 (Vilber Lourmat, Germany). ß-actin served as a loading control.

4.12. siRNA-mediated gene silencing

siRNA targeting APOL2, CES2, PTTG1IP and MGARP protein (all ThermoFisher, Germany, cat. no. 4392429) were used at a concentration of 5 mM according to manufacturer´s protocol. NHDF were seeded in 96-well plates at a concentration of 10´000 cells/well. The next day, NHDF were treated with corresponding siRNA every 72 hours according to manufacturer´s protocol, as previously explained. Scramble siRNA (cat. no. 4390844), siRNA targeting GAPDH (cat. no. 4390850), transfection reagent (Lipofectamine 3000) and "untreated cells" served as controls.

4.13. ATP assay

Cytotoxic effect of autophagy modulation in senescent WS1 fibroblasts and 4 candidates silencing in NHDF was monitored using the ATPlite™ 1step Luminescence Assay System (PerkinElmer, USA) according to manufacturer's protocol. Briefly, cells were cultured in 96-well plates under standard cell culture conditions (37°C and 5 % CO_2). After treatment (siRNA, autophagy modulators and carbohydrates), 100 µL/well culture medium were removed and refiled with 100 µL/well reconstituted reaction reagent (provided in the kit). Plates were subsequently shacked for 5 minutes at 700 rpm and at room temperature, protected from light, using an orbital microplate shaker, with an orbit diameter of 3 mm. Luminescence was detected using a Spark® 20M multiplate reader (TECAN, Switzerland). Untreated cells served as negative control. Cells treated with 7.5% Tween80 (G Biosciences, USA) as positive control.

4.14. Electron microscopy

Normal human dermal fibroblasts were induced senescent using doxorubicin, as previously explained. After 2 weeks of recovery time, NHDF were cryo-fixed within a few milliseconds at a pressure of 200 bar using a high-pressure freezer Compact 1 (Wohlwend GmbH, Switzerland). Freez-substitution was conducted using a Leica EM AFS 2 device (Leica Microsystems, Germany). Here, the substitution / staining medium (acetone p.a., 0.2% osmium tetroxide, 0.1% uranylacetate and 5% water) was pre-cooled to -90 °C before samples were added. Finally, the samples were embedded in EPON 812 and sectioned at room temperature using a diamond knife. Examination of the thin sections was conducted with a FEI Tecnai F20 transmission electron microscope (FEI, USA) operated at an acceleration voltage of 200 kV. Conventional bright field images were acquired using a Gatan US1000 slow scan CCD camera (Gatan Inc., USA).

4.15. Statistical analysis

All experiments were conducted with at least 3 technical replicates. Statistical analysis was performed using GraphPad Prism 7 (GraphPad Software, USA). One-way ANOVA followed by Tukey's multiple comparison test was performed for treatments individually or whole data sets as indicated. $\alpha = 0.05$. Significances (****): $p < 0.0001$, (***): $p < 0.001$, (**): $p < 0.01$, (*): $p < 0.05$, (ns): $p \geq 0.05$.

5. Results

5.1. Induction and monitoring of cellular senescence in WS1 fibroblasts

Premature senescence was induced using doxorubicin (Dox) in WS1 fibroblasts. To assess whether Dox- treatment induced senescence, two methods based on the activity of the Senescence-Associated beta- galactosidase (SA-β-gal), known as a biomarker of cellular senescence, were used. First, SA-β-gal activity was measured in cell lysates using a fluorometric substrate. Second, fixed cells were provided a modified galactosidase substrate (X-gal), metabolized upon enzyme activity and detectable by light microscopy as blue precipitate.

5.1.1. SA-β-gal activity is increased in senescent WS1 fibroblasts

WS1 fibroblasts were treated with 0.5 µM Dox for 24 hours to induce premature senescence and allowed to recover for 14 days. After 14 days, SA-β-gal activity from Dox-treated (SC) cells was compared to untreated (UT) (see sections 4.2 and 4.4). The fluorescence signal was significantly 2.6-fold increased in SC compared to UT WS1, indicating higher SA-β-gal activity and development of senescence [Fig. 10a]. To confirm senescence in Dox-treated WS1 fibroblasts, untreated- and Dox-treated cells were fixed and stained for SA-β-gal activity. Dox-treated WS1 showed strong staining [Fig. 10b, right] compared to untreated WS1 [Fig. 10b, left].

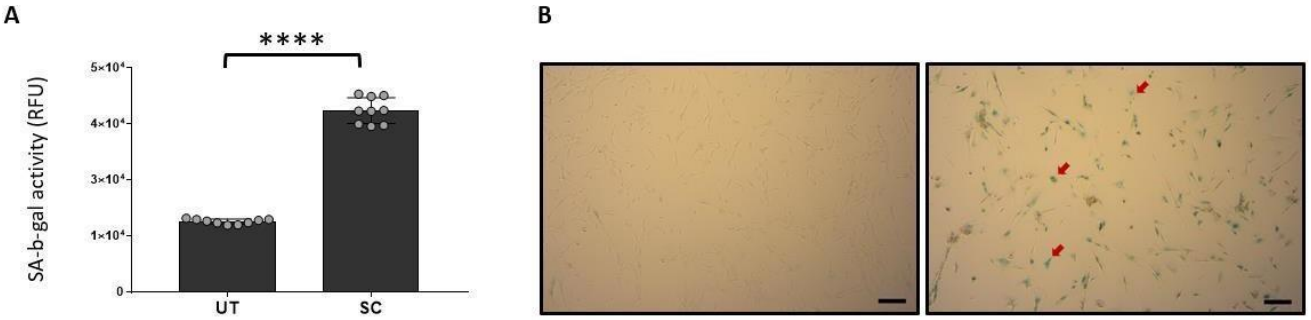

Figure 10: Cellular senescence activity assay in WS1 fibroblasts. SIPS was induced in NHDF using doxorubicin. After 14 days of recovery time, SA-β-gal activity was measured. (**A**) SA-β-gal activity of lysate from Dox-treated cells (SC) was compared to untreated (UT). Values obtained from 3 biological replicates, each in 3 technical replicates and expressed in Relative Fluorescent Unit (RFU). Means ± SEM are shown. Means compared using unpaired t-test: (****): <0.0001. (**B**) SA-β-gal staining. Blue staining indicates senescent cells (red arrows). Scalebar: 100 µM.

5.2. Differential proteome analysis of senescent NHDF by 2D-LC-MS/MS labeling-assisted proteomics

Molecular mechanisms underlying cellular senescence remain poorly understood. The proteome of senescent skin fibroblasts was analyzed by 2D-LC-MS/MS labeling-assisted proteomics.

Stress-induced premature senescence (SIPS) was triggered in normal human dermal fibroblasts (NHDF) using doxorubicin (Dox). As previously described, Dox-treated cells require a few days to recover and develop a senescent phenotype[149]. 14 days after SIPS induction, senescence phenotype was assessed by SA-β-gal staining [Fig. 11] and subsequent differential proteome analysis was conducted by 2D-LC MS/MS labeling-assisted proteomics (see sections 4.6 to 4.8).

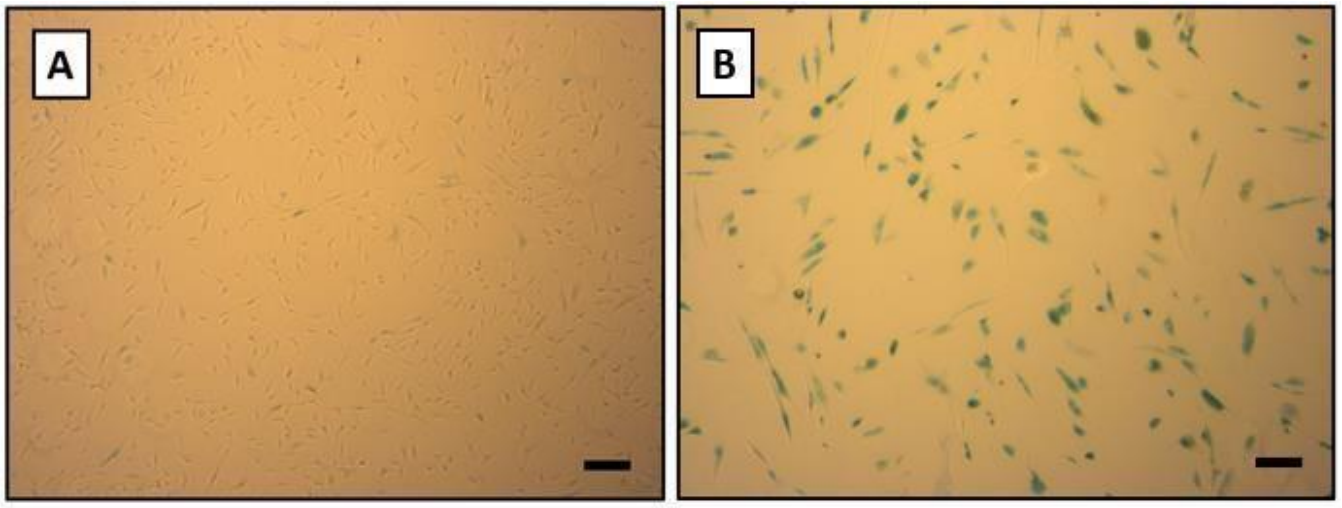

Figure 11: SA-β-gal staining of Normal Human Dermal Fibroblasts. SIPS was induced in NHDF using doxorubicin. After 14 days of recovery time, cells were stained for SA-β-gal activity. Blue staining indicates senescent cells. Scale bar: 100 µM.

A total of 4147 proteins were identified at a 1% false discovery rate (FDR), among which 20 proteins were specific to proliferating NHDF and 19 to senescent NHDF [Table 1a and 1b, respectively].

Accession	Description	Gene Symbol
Q9Y5Q8	General transcription factor 3C polypeptide 5	GTF3C5
P58044	Isopentenyl-diphosphate Delta-isomerase 1	IDI1
O00221	NF-kappa-B inhibitor epsilon	NFKBIE
Q3SWX9	Double-strand-break repair protein rad21 homolog	RAD21
O15254	Peroxisomal acyl-coenzyme A oxidase 3	ACOX3
Q13356	RING-type E3 ubiquitin-protein ligase PPIL2	PPIL2
Q5R746	3'-5' RNA helicase YTHDC2	YTHDC2
Q9Y6G3	39S ribosomal protein L42, mitochondrial	MRPL42
P41742	Tubulin beta chain	TUB2
Q9GL73	Zinc phosphodiesterase ELAC protein 2	ELAC2
Q68D10	Protein SPT2 homolog	SPTY2D1
Q53GL7	Protein mono-ADP-ribosyltransferase PARP10	PARP10
Q96PZ2	Protein FAM111A	FAM111A
Q9N0Y0	Vesicle-associated membrane protein 2	VAMP2

Q4R588	Hsp70-binding protein 1	HSPBP1
Q91WK7	Ankyrin repeat domain-containing protein 54	Ankrd54
Q86YV9	Hermansky-Pudlak syndrome 6 protein	HPS6
P24386	Rab proteins geranylgeranyltransferase component A 1	CHM
Q8TEB9	Rhomboid-related protein 4	RHBDD1
O95365	Zinc finger and BTB domain-containing protein 7A	ZBTB7A

Table 1a: Proteins specific to proliferating NHDF as identified by 2D-LC MS/MS labeling-assisted proteomics. Differential proteome analysisby 2D-LC-MS/MSidentified 20 proteinsonlyfoundin proliferating NHDF.

Accession	Description	Symbol
O95210	Starch-binding domain-containing protein 1	STBD1
P55288	Cadherin-11	CDH11
Q71U07	Thrombomodulin	THBD
P82930	28S ribosomal protein S34, mitochondrial	MRPS34
Q6PCT5	Polyglutamine-binding protein 1	PQBP1
Q04690	Neurofibromin	NF1
O75420	GRB10-interacting GYF protein 1	GIGYF1
Q15283	Ras GTPase-activating protein 2	RASA2
O95396	Adenylyltransferase and sulfurtransferase MOCS3	MOCS3
Q16611	Bcl-2 homologous antagonist/killer	BAK1
Q9L6W9	S-adenosylmethionine tRNA ribosyltransferase-isomerase	QUEA
Q5R801	5'-AMP-activated protein kinase subunit beta-1	PRKAB1
Q60592	Microtubule-associated serine/threonine-protein kinase 2	MAST2
Q5HYI8	Rab-like protein 3	RABL3
P25311	Zinc-alpha-2-glycoprotein	AZGP1
Q9NZQ3	NCK-interacting protein with SH3 domain	NCKIPSD
Q96LJ7	Dehydrogenase/reductase SDR family member 1	DHRS1
Q96B49	Mitochondrial import receptor subunit TOM6 homolog	TOMM6
O75427	Leucine-rich repeat and calponin homology domain-containing protein 4	LRCH4

Table 1b: Proteins specific to senescent NHDF as identified by 2D-LC MS/MS labeling-assisted proteomics. Differential proteome analysis by 2D-LC-MS/MS identified 19 proteins only found in senescent NHDF.

If not otherwise specified, only proteins with at least two unique peptides were selected for further analysis. Among the 4´147 proteins, 2´642 proteins respected this latest criterion. To identify differentially expressed proteins (DEPs) in senescent NHDF, means S/P abundance of each protein were displayed in a volcano plot [Fig. 12]. With a threshold set at ±1.5-fold change, 230 and 228 proteins were found to be significantly up- and down-regulated in senescent NHDF, respectively.

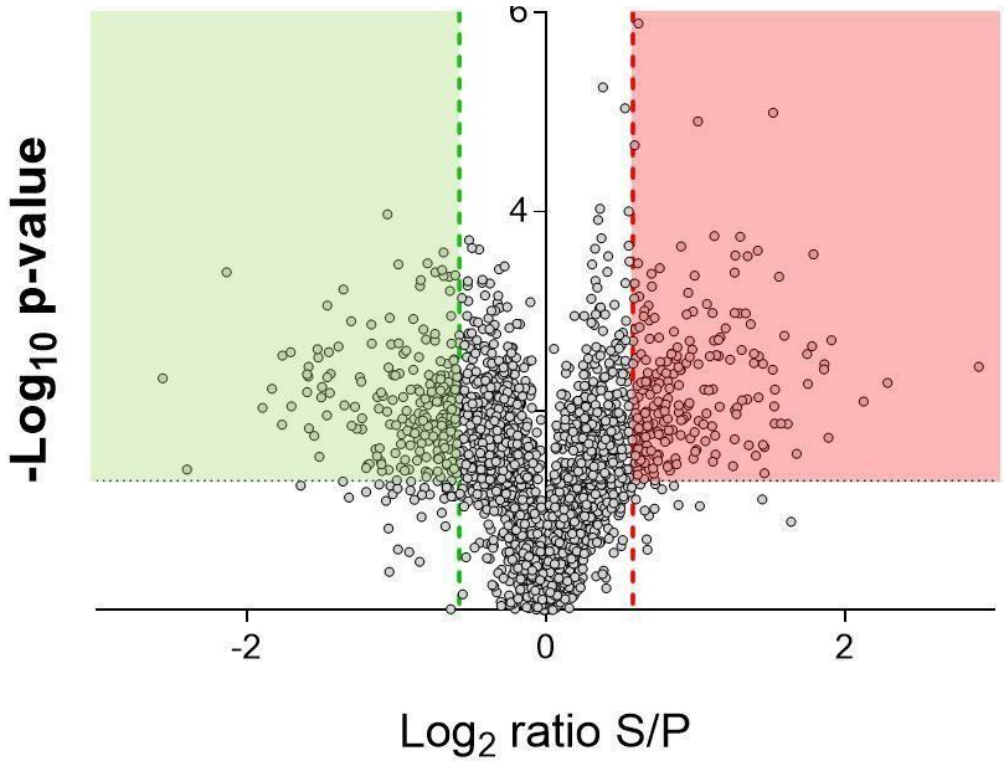

Figure 12: Differentially expressed proteins in senescent normal human dermal fibroblasts. For each protein detected by 2D-LC-MS/MS, the mean abundance ratio "senescence/proliferating" of each detected proteins (log_2) was plotted against its corresponding p-value ($-log_{10}$). P-values were calculated from 3 biological replicates (n=3). Proteins with at least ±1.5 fold changed expression are displayed in green (downregulated, 228) and red (upregulated, 230).

5.3. Gene set enrichment analysis

A gene set enrichment analysis (GSEA) is a method to identify biological pathways that are enriched in a genes list, more than what would be expected by chance[150]. To have an insight of biological pathways impaired in senescent NHDF, down- and up-regulated proteins were separately subjected to a GSEA, mining Gene Ontology: Biological process (GO:BP) and Reactome (REAC) databases.

5.3.1. GSEA of downregulated proteins

GSEA of the 228 downregulated proteins was conducted using g:Profiler webtool. Mining Gene Ontology: Biological Process (GO:BP) and Reactome (REAC) databases, 532 GO:BP biological processes (BPs) and 149 REAC pathways were found significantly enriched due to downregulated proteins in senescent NHDF [Fig. 13].

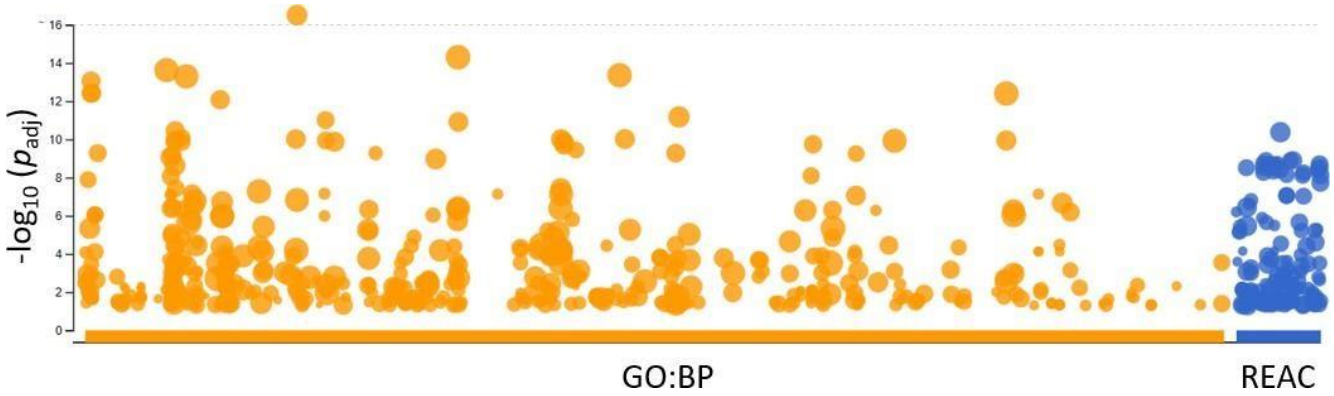

Figure 13: Downregulated proteins enrichment analysis. Proteins found to be downregulated in senescent NHDF were subjected to a gene set enrichment analysis, mining two databases: (**1**) Gene Ontology: Biological Process (GO:BP) and (**2**) Reactome (REAC). Each dot on the graph represent a biological process or a pathway. **X-axis**: mining GO:BP database, 532 biological processes were identified (orange). Mining REAC, 149 pathways were identified (blue). **Y-axis**: Adjusted *p*-values associated with each biological process and pathway.

To visualize the GSEA, impaired BPs and pathways were further mapped using Cytoscape software and manually grouped into clusters of similar functions as previously described[150] (see section 4.9) [Fig. 14].

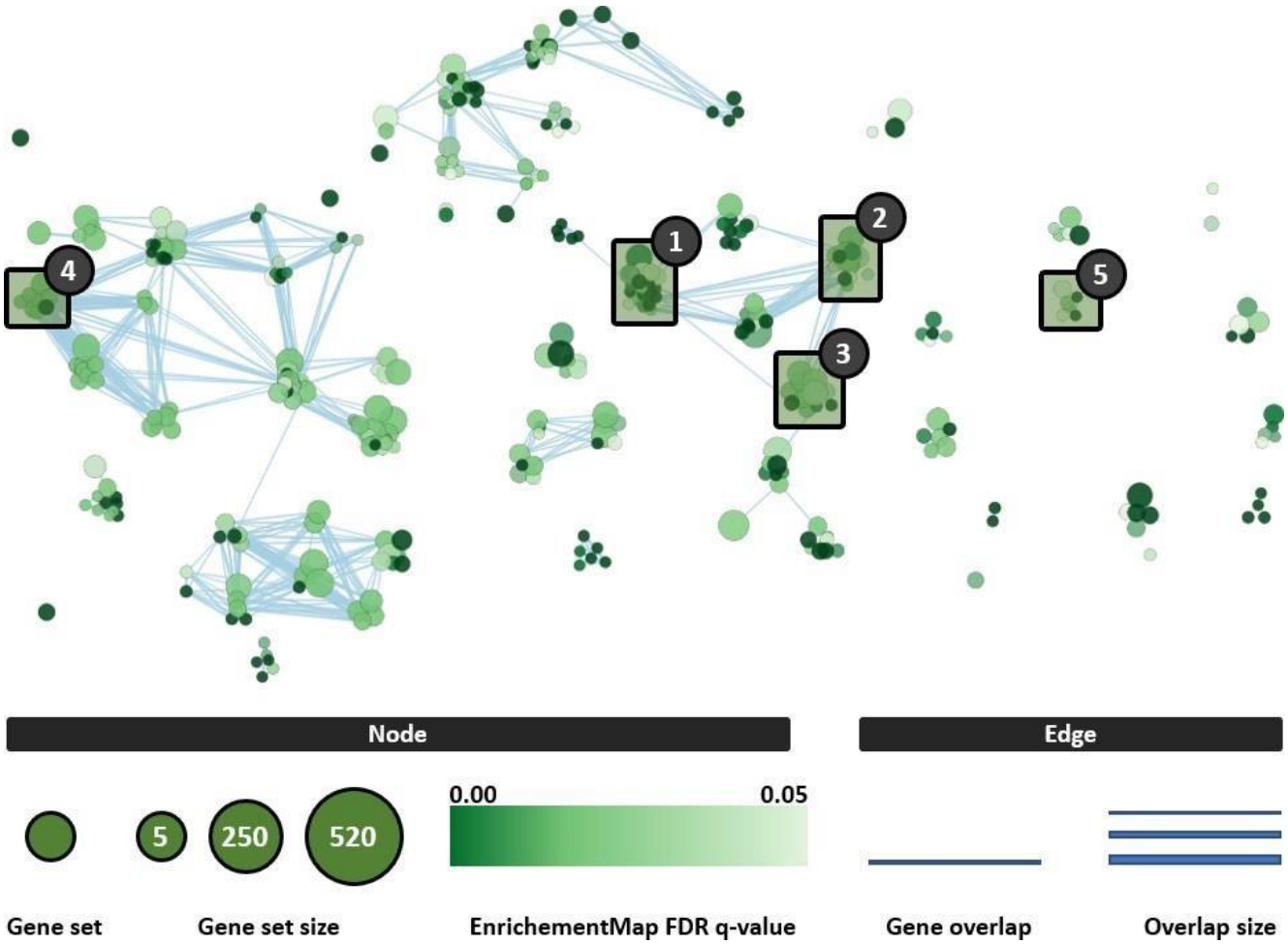

Figure 14: Enrichment map of downregulated proteins GSEA. All BPs and pathways enriched in senescent NHDF due to downregulated proteins were mapped and manually arranged according to function similarities. Each node (circle) represents a distinct biological process (GO:BP) or pathway (REAC), involving between 5 and 520 genes. Color gradient describes the statistic linked to the identification of the biological processes and pathways. Edges (blue lines) represent the number of genes overlapping between two biological processes or pathways, determined using the similarity coefficient. Numbers (**1**-**5**) represent clusters of similar biological processes or pathway. (**1**) BPs involved in DNA repair, (**2**) BPs involved in DNA replication, (**3**) BPs involved in telomere maintenance, (**4**) BPs involved translation initiation and (**5**) BPs involved in nucleus organization.

Visualization and grouping of the GSEA data identified BPs expected to be impaired in senescent cells, including BPs involved in DNA repair, DNA replication, telomere maintenance, initiation of translation and nucleus organization [numbered 1-5 on fig. 14 and table 2].

No.	Database	Accession	Description	FDR q-value
1	REAC	REAC:R-HSA-73894	DNA repair	1.69E-02
2	GO:BP	GO:0033260	Nuclear DNA replication	3.43E-02
3	GO:BP	GO:0007004	Telomere maintenance	1.91E-02
4	GO:BP	GO:0006413	Translation initiation	5.00E-8
5	REAC	REAC:R-HSA-2995410	Nuclear envelope reassembly	2.89E-02

Table 2: List of BPs and pathways known to be impaired in senescent cells. Table lists BPs and pathways identified on figure 4 with corresponding database, accession number and FDR q-value.

Along with expected BPs, GSEA of downregulated proteins identified 34 BPs and pathways directly involved in viral defense and 53 involved in immune response, together counting for 13% of all enriched BPs in senescent NHDF [Appendix 1a and 1b, p. 103**]**.

5.3.2. GSEA of upregulated proteins identified enriched autophagy-related processes in senescent NHDF

Mining GO:BP and REAC, gene set enrichment analysis of the 230 upregulated proteins identified 490 Gene Ontology biological processes and 32 Reactome pathways to be significantly enriched in senescent NHDF [Fig. 15].

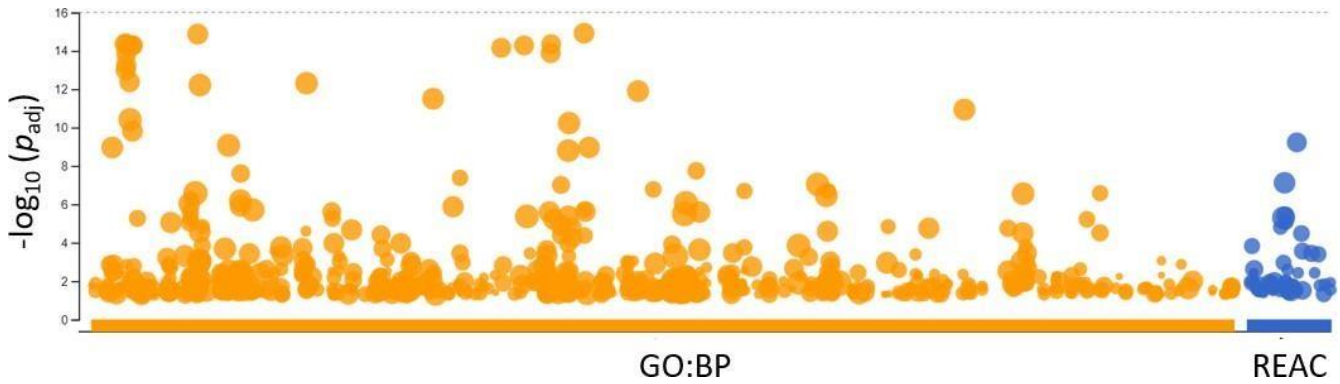

Figure 15: Upregulated proteins enrichment analysis. Proteins found to be upregulated in senescent NHDF were subjected to a gene set enrichment analysis mining two databases: (**1**) Gene Ontology: Biological Process (GO:BP) and (**2**) Reactome (REAC). Each dot on the graph represent a biological process or a pathway. **X-axis**: mining GO:BP database, 280 biological processes were identified (orange). Mining REAC, 32 pathways were identified (blue). **Y-axis**: Adjusted *p*-values associated with each biological process and pathway.

To visualize the GSEA of upregulated proteins, impaired BPs and pathways were further mapped and manually grouped into clusters of similar functions [Fig. 16].

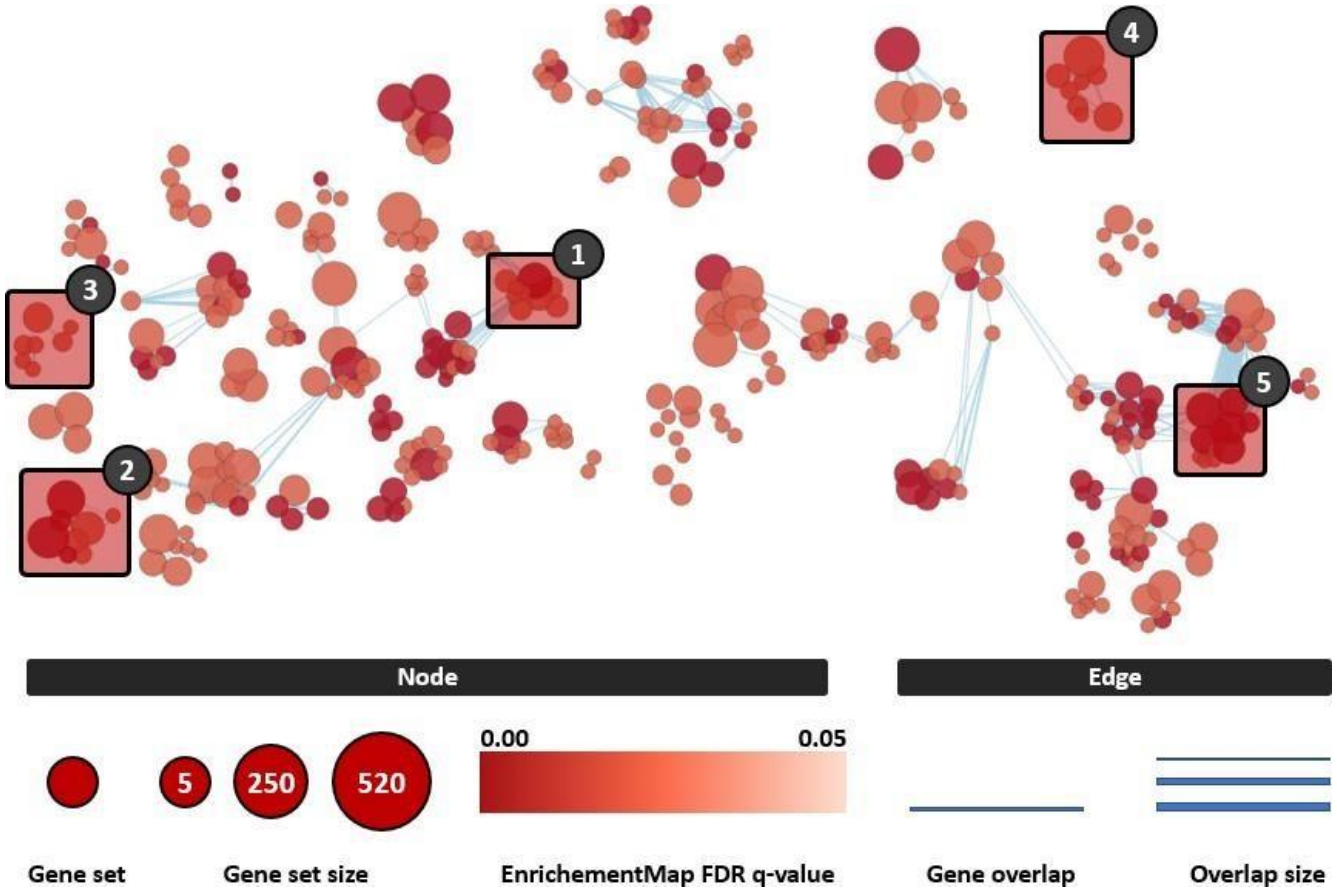

Figure 16: Enrichment map of upregulated proteins GSEA. All BPs and pathways enriched in senescent NHDF due to upregulated proteins were mapped and manually arranged according to function similarities. Each node (circle) represents a distinct biological process (GO:BP) or pathway (REAC), involving between 5 and 520 genes. Color gradient describes the statistic linked to the identification of the biological processes and pathways. Edges (blue lines) represent the number of genes overlapping between two biological processes or pathways, determined using the similarity coefficient. Numbers (**1**-**5**) represent clusters of similar biological processes or pathway. (**1**) BPs involved in viral life cycle, (2) BPs involved in extracellular matrix organization, (**3**) BPs involved in cell cycle arrest, (**4**) BPs involved in apoptotic signaling and (**5**) BPs involved in lipid metabolism.

Visualization and grouping of the GSEA data identified numerous BPs among which (**1**) viral life cycle (GO:0019058, FDR q-value =1.37E-5), (**2**) Extracellular matrix organization (GO:0030198, FDR q-value =3.80E-5), (**3**) cell cycle arrest (GO:0007050, FDR q-value =0.009), (**4**) apoptotic signaling (GO:2001233, FDR q-value =0.0285), and (**5**) lipid metabolism (GO:0006643, FDR q-value =1.01E-5), numbered 1-5 on Fig. 16. GSEA also identified 9 clusters on BPs (38) directly or indirectly related to autophagy [Fig. 17], accounting for 8% of all enriched BPs in senescent NHDF, among which lysosome organization (GO:0007040, FDR q-value=$1.37x10^{-5}$), regulation of macroautophagy (GO:0016241, FDR q-value=$1.28x10^{-3}$), lysosomal transport (GO:0007041, FDR q-value=$1.47x10^{-3}$) and regulation of mTOR signaling (GO:0032006, FDR q- value=$3.09x10^{-2}$).

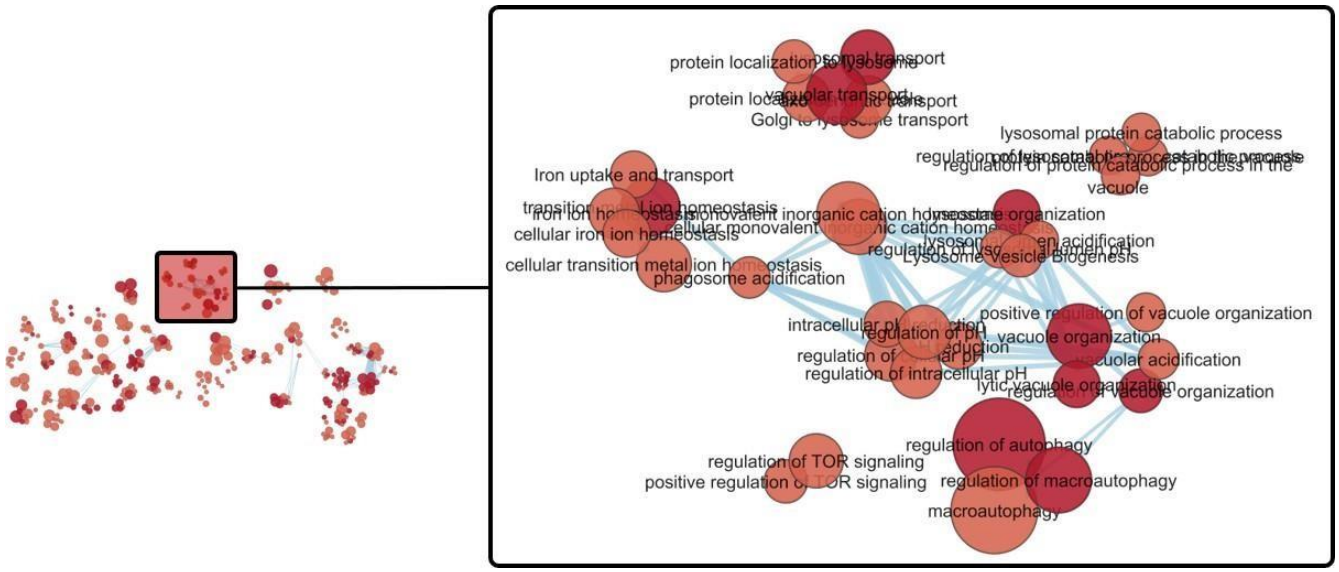

Figure 17: Enrichment map of upregulated proteins GSEA – Magnification of autophagy-related clusters. GSEA identified 9 clusters of biological processes directly or indirectly related to autophagy, accounting for 8% of all enriched biological processes in senescent NHDF.

5.4. Rapamycin and chloroquine modulate autophagy in WS1 fibroblasts

The mTOR inhibitor Rapamycin (Rap) was used as autophagy *activator*. With its ability to block the fusion lysosomes-autophagosomes, Chloroquine (Cq) was used as autophagy *inhibitor*. Wortmannin and siRNA targeting Atg5 and Atg7 as inhibitors of autophagosomes formation and maturation.

Autophagic activity was assessed in WS1 fibroblasts by two methods. First, levels of Microtubule-associated protein 1A/1B-light chain 3 (LC3), a central protein in the maturation of autophagosomes, were measured by Western blot analysis. LC3 exists in two forms; LC3 (cytosolic) and LC3ii (membrane bound). Upon autophagy activation, LC3i is converted into LC3ii, and the ratio LC3ii/LC3i reflects autophagic activity. Second, a fluorescent dye specific for autophagosomes and autolysosomes was used in a live cell setting to quantify autophagic vesicles (AV).

WS1 fibroblasts were treated with Rap, Cq, or a combination of both for 24 hours and were subsequently stained for AV. The nuclear counterstain Hoechst 33342 served for the normalization of AV to the number of cells. Rap-treated cells showed no significant difference compared to untreated cells, whereas Cq treatment led to a 7.2- fold increase. Cells treated with a combination of Rap and Cq showed a 9-fold increase in AV compared to untreated cells, which was significantly higher that Cq-treatment alone [Fig. 18a].

Levels of LC3 proteins in WS1 treated with Rap, Cq and a combination of both for 24 hours were assessed by Western blot analysis. Untreated- and DMSO-treated cells served as controls. Untreated cells showed expression of LC3i and LC3ii, indicating basal autophagic activity. DMSO- and Rap-treated cells showed no increase in LC3 turnover, whereas treatment with Cq or Rap+Cq led to increased abundance of LC3ii [Fig. 18b]. LC3ii abundance as well as LC3 ratio were higher for WS1 treated with a combination of Rap and Cq compared to cells treated with Cq only [Fig. 18b and 18c].

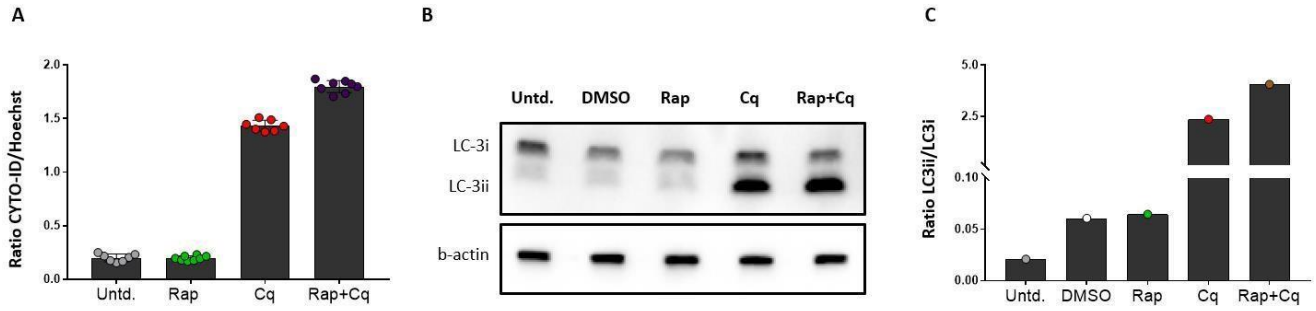

Figure 18: Measurement of autophagic activity in WS1 fibroblasts. WS1 were treated with Rap, Cq or with a combination of Rap and Cq for 24 hours. Autophagic activity was subsequently assessed by two methods. (**A**) quantification of autophagic vesicles using a fluorescent dye, normalized to cell number. (**B**) Western blot analysis of LC3i (cytosolic) and LC3ii (membrane bound) and (**C**) ratio LC3ii/LC3i expressed in a bar plot.

5.5. Stimulation of autophagy *prior* to SIPS induction delays the onset of senescence in WS1

To assess whether autophagy is responsible for the trigger of premature senescence in WS1 fibroblasts, autophagy was either stimulated using Rap or inhibited using CQ for 24 hours *prior* to Dox-mediated induction ofsenescence. Autophagy and SA-β-gal activity were monitored, as previously described [Sections 4.8 and 4.9], directly after autophagy modulation (D-1), directly after senescence induction (D0) and at different time points during the recovery time [Fig. 19]. Autophagy-untreated WS1 were used as control.

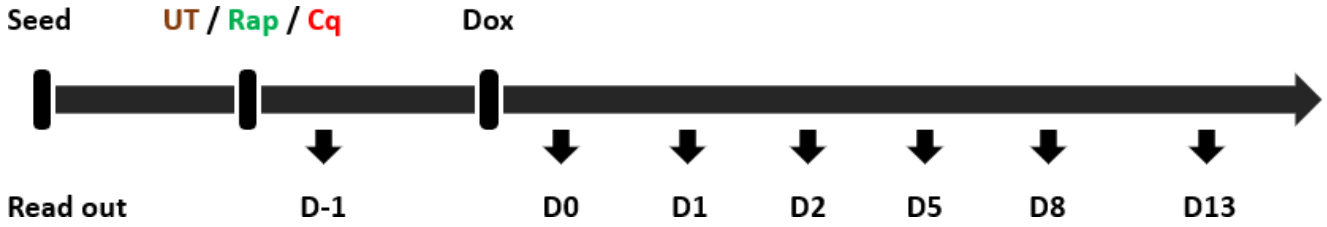

Figure 19: **Experimental design to evaluate the relevance of autophagy in triggering senescence in WS1 fibroblasts.** Autophagy was either left unmodulated (Untd.), stimulated (Rap) or inhibited (CQ) for 24 hours before induction of senescence (Dox). Following Dox treatment, WS1 were allowed to recover for 13 days. Autophagy and SA-β-gal activity were monitored at day -1, day 0 and days 1, 2, 5, 8 and 13 using methods previously described.

5.5.1. Inhibition of autophagy prior to senescence induction changes the autophagic profile during the development of senescence in WS1 fibroblasts

Autophagic activity was assessed by Western blot analysis of LC3i and LC3ii [Fig. 20].

Untreated cells showed basal level of autophagic activity, as both forms of LC3 were detected [Fig. 20a, D-1].

Following Dox treatment (D0), LC3ii was greatly increased compared to D-1, indicating increased autophagic

activity. 1 day after Dox treatment (D1), LC3i expression was decreased compared to D-1. Abundance of LC3ii gradually increased during the development of SIPS (D2- D13), suggesting that autophagic activity is increased in senescent WS1

Stimulation of autophagy through Rap slightly increased LC3ii abundance compared to untreated cells, indicating increased autophagy activity [Fig. 20b, D-1]. Directly after Dox-treatment (D0), both LC3 abundances were the same as in untreated cells. 1 day after Dox treatment (D1), LC3 abundances were similaras the one observed in untreated cells. During the development of SIPS (D2-D13), LC3 expression was similar compared to untreated cells.

Inhibition of autophagy through Cq led to an increase in LC3ii and a decrease in LC3i abundances compared to untreated cells [Fig. 20c, D-1], indicating inhibition of the autophagic flux. Directly after Dox treatment (D0), LC3ii expression was higher compared to untreated and Rap treated WS1. 1 day after Dox treatment (D1), expression of LC3i was slightly decreased compared to untreated and Rap treated cells. During the development of SIPS (D2-D13), expressions of LC3i and LC3ii were significantly decreased compared to untreated and Rap treated cells.

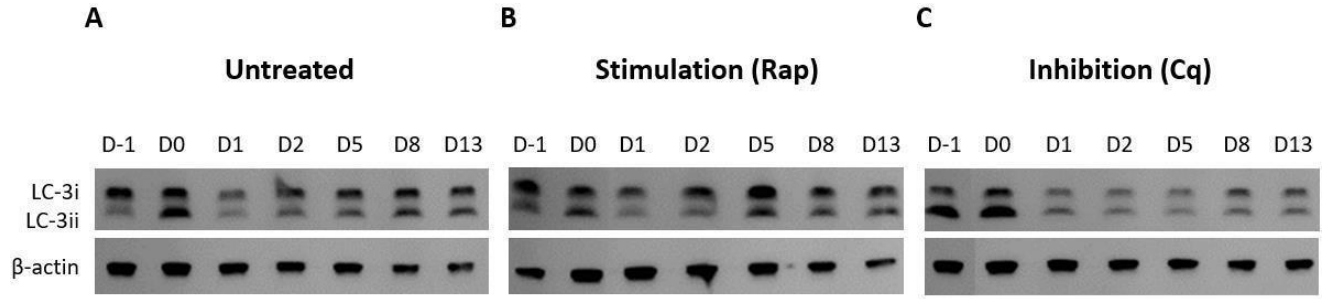

Figure 20: Western blot analysis of LC3i and LC3ii. Autophagy was either stimulated (Rap), inhibited (Cq) or left untreated (control) prior to senescence induction in WS1 fibroblasts. At different timepoints, 15 µg protein lysate were used to assess the expression of LC3i (cytosolic form) and LC3ii (autophagosomal form). β- actin served as loading control. Representative pictures of 3 biological replicates are shown.

To evaluate the autophagic flux, ratios LC3ii/LC3i [Fig. 20] were shown in a bar plot [Fig. 21].

Untreated cells showed basal autophagic activity [Fig. 21a, D-1]. LC3 ratio significantly increased following Dox treatment (D0). Although not statistically significant, LC3 ratio was higher 1 day after Dox treatment(D1), which is explained by the lower LC3i expression previously observed [Fig. 20a, D1]. During the development of SIPS (D2-D13), LC3 ratio gradually increased.

Stimulation of autophagy through Rap slightly increased the LC3 ratio at D-1, as LC3ii abundance was higher compared to untreated cells [Fig 20b, D-1]. Directly after Dox treatment (D0), LC3 ratio was significantly higher compared to D-1 [Fig. 21b, D0], but lower compared to untreated cells. During the development of SIPS (D2-D13), LC3 ratio increased over time in a similar fashion as observed in untreated cells.

Inhibition of autophagy through Cq significantly increased the LC3 ratio, as LC3ii expression was higher compared to other treatments [Fig. 21c, D-1]. Directly after Dox treatment (D0), LC3 ratio was higher compared to other treatments. Although not significant, LC3 ratio at D0 was decreased compared to D-1 [Fig. 21, D0]. During the development of SIPS, LC3 ratios were slightly higher as compared to other treatments. At day 13, LC3 ratio was not different from the one observed in other treatments.

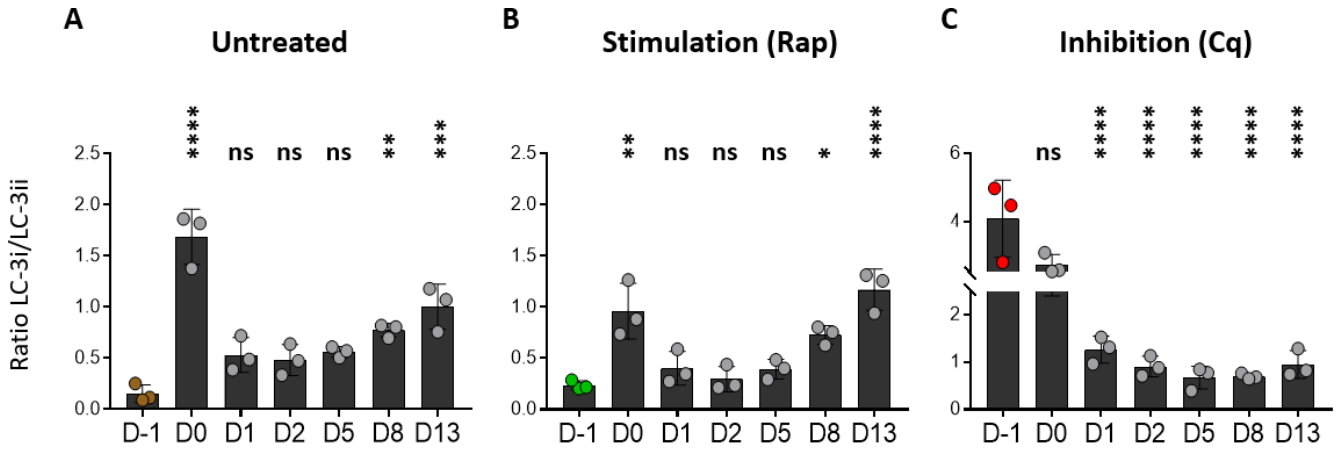

Comp.	Sig.?	Sum.	Adj. p
d-1 – d0	Yes	****	<0.0001
d0 - d1	Yes	****	<0.0001
d-1 – d1	No	ns	0.1371
d-1 – d13	Yes	***	0.0003

Comp.	Sig.?	Sum.	Adj. p
d-1 – d0	Yes	**	0.001
d0 - d1	Yes	*	0.0101
d-1 – d1	No	ns	0.8464
d-1 – d13	Yes	****	<0.0001

Comp.	Sig.?	Sum.	Adj. p
d-1 – d0	No	Ns	0.05
d0 - d1	Yes	*	0.0351
d-1 – d1	Yes	****	<0.0001
d-1 – d13	Yes	****	<0.0001

Figure 21: Ratio analysis of LC3i/LC3ii. Autophagy was either stimulated (Rap), inhibited (Cq) or left untreated (control) prior to senescence induction in WS1 fibroblasts. Values obtained from Western blots [Fig. 20] ofthree biological replicates. Means ± SEM are shown. Means compared using one-way ANOVA. Adjusted p-values of Turkey´s multiple comparisons tests: (****): <0.0001, (***):0.001, (**): <0.01, (*): <0.05 and (ns): not significant.

5.5.2. Early stimulation of autophagy decreases SA-β-gal activity during the development of senescence in WS1 fibroblasts

Senescence was measured at different time points by providing the SA-β-gal a fluorescent substrate [Fig. 22].In autophagy-untreated WS1, Dox-mediated induction of senescence (D0) resulted in a 1.5-fold increase in SA- β-gal activity compared to autophagy/senescence-untreated WS1. During the recovery time (D1-D13), levels of SA-β-gal activity remained significantly above the level of activity after 1 day of recovery time. D13. All comparisons and corresponding *p*-values can be found in appendix [Appendix 2a-2c, p. 106].

WS1 treated with Rap before the induction of senescence showed no significant increase in SA-β-gal activity after Dox-treatment, or after 2 and 8 days or recovery. After 1, 5 and 13 days of recovery, SA-β-gal activity was significantly higher compared to Dox-untreated cells.

WS1 treated with Cq before the induction of senescence showed a significant 1.9-fold increase in SA-β-gal activity compared to Dox-untreated WS1. After one day of recovery (D1), SA-β-gal activity increased significantly compared to day 0. During the recovery time (D2-D13), SA-β-gal activity remained significantly above the level of activity observed prior to senescence induction, but did not change significantly compared to day 1.

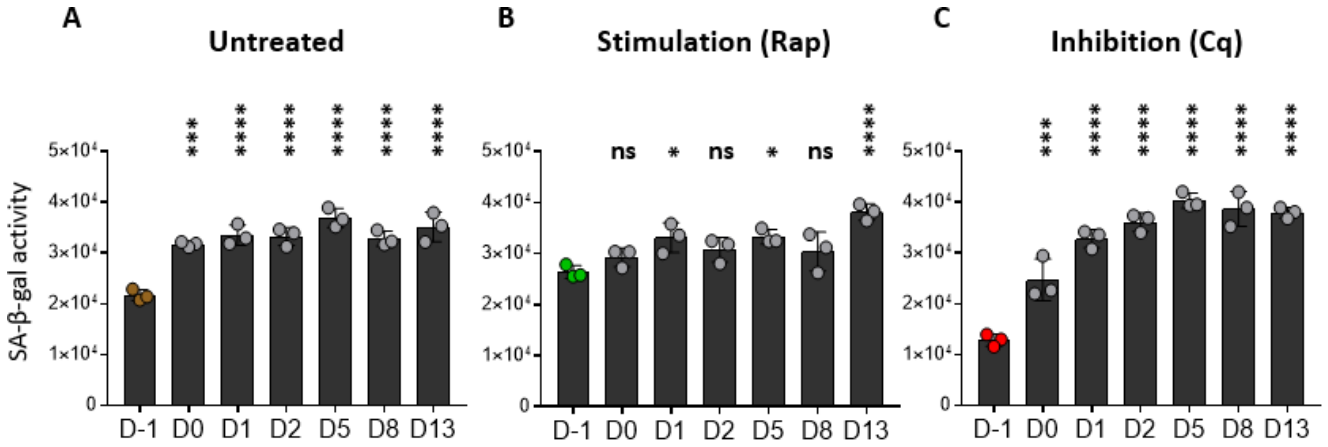

Comp.	Sig.?	Sum.	Adj. p
d-1 – d0	Yes	***	0.0001
d1 – d5	No	ns	0.2992
d5 – d13	No	ns	0.8844
d-1 – d13	Yes	****	<0.0001

Comp.	Sig.?	Sum.	Adj. p
d-1 – d0	No	ns	0.7313
d-1 – d8	No	ns	0.4002
d8 – d13	Yes	*	0.0166
d-1 – d5	Yes	*	<0.0358

Comp.	Sig.?	Sum.	Adj. p
d-1 – d0	No	ns	0.05
d0 - d1	Yes	*	0.0351
d-1 – d1	Yes	****	<0.0001
d-1 – d13	Yes	****	<0.0001

Figure 22: SA-β-galactosidase activity when autophagy was modulated prior to SIPS induction in WS1. Autophagy was either (**A**) left untreated, (**B**) stimulated or (**C**) inhibited prior to senescence induction in WS1 fibroblasts. At different timepoints, cellular senescence was measured using a fluorescent dye. Significances showed on the graph are in comparison with D-1. Values obtained from three biological replicates, each measured in triplicate (expression in Relative Fluorescent Units (RFU). Means ± SEM are shown. Means compared usingone-way ANOVA. Adjusted p-valuesof Turkey´s multiple comparisonstests: (****): <0.0001, (***):0.001, (**): <0.01, (*): <0.05 and (ns): not significant.

5.5.3. Early stimulation of autophagy decreases the number of SA-β-gal positive fibroblasts during the development of senescence

To validate SA-β-gal activity measurement, WS1 were stained for SA-β-gal activity [Fig. 23]. Independent of the treatment, WS1 developed a faint blue staining after one day of recovery (D1). After five days of recovery (D5), Rap-treated cells showed less intense staining compared to autophagy-untreated and Cq-treated cells.

WS1 treated with Cq before induction of senescence showed no visible difference compared to untreated cells at any time points. At day 13 (D13), all cells showed a similar senescent phenotype.

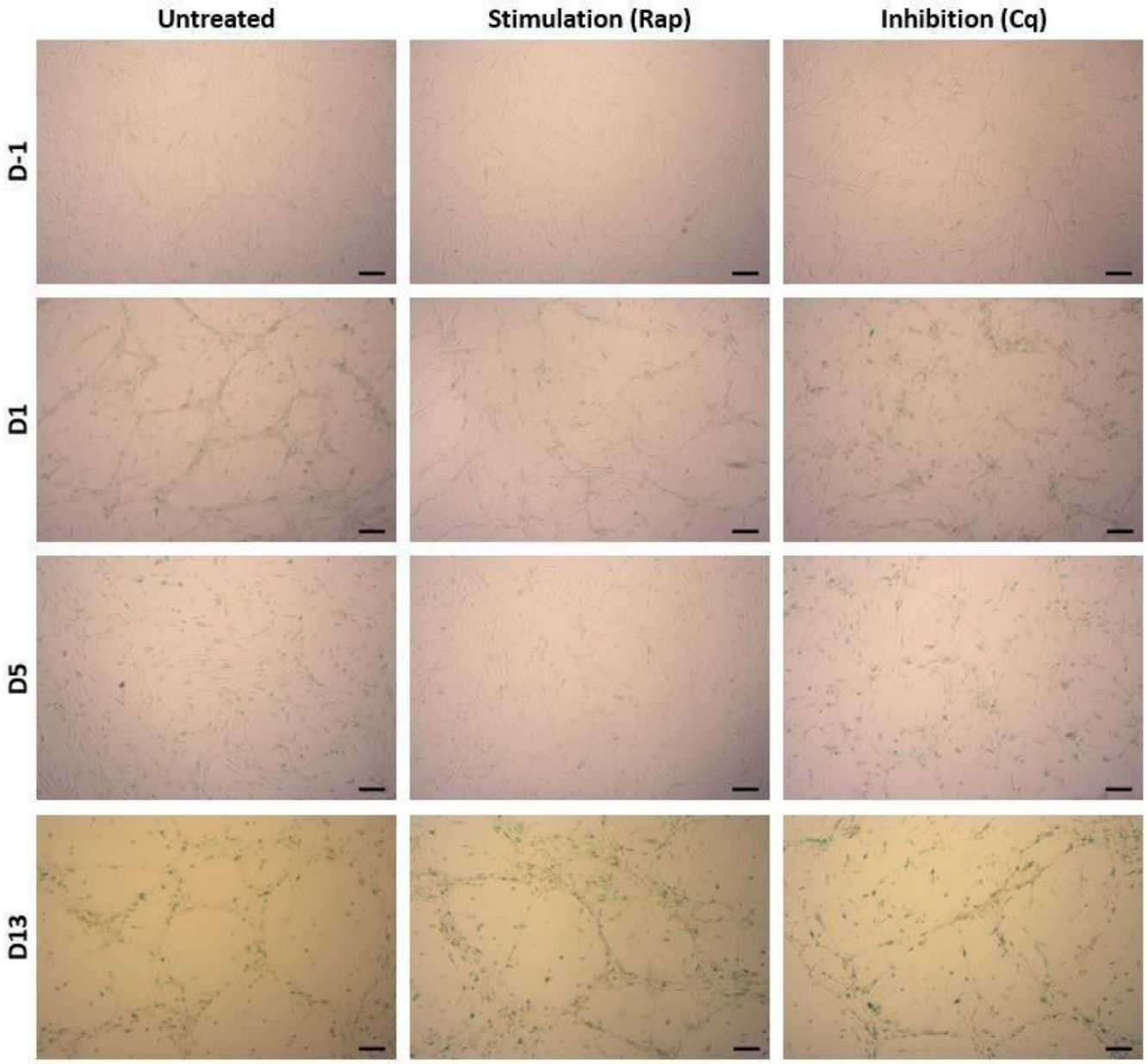

Figure 23: SA-β-galactosidase staining of WS1 when autophagy was modulated prior to SIPS induction. Autophagy was either stimulated (Rap), inhibited (Cq) or left untreated (control) prior to senescence induction in WS1 fibroblasts. At different timepoints, cells were stained for SA-β-gal activity. Blue staining indicates senescent cells. Representative figures from three biological replicates are shown. Scalebar: 100 µM.

5.6. Inhibition of autophagy *during* SIPS development lead to cell death in WS1

To assess whether autophagy is responsible for the development of premature senescence in WS1 fibroblasts, autophagy was either stimulated using Rap or inhibited using Cq for 24 hours *after* Dox-mediated induction of senescence. Autophagy and SA-β-gal activity were monitored before senescence induction (D-1), directly after (D0), and at different time points during the recovery time [Fig. 24]. Autophagy-untreated WS1 were used as control.

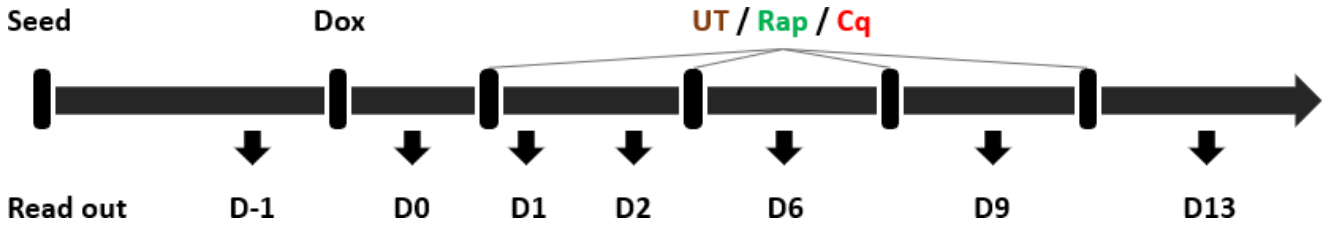

Figure 24: Experimental design to evaluate the relevance of autophagy during the development of senescence in WS1 fibroblasts. During the recovery time, autophagy was either left unmodulated (UT), stimulated (Rap) or inhibited (Cq) for 24 hours. Following Dox treatment, WS1 were allowed to recover for 13 days. Autophagy and SA-β-gal activity were monitored at day -1, day 0 and days 1, 2, 6, 9 and 13 using methods previously described.

5.6.1. Autophagy inhibition during the development of senescence increases LC3ii in WS1

Autophagic activity was assessed by Western blot analysis of LC3i and LC3ii [Fig. 25].

Untreated cells showed basal level of autophagic activity, as both forms of LC3 were detected [Fig. 25a, D-1]. Following Dox treatment (D0), LC3ii was greatly increased compared to D-1, indicating increased autophagic activity. After 1 and 2 days following Dox treatment (D1 and D2), LC3i expression were significantly decreased compared to D-1. During the development of SIPS (D6-D13), LC3i and LC3ii expression increases compared to D1 and D2.

Directly after Dox-treatment [Fig. 25b, D0], LC3ii expression was increased compared to untreated WS1 (D-1), indicating that Dox treatment increases autophagy as previously observed [Section 5.6]. 1 day after Dox treatment (D1), LC3i expression was lower compared to untreated cells. 2 days after Dox treatment (D2), expressions of both LC3i and LC3ii were the same as observed in untreated WS1. During the development of SIPS (D6-D13), expression of LC3ii gradually increased.

Unexpectedly, both LC3i and LC3ii expression where lower at D-1 and D0 compared to untreated and Rap treated WS1 [Fig. 25c, D-1 and D0]. 1 day after Dox treatment (D1), LC3ii expression was significantly higher compared to the one observed in untreated and Rap treated cells. During the development of SIPS (D2-D13), expression of LC3 did not change over time, and expression of LC3ii was significantly higher as observed in theother treatments.

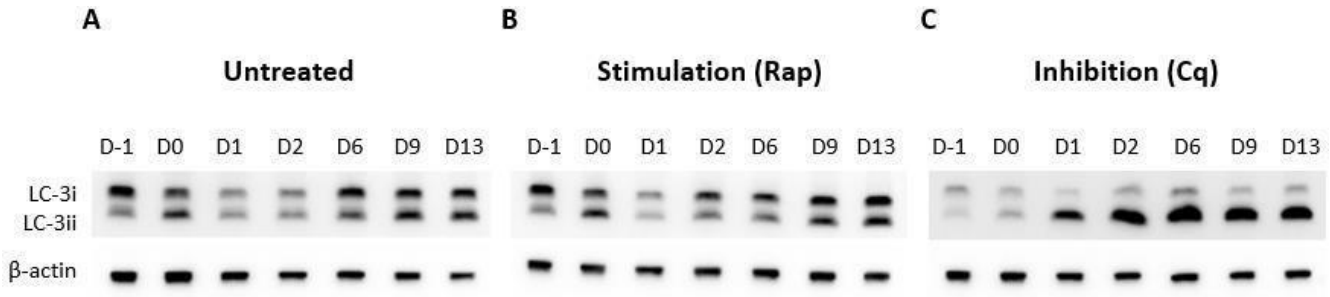

Figure 25: Western blot analysis of LC3i and LC3ii. Autophagy was either stimulated (Rap), inhibited (Cq) or left untreated (control) after senescence induction in WS1 fibroblasts. At different timepoints, 15 µg protein lysate were used to assess the expression of LC3i (cytosolic form) and LC3ii (autophagosomal form). B-actin served as loading control. Representative pictures of 3 biological replicates are shown

To evaluate the autophagic flux, ratios LC3ii/LC3i [Fig. 25] were shown in a bar plot [Fig. 26].

Untreated cells showed basal autophagic activity [Fig. 16a, D-1]. LC3 ratio significantly increased following Dox treatment (D0). Although not significant, LC3 ratio 1 day after Dox treatment (D1) was lower comparedto D0. Between day 2 and day 6, LC3 ratio did not change compared to day 1, but was significantly increased at day 9 and 13.

Stimulation of autophagy through Rap led to a similar trend in LC3 ratios compared to untreated cells [Fig.26b]; directly after Dox treatment (D0), LC3 ratio was significantly higher compared to before Dox treatment (D-1). 1 day after Dox treatment (D1), LC3 ratio was significantly lower compared to D0 and, although not significant, tend to increase during the development of SIPS (D2-D13).

Inhibition of autophagy through Cq significantly increased LC3 ratios compared to cells before Dox treatment and directly after [Fig. 26c]. This ratio were approximatively 10-fold increases compared to untreated [Fig. 26a] and Rap treated WS1 [Fig. 26b].

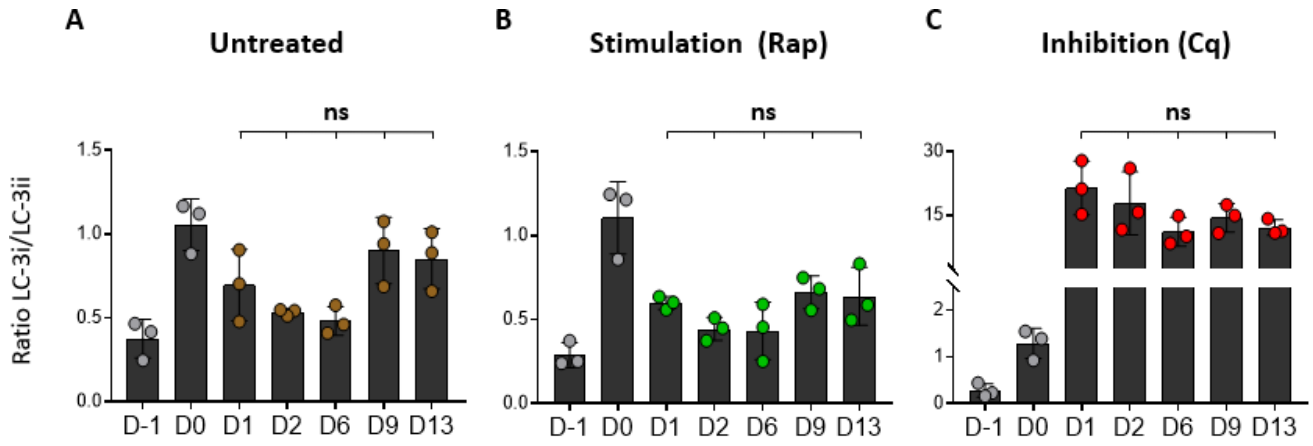

Comp.	Sig.?	Sum.	Adj. p
d-1 – d0	Yes	**	0.0012
d0 - d1	No	ns	0.1185
d-1 – d1	No	ns	0.2049
d-1 – d13	Yes	*	0.023

Comp.	Sig.?	Sum.	Adj. p
d-1 – d0	Yes	****	<0.0001
d0 - d1	Yes	**	0.0056
d-1 – d1	No	ns	0.1364
d-1 – d13	No	ns	0.0736

Comp.	Sig.?	Sum.	Adj. p
d-1 – d0	No	ns	>0.9999
d0 - d1	Yes	***	0.0006
d-1 – d1	Yes	***	0.0004
d-1 – d13	Yes	*	0.0454

Figure 26: **LC3i/LC3ii ratio analysis when autophagy was modulated during the development of SIPS in WS1.** Autophagy was either stimulated (Rap), inhibited (Cq) or left untreated (control) after senescence inductionin WS1 fibroblasts. Values obtained from Western blots [Fig. 25] ofthree biological replicates. Means ± SEM are shown. Means compared using one-way ANOVA. Adjusted p-values of Turkey´s multiple comparisons tests: (****): <0.0001, (***):0.001, (**): <0.01, (*): <0.05 and (ns): not significant.

5.6.2. Inhibition of autophagy during the development of senescence decreases SA-β-gal activity in WS1 fibroblasts

For each treatment, SA-β-gal activity means were compared using one-way ANOVA [Fig. 27]. As previously observed [Fig. 22a], Dox-mediated induction of senescence significantly increased SA-β-gal activity (D0) for untreated and Cq-treated WS1, but not in Rap-treated cells.

Autophagy-untreated WS1 show a significant increase in SA-β-gal activity during the recovery time (D1-D13) compared to untreated cells (D-1). During the recovery time, SA-β-gal activities at different time points were not significantly different, except for D13 [Fig. 27a]. All comparisons and corresponding *p*-values can be found in appendix [Appendix 3a-3c, p. 109].

WS1 treated with Rap after induction of senescence SA- β-gal activity was not different from untreated cells until day 6 (D6). Between day 6 and 13 (D6-D13), SA- β-gal activity was significantly higher as compared to untreated cells [Fig. 27b].

Cq-treated WS1 had significantly higher SA- β-gal activity after induction of senescence (D0). After 6 days of recovery time (D6), SA- β-gal activity was significantly lower as compared to untreated cells (D-1). Between day 6 and day 13 (D6-D13), SA- β-gal activity increased and was significantly higher compared to untreated cells at day 13 (D13) [Fig. 27c].

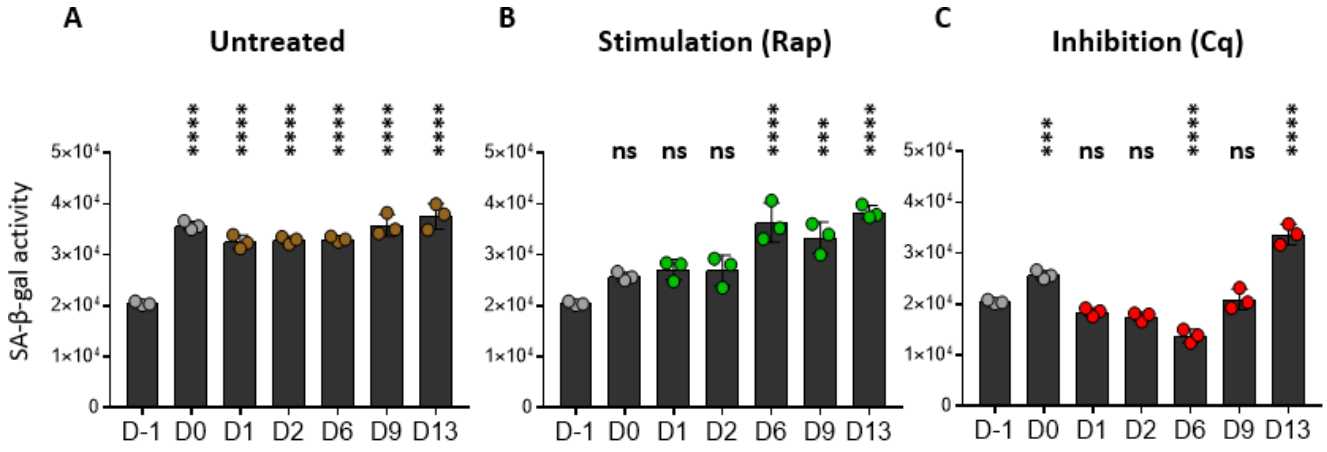

Comp.	Sig.?	Sum.	Adj. p
d-1 – d0	Yes	****	<0.0001
d0 - d1	No	ns	0.1491
d-1 – d1	Yes	****	<0.0001
d-1 – d13	Yes	****	<0.0001

Comp.	Sig.?	Sum.	Adj. p
d-1 – d0	No	ns	0.1655
d0 - d1	No	ns	0.9908
d-1 – d1	No	ns	0.0507
d-1 – d13	Yes	****	<0.0001

Comp.	Sig.?	Sum.	Adj. p
d-1 – d0	Yes	**	0.0035
d0 - d1	Yes	***	0.0002
d-1 – d1	No	ns	0.5550
d-1 – d13	Yes	****	<0.0001

Figure 27: SA-β-galactosidase activity when autophagy was modulated during the development of SIPS in WS1. Autophagy was either (**A**) left untreated, (**B**) stimulated or (**C**) inhibited after induction of senescence in WS1 fibroblasts. At different timepoints, cellular senescence was measured using a fluorescent dye. Significances showed on thegraph arein comparison with D-1. Values obtained from three biological replicates, each measured in triplicate (expression in Relative Fluorescent Units (RFU). Means ± SEM are shown. Means compared using one-way ANOVA. Adjusted p-values of Turkey´s multiple comparisonstests: (****): <0.0001, (***):0.001, (**): <0.01, (*): <0.05 and (ns): not significant.

5.6.3. Inhibition of autophagy during the development of senescence leads to cell death in WS1 fibroblasts

Proliferating cells (D-1) showed faint staining in some cells. After Dox-treatment (D0), WS1 cells showed increased blue staining [Fig. 28]. Following senescence induction, WS1 were subsequently either left untreated for autophagy or treated with Rap (stimulation) or Cq (inhibition) for 13 days [Fig. 29].

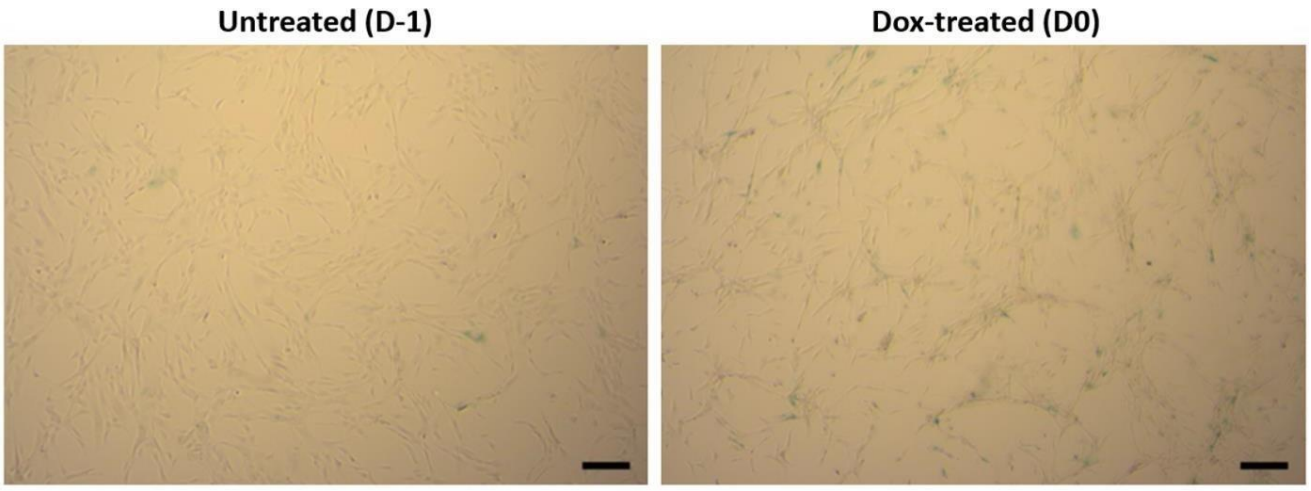

Figure 28: SA-β-galactosidase staining of untreated and Dox-treated WS1. SIPS was induced in WS1 fibroblasts using Dox. Directly after treatment (D0, right), WS1 were stained for SA-β-gal activity. Staining of untreated cellsserved as control (D-1, links). Blue stainingindicatessenescent cells. Representative figures from three biological replicates are shown. Scalebar: 100 µM.

After induction of senescence, autophagy-untreated cells showed SA-β-gal activity after two days (D2), which progressively increased until day 13 (D13). After 2 days of Rap-treatment, cells showed less staining as compared to untreated cells. After 6 days of Rap-treatment, no more difference could be observed between untreated and Rap-treated cells whereas after 13 days of Rap-treatment untreated WS1 showed deeper staining. After 2 days of Cq-treatment (D2), fewer SA-β-gal-positive WS1 were detected as compared to untreated cells. After six days of Cq treatment (D6), cell number was decreased and only some of the remaining cells showed a faint blue staining compared to untreated. After 16 days of Cq treatment almost no cells were left and few WS1 were SA-β-gal-positive.

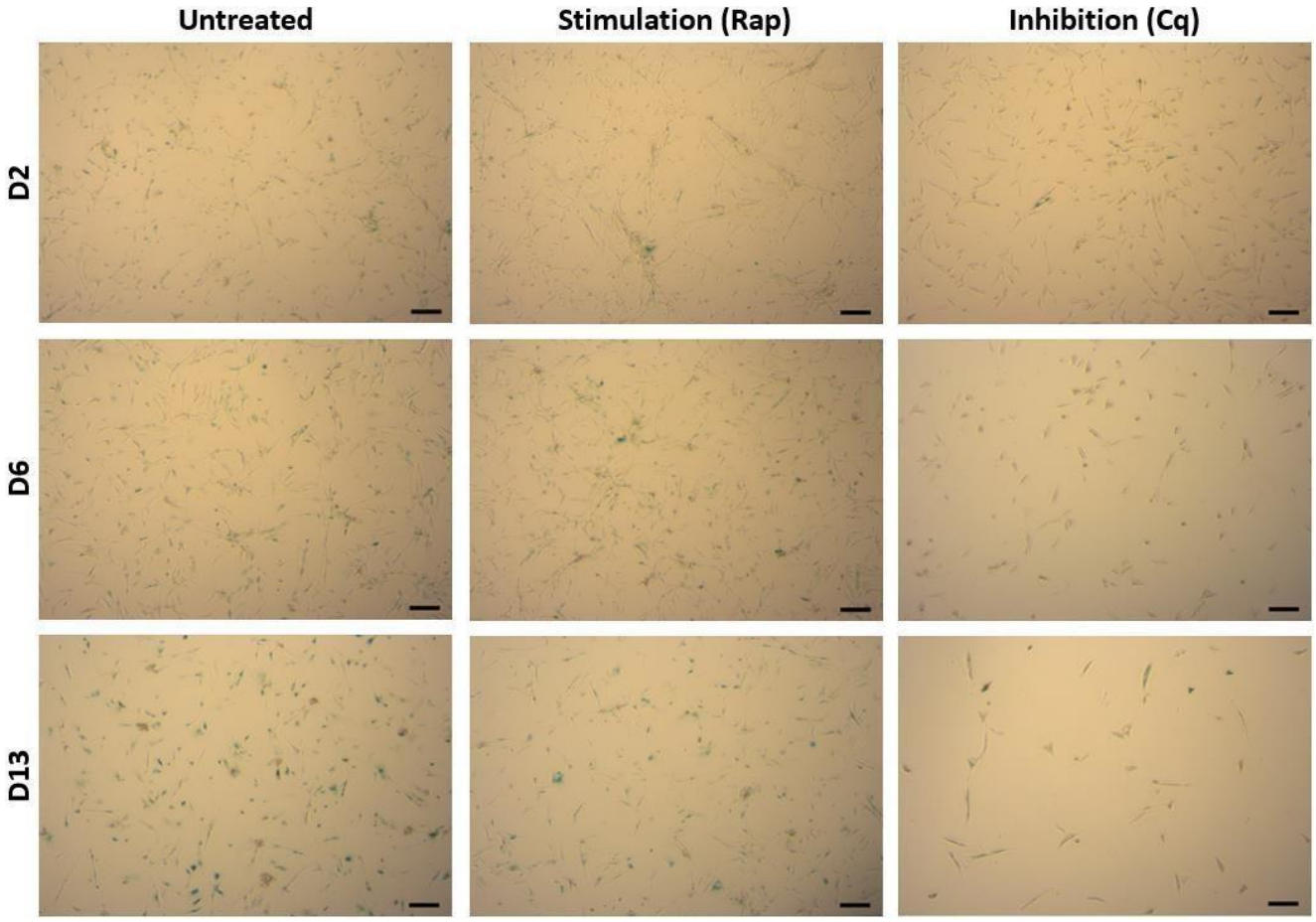

Figure 29: SA-β-galactosidase staining of WS1 when autophagy was modulated during the development of SIPS. Autophagy was either stimulated (Rap), inhibited (Cq) or left untreated (control) after induction of senescence in WS1 fibroblasts. At different timepoints, cells were stained for SA-β-gal activity. Blue staining indicates senescent cells. Representative figures from three biological replicates are shown. Scalebar: 100 µM.

5.7. Inhibition of autophagy *in* senescent WS1 leads to cell death

To assess whether autophagy is relevant for the phenotype of senescence, autophagy was either left untreated, or stimulated using Rap or inhibited using Cq for 24 hours *in* senescent WS1. Autophagy and SA-β-gal activity were monitored before senescence induction (D-1), after 14 days of recovery time (D14), and after 15 (D15) and 22 days [Fig. 30].

Figure 30: Experimental design to evaluate the relevance of autophagy in senescent WS1. Senescence was induced in WS1 and cells were allowed to recover for 14 days. Autophagy was either left untreated (UT), stimulated (Rap) or inhibited (Cq) for 24 hours in senescent WS1. SA-β-gal activity, autophagic activity and cell viability were monitored at day -1, day 14, 15 and 22 using methods previously described.

5.7.1. Measurement of autophagic activity

For representation purpose, LC3 ratios of untreated (D-1) and senescent cells (D14) were used for all treatment in Figure 31a. As previously observed [Section 5.6], untreated cells displayed basal autophagic activity, as both LC3i and LC3ii were detected [Fig. 31a and 31c, D-1]. As previously observed, autophagic activity is increased 14 days after Dox treatment, as expression of LC3i is decreased, and expression of LC3ii increased compared tountreated cells. [Fig. 31a and 31b, D14].

Unexpectedly, expression of LC3ii was slightly decreased at D15 and D22 compared to D14 [Fig. 31a], resulting in a smaller LC3 ratio [Fig. 31b].

Stimulation of autophagy through Rap decreased LC3i expression at D15 and D22, lowering corresponding LC3 ratios [Fig. 31b], suggesting an increased autophagic activity.

Inhibition of autophagy through Cq gradually increased LC3ii expression (D15 and D22), significantly increasing corresponding ratios [Fig. 31b] and suggesting an accumulation of autophagic vesicles.

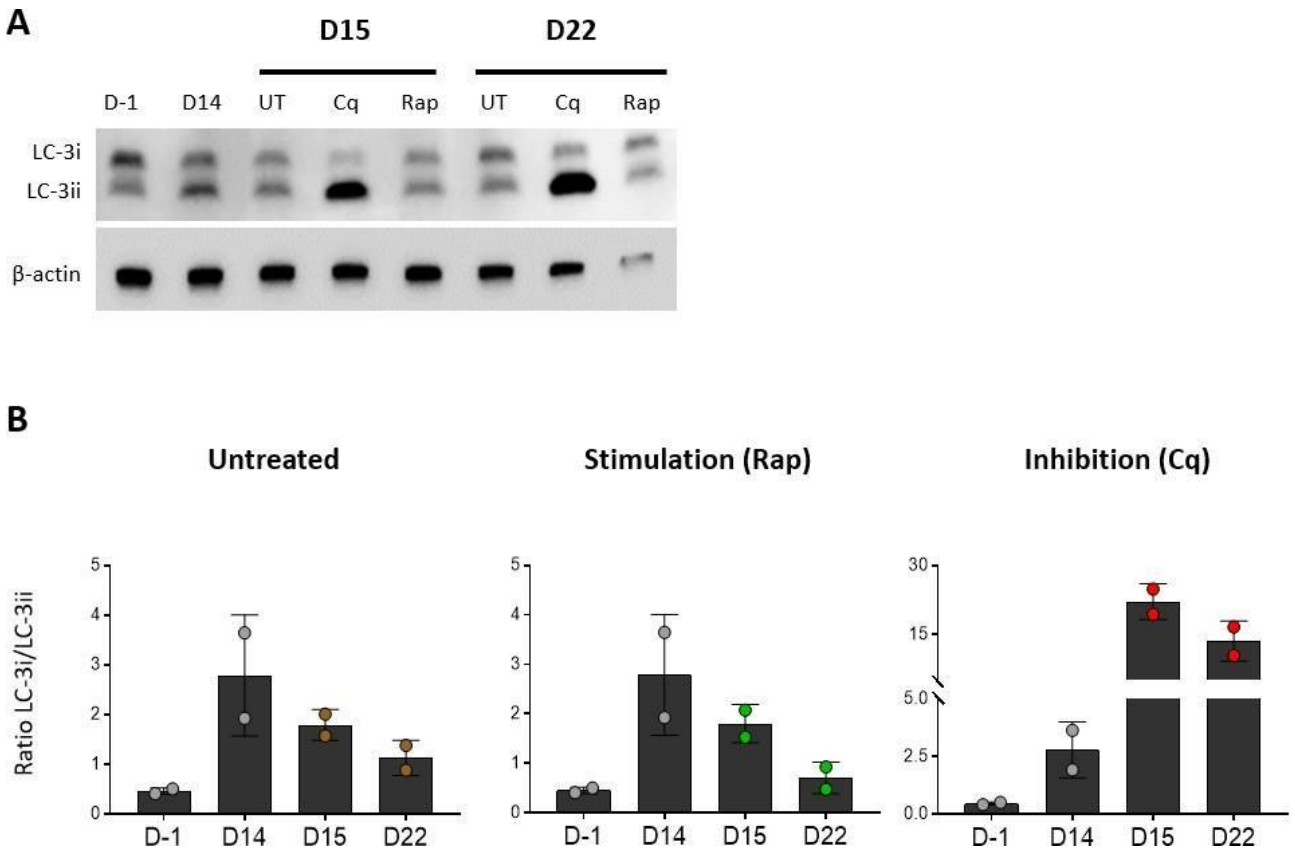

Figure 31: LC3i/LC3ii ratio analysis when autophagy was modulated in senescent WS1. LC3ii/LC3i ratios were measured in non-senescent WS1 (D-1), in senescent WS1 (D14) and in senescent WS1 where autophagy was modulated for 1 day (D15) and 7 days (D22). (**A**) Western Blotof LC3. 10 µglysate from different time points were used. B-actin served as loading control. Representative figure from 2 biological replicates is shown. (**B**) Ratio of LC3ii and LC3i abundance. Same data for non-senescent (D-1) and senescent (D14) are depicted three times. Means ± SEM are shown

5.7.2. Measurement of SA-β-gal activity

After 2 weeks of recovery, senescent WS1 showed a 2.6-fold increase in SA-β-gal activity compared to non-senescent WS1 [Fig. 32, D14], which remained constant after 1 week of treatment (D22).

Rap-treatment showed a similar trend compared to untreated cells, whereas Cq treatment led to a decrease in SA-β-gal activity after 1 (D15) and 7 (D22) autophagy inhibition [Fig. 32b and 32c]. Corresponding SA-β-gal staining can be found in appendix [Appendix 4, p. 112].

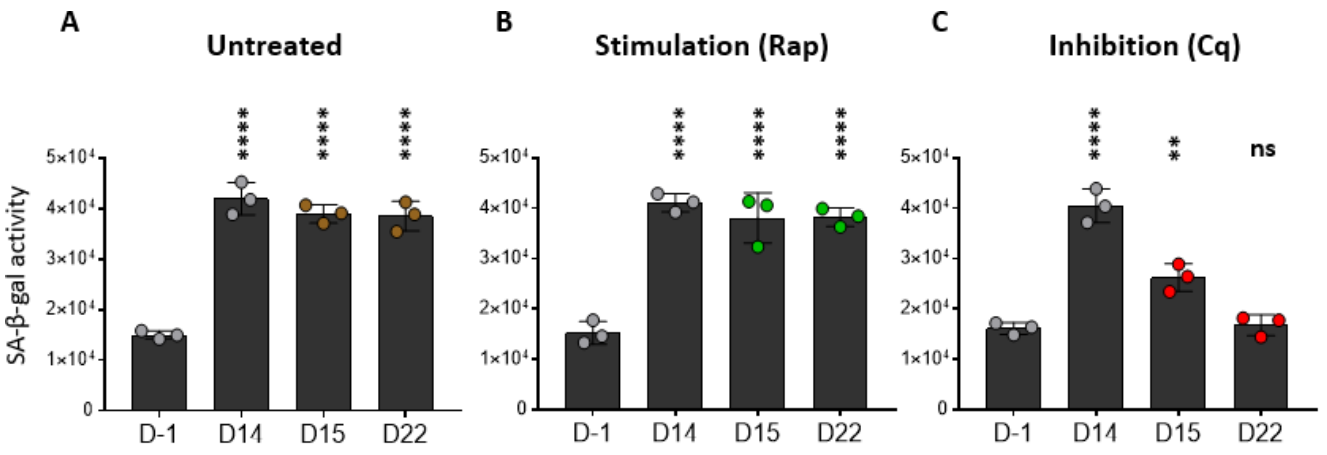

Comp.	Sig.?	Sum.	Adj. p
D14 – D15	No	ns	0.4546
D14 – D21	No	ns	0.354
D15 – D21	No	ns	0.9962

Comp.	Sig.?	Sum.	Adj. p
D14 – D15	No	ns	0.6335
D14 – D21	No	ns	0.6613
D15 – D21	No	ns	>0.9999

Comp.	Sig.?	Sum.	Adj. p
D14 – D15	Yes	***	0.0005
D14 – D21	Yes	****	<0.0001
D15 – D21	Yes	**	0.0067

Figure 32: SA-β-galactosidase activity when autophagy was modulated in senescent WS1. Autophagy was either stimulated (Rap), inhibited (Cq) or left untreated (control) in senescent WS1 fibroblasts. After 1 day (D15) and 7 days (D22) of treatment, cellular senescence was measured using a fluorescent dye. Significances shown on thegraph are in comparison with D-1. Values obtained from three biological replicates, each measuredin triplicate (expression in Relative Fluorescent Units (RFU). Means ± SEM are shown. Means compared using one-way ANOVA. Adjusted p-values of Turkey´s multiple comparisons tests: (****): <0.0001, (***):0.001, (**): <0.01, (*): <0.05 and (ns): not significant.

5.7.3. Inhibition of autophagy in senescent WS1 decreases viability

Cell viability can be determined by measuring the release of ATP in the culture medium using a luciferase-based assay (see section 4.14). To assess whether modulation of autophagy in senescent WS1 fibroblasts has cytotoxic effects, an ATP assay was performed in senescent WS1 after 3-, 6- and 9-days of autophagy modulation [Fig. 33]. When autophagy was left unmodified, senescent WS1 showed a significant decrease in viability after 6 days in culture compared to 3 days. After 9 days in culture, viability stabilized and was not different compared to 6. Similar trend was observed when autophagy was stimulated in senescent WS1.

When autophagy was inhibited, viability of senescent WS1 also decreased after 6 days treatment. After 9 days of inhibition, viability was significantly lower as compared to days 3 and 6.

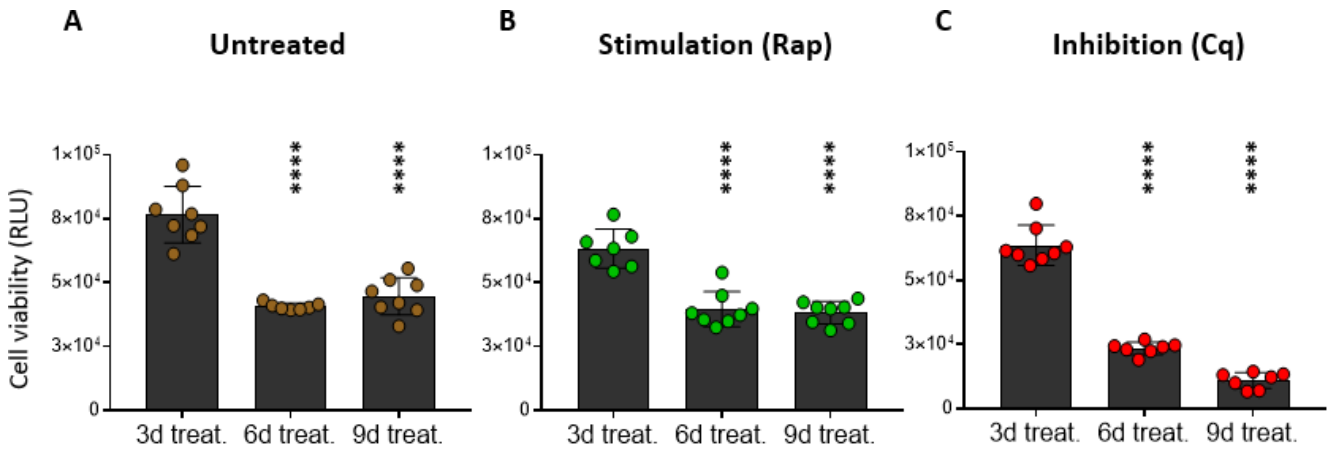

Comp.	Sig.?	Sum.	Adj. p
D3 – D6	Yes	****	<0.0001
D3 – D9	Yes	****	<0.0001
D6 – D9	No	ns	0.6009

Comp.	Sig.?	Sum.	Adj. p
D3 – D6	Yes	****	<0.0001
D3 – D9	Yes	****	<0.0001
D6 – D9	No	ns	0.9095

Comp.	Sig.?	Sum.	Adj. p
D3 – D6	Yes	****	<0.0001
D3 – D9	Yes	****	<0.0001
D6 – D9	Yes	***	0.0007

Figure 33: Senescent WS1 viability following autophagy modulation in senescent WS1. Autophagy was either left untreated, or stimulated (Rap) or inhibited (Cq) for 3-, 6-, and 9-days in senescent WS1. Cell viability measured using ATP assay (expression in Relative Luminescence Units). Values obtained from 8 biological. Means ± SEM are shown. Means compared using one-way ANOVA. Adjusted p-values of Turkey´s multiple comparisons tests: (****): <0.0001, (***):0.001, (**): <0.01, (*): <0.05 and (ns): not significant.

5.8. Inhibition of autophagy in senescent Normal Human Dermal Fibroblasts decreases cell viability

Results obtained in sections 5.6 and 5.7 suggest that inhibition of autophagy induces cell death in senescent WS1 fibroblasts. Because Cq blocks the fusion between autophagosomes with lysosomes, it was hypothesized that cells die due to an over-accumulation of autophagosomes. To test this hypothesis, autophagy was blocked in senescent Normal Human Dermal Fibroblasts (NHDF) by inhibiting the maturation of autophagosomes. Senescent NHDF were treated with Wortmannin (Wort), Cq, siRNA targeting Atg5 and 7 and siRNA in a combination with Cq. Treatments were applied for 3-, 6- and 9-days and cell viability assessed using ATP assays [Fig. 34a and 34b].

After 3 days of treatment, all autophagy inhibitors significantly decreased the viability of NHDF compared to untreated cells. Cell viability kept decreasing over time. After 9 days of treatment, inhibition of autophagy induced death of almost all senescent NHDF. All comparisons among treatments can be found in appendix [Appendix 5a-5c]. Decreased viability of senescent NHDF was further validated by counting the number of floating cells (dead cells) in culture medium [Appendix 5d].

A

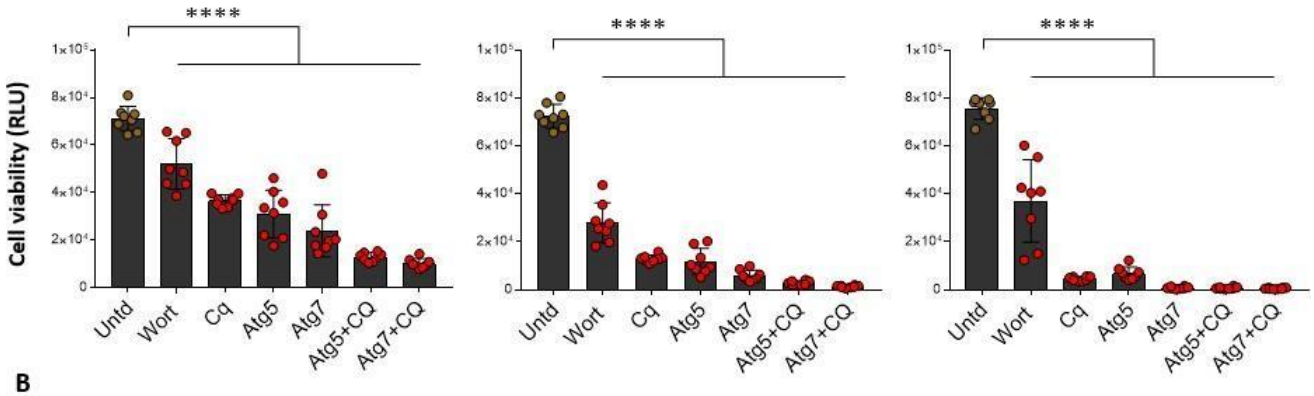

B

Untreated VS...	% decrease
Wort	-26%
Cq	-49%
siRNA Atg5	-56%
siRNA Atg7	-66%
siRNA Atg5 + Cq	-81%
siRNA Atg7 + Cq	-85%

Untreated VS...	% decrease
Wort	-61%
Cq	-82%
siRNA Atg5	-84%
siRNA Atg7	-92%
siRNA Atg5 + Cq	-96%
siRNA Atg7 + Cq	-98%

Untreated VS...	% decrease
Wort	-50%
Cq	-94%
siRNA Atg5	-91%
siRNA Atg7	-99%
siRNA Atg5 + Cq	-99%
siRNA Atg7 + Cq	-99%

Figure 34: Viability following inhibition of autophagy in NHDF. Autophagy was inhibited in senescent NHDF using Wort, Cq, siRNA targeting Atg5/Atg7 and in a combination with Cq for 3-, 6- and 9-days. (**A**) Cell viability measured using ATP assay (expression in Relative Luminescence Units). Values obtained from 8 biological. Significances shown on the graph are in comparison with untreated NHDF. Means ± SEM are shown.Means compared using one-way ANOVA. Adjusted p-values of Turkey´s multiple comparisons tests: (****): <0.0001. (**B**) Cell viability decrease for each treatment, expressed as percentage compared to untreated NHDF.

5.9. Modulation of autophagy using carbohydrates

10 sugars and sugars derivatives [Fig. 35] were tested for their ability to modulate autophagy in skin fibroblasts by measuring LC3 ratios and number of autophagic vesicules (AV). To further assess whether the modulation of autophagy was mTOR-dependent or independent, Western blot of key phosphorlyation sites of mTOR, Raptor and Rictor were performed.

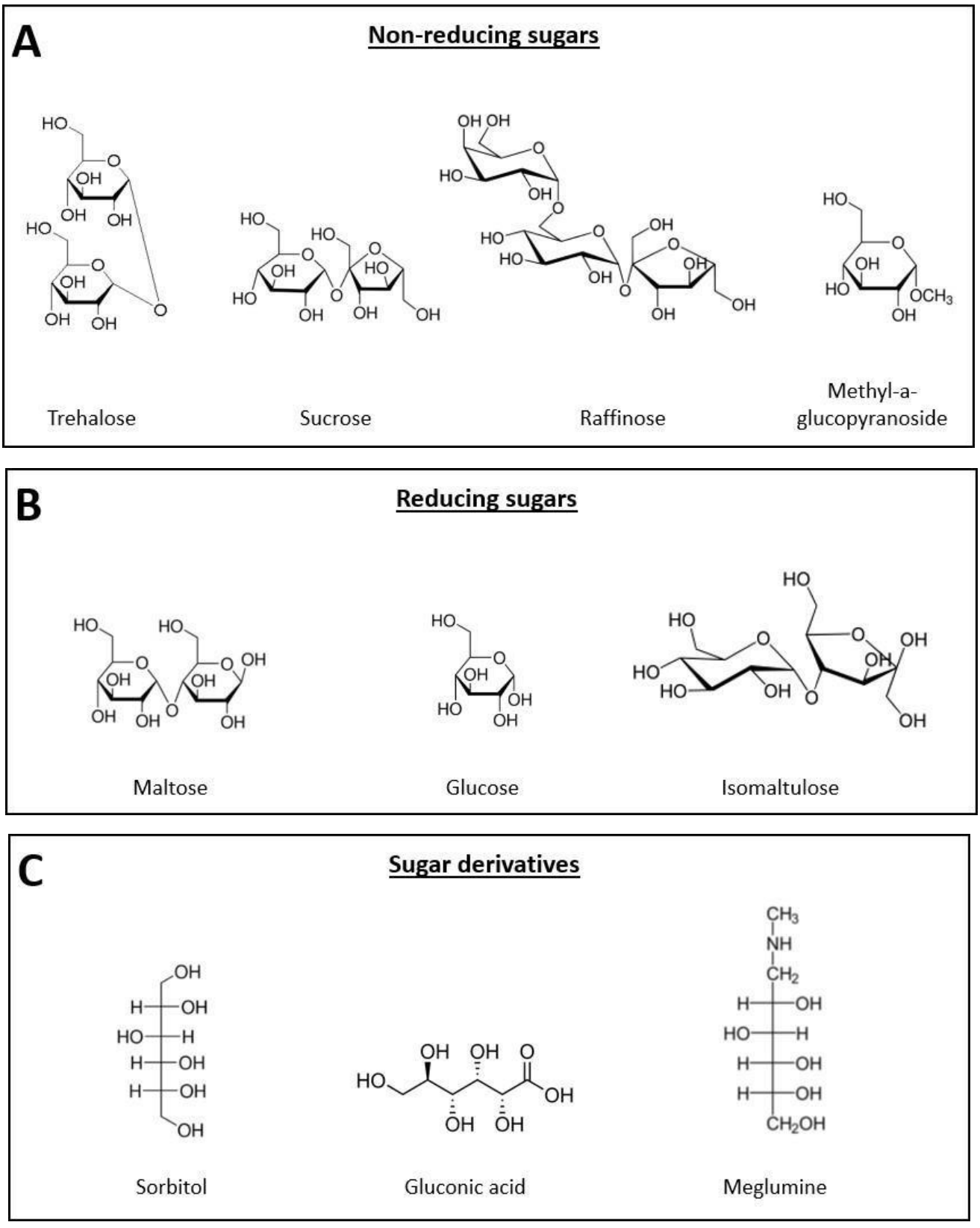

Figure 35: Haworth projection of sugar structures used to modulate autophagy. (**A**) non-reducing sugars (trehalose, sucrose, raffinose and methyl-a-glucopyranoside), (**B**) reducing sugars (maltose, glucose and isomaltulose) and (**C**) sugars derivatives (sorbitol, gluconic acid and meglumine).

5.9.1. Quantification of autophagic vesicles in WS1 treated with non-reducing sugars

WS1 fibroblasts were treated with 50 mM, 100 mM and 200 mM sugars in presence or absence of Cq for 24 hours. Impact on autophagy was assessed using a fluorescent dye specifically staining A). Units expressed as ratio CYTO-ID/Hoechst. Untreated WS1 (Untd.), as well as Rap-, Cq- and Rap+Cq-treated cells served as control.

All non-reducing sugars tested for their ability to modulate autophagy increased AV number in a dose- dependent manner [Fig. 36].

When treated with trehalose, WS1 showed a significant 5-fold (50 mM) and 6.7-fold (100 mM) increase in AV as compared to untreated cells, whereas 200 mM had cytotoxic effects (data not shown) [Fig. 36a].

Sucrose treatment induced a significant 4.3-fold (50 mM), 6.2-fold (100 mM) or 7.6-fold increase of AV compared to untreated WS1 [Fig. 36b].

Raffinose treatment induced a significant 4.8-fold (50 mM), 6.8-fold (100 mM) or 8.9-fold increase of AV compared to untreated WS1 [Fig. 36c].

Treatment with 50 mM and 100 mM methyl-α-glucopyranoside did not impact the amount of AV compared to untreated cells. When WS1 were treated with 200 mM methyl-α-glucopyranoside, number of AV was 2.8-fold increased compared to untreated cells [Fig. 36d].

Treatment with sugars in the presence of Cq resulted in significant increases in AV compared to WS1 treated with Cq only for sucrose (100 mM and 200 mM), raffinose (100 mM and 200 mM) and methyl-α- glucopyranoside (100 mM and 200 mM).

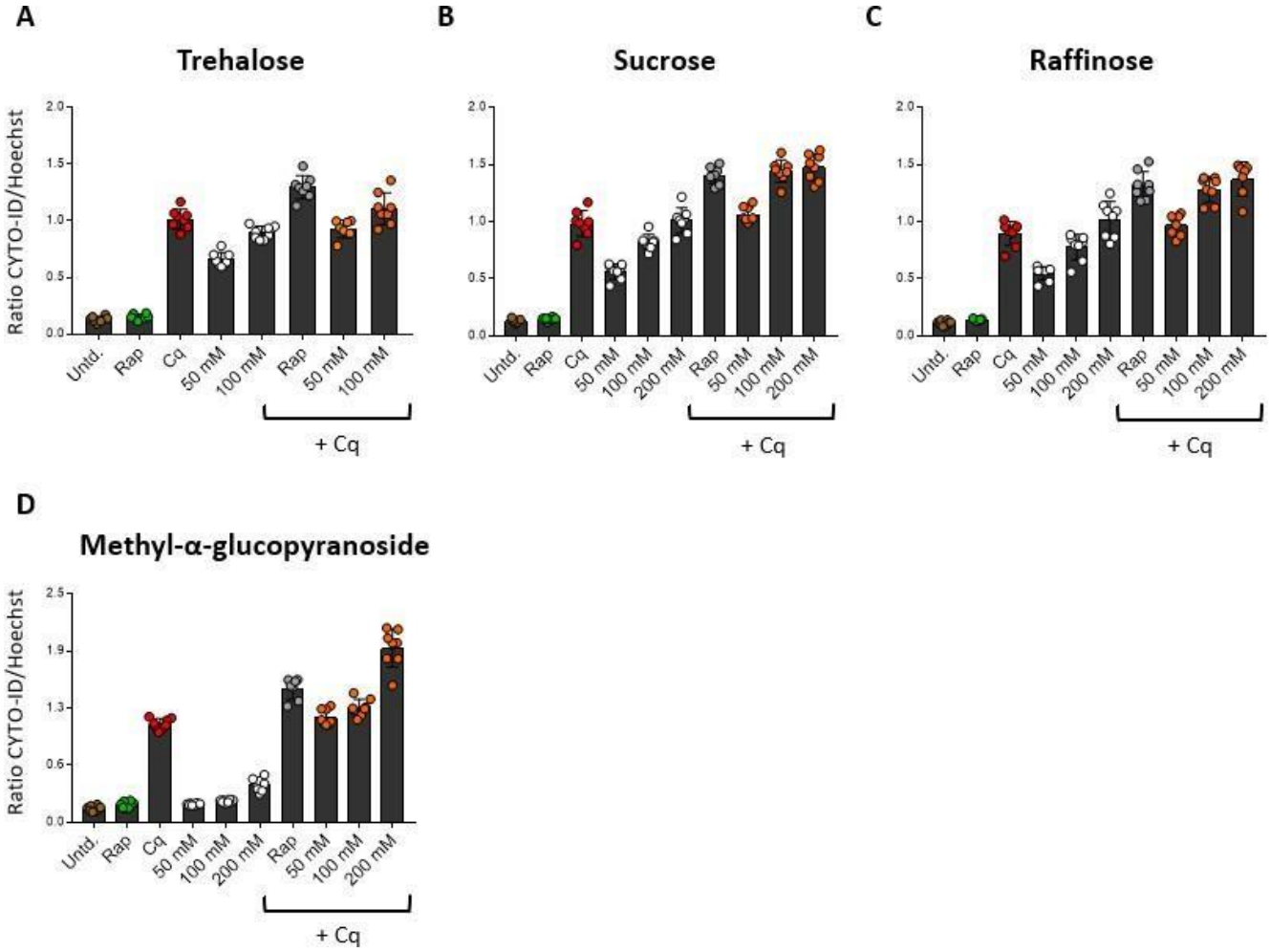

Figure 36: Quantification of autophagic vesicles in WS1 fibroblasts treated with non-reducing sugars. WS1 were treated with indicated concentration of (**A**) trehalose, (**B**) sucrose, (**C**) raffinose and (**D**) methyl-α-glucopyranoside in absence or presence of Cq. Untreated (Untd.), Rap-, Cq- and Rap+Cq-treated cells served as control. Level of autophagy was assessed by measuring the number of autophagic vesicle (see section 4.11). Ratios of fluorescent signals of CYTO-ID (autophagic vesicles) and Hoechst (nuclear dye) in WS1 after 24h treatment are shown. Values were obtained from n ≥ 7 biological replicates. Means ± SEM are shown. Adjusted *p*-values of Tukey's multiple comparison test: (****): < 0.0001, (**): < 0.01, (ns): not significant.

5.9.2. Quantification of autophagic vesicles in WS1 treated with reducing sugars

Reducing sugars tested in the scope of this work showed variable effects on autophagy in WS1 [Fig. 27]. Tested at different concentrations, maltose and glucose had no effect of AV levels in WS1 compared to untreated cells. Levels of AV were not different from Cq-treated cells when maltose and glucose were combined with Cq. Treatment of WS1 with isomaltulose resulted in a significant 2.3-fold (50 mM), 3.9-fold (100 mM) and 5.7-fold (200 mM) increase in AV compared to untreated. In combination with Cq, isomaltulose showed increased AV levels as compared to Cq only.

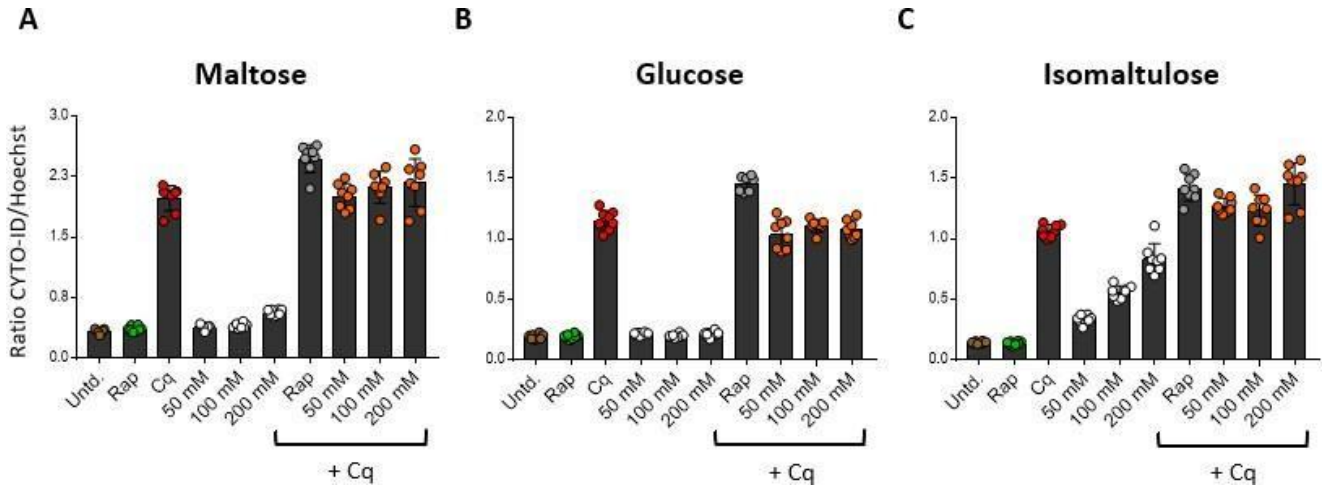

Figure 37: Quantification of autophagic vesicles in WS1 fibroblasts treated with reducing sugars. WS1 were treated with indicated concentration of (**A**) maltose, (**B**) glucose and (**C**) isomaltulose, in presence or absence of Cq. Untreated (Untd.), Rap-, Cq- and Rap+Cq-treated cells served as control. Level of autophagy was assessed by measuring the number of autophagic vesicle (see section 4.11). Ratios of fluorescent signals of CYTO-ID (autophagic vesicles) and Hoechst (nuclear dye) in WS1 after 24h treatment are shown. Values were obtained from n ≥ 7 biological replicates. Means ± SEM are shown. Adjusted P values of Tukey's multiple comparison test: (****): < 0.0001, (**): < 0.01, (ns): not significant.

5.9.3. Quantification of autophagic vesicles in WS1 treated with sugars derivatives

Sugar derivatives tested showed variable effects on autophagy in WS1 fibroblasts. Used at 50 mM and 100 mM, gluconic acid and meglumine did not increase AV levels in WS1 [Fig. 38b and c], whereas both had cytotoxic effect when used at a concentration of 200 mM (data not shown). Levels of AV detected when they were used in a combination with Cq were not different from Cq alone. Sorbitol induced a dose-dependent increase of AV in WS1 [Fig. 38a]. When used at concentrations of 100 mM and 200 mM in combination with Cq, AV levels were significantly higher as compared to Cq only.

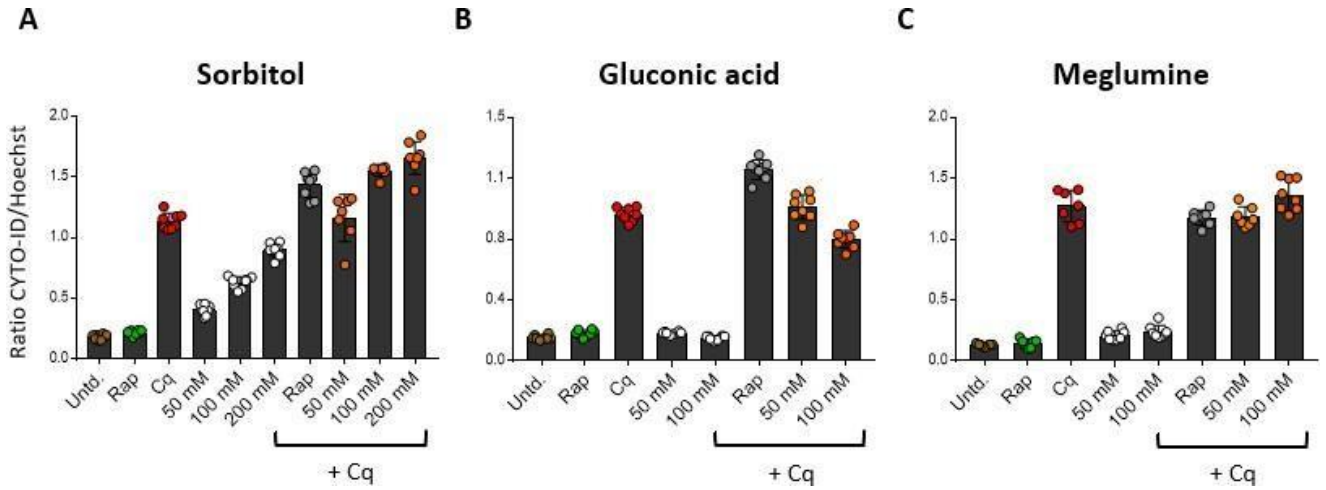

Figure 38: Quantification of autophagic vesicles following carbohydrates treatment in WS1 fibroblasts. WS1 were treated withindicated concentration of(**A**) sorbitol, (**B**) gluconic acid and (**C**) meglumine, in presence or absence of Cq. Untreated (Untd.), Rap-, Cq- and Rap+Cq-treated cells served as control. Level of autophagy was assessed by measuring the number of autophagic vesicle (see section 4.11). Ratios of fluorescent signals of CYTO-ID (autophagic vesicles) and Hoechst (nuclear dye) in WS1 after 24h treatment are shown. Values were obtained from n ≥ 7 biological replicates. Means ± SEM are shown. Adjusted P values of Tukey's multiple comparison test: (****): < 0.0001, (**): < 0.01, (ns): not significant.

5.9.4. Effect of raffinose, maltose and isomaltose on autophagic activity

To assess sugars ability to modulate autophagy, LC3 levels and ratio were monitored in WS1 treated with 100 mM raffinose (non-reducing, shown to increase AV), isomaltulose (reducing, shown to increase AV) and maltose (reducing, with no effect on AV) by Western blot analysis [Fig. 39]. Sugars were used alone or in a combination with Cq. Untreated (Untd.), Rap-, Cq- and Rap+Cq served as controls.

Untreated cells showed basal expression of LC3i and LC3ii, suggesting a basal autophagic activity. Treatment of WS1 with 100 mM raffinose (Raff) and 100 mM isomaltulose (Isom) increased abundance of LC3ii compared to untreated [Fig. 39a], while LC3i abundance did not change, resulting in higher LC3 ratios [Fig. 39b]. In combination with Cq, raffinose and isomaltulose increased LC3ii abundance compared to cells treated with Cq only. Treatment with 100 mM maltose did not change abundances of LC3ii nor LC3i compared to untreated WS1, resulting in a similar ratio. When used in a combination with Cq, maltose also induced increase in LC3 ratio, and band intensities resembled the one observed for Cq treatment only [Fig. 39a].

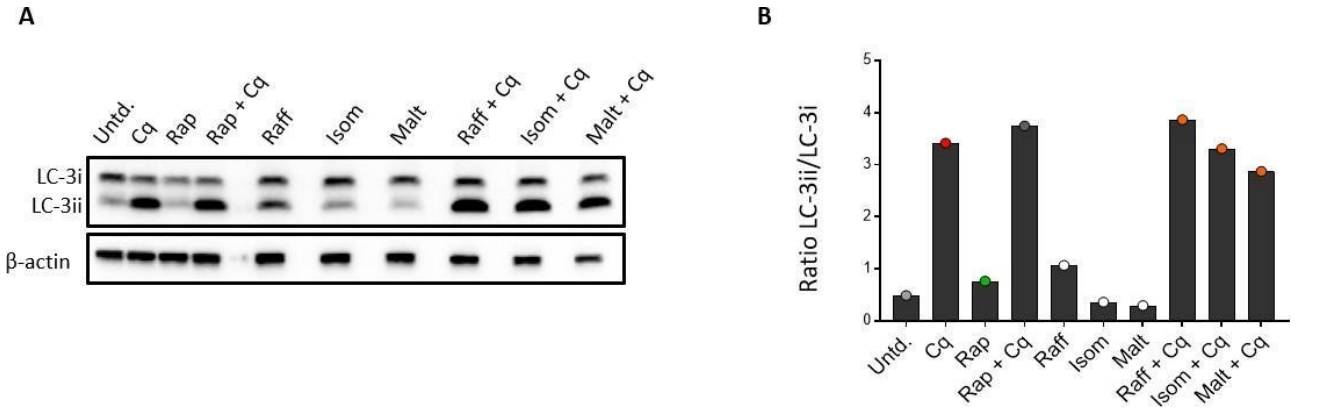

Figure 39: **Western blot analysis of LC3 in WS1 treated with 100 mM raffinose, isomaltulose and maltose.** Treatment in the presence or absence of Cq. Untreated (untd.), Rap-, Cq- and Rap+Cq-treated cells served as control. (**A**) Western blot LC3. Following 24h treatment with sugars, proteins were isolated, and 12 µg protein lysate loaded. β-actin served as loading control. Representative figure of 3 biological replicates is shown. (**B**) Ratio LC3ii/LC3i. Values obtained from 3 biological replicates. Means ± SEM are shown.

5.9.5. Effect of raffinose, maltose and isomaltose on mTOR, Raptor and Rictor

To assess whether sugar-mediated activation of autophagy in WS1 is mTOR-dependent or independent, abundances and phosphorylation levels of mTOR (Ser2481), Raptor (Ser792) and Rictor (Thr1135) were assessed by Western blot analysis. Cells were treated with 100 mM raffinose (non-reducing, shown to increase AV), isomaltulose (reducing, shown to increase AV) and maltose (reducing, with no effect on AV) for 24 hours.Rap-treated cells served as control [Fig. 40].

Neither Rap treatment, nortreatment with raffinose, isomaltulose or maltose induced changes in mTOR, Raptor or Rictor expression [Fig. 40a]. Rap treatment induced a slight migration of Rictor as compared to untreated cells [Fig. 40a]. Rap treatment decreased abundance of phosphorylated mTOR, while sugars had no effect [Fig. 40b]. Phosphorylation of Raptor on Ser792 was increased in Rap-treated cells, but did not change upon any sugar treatments. Rap-treated cells showed lower level of phosphorylated Rictor compared to untreated cells, whereas phosphorylation levels where higher upon sugars treatment [Fig. 40b].

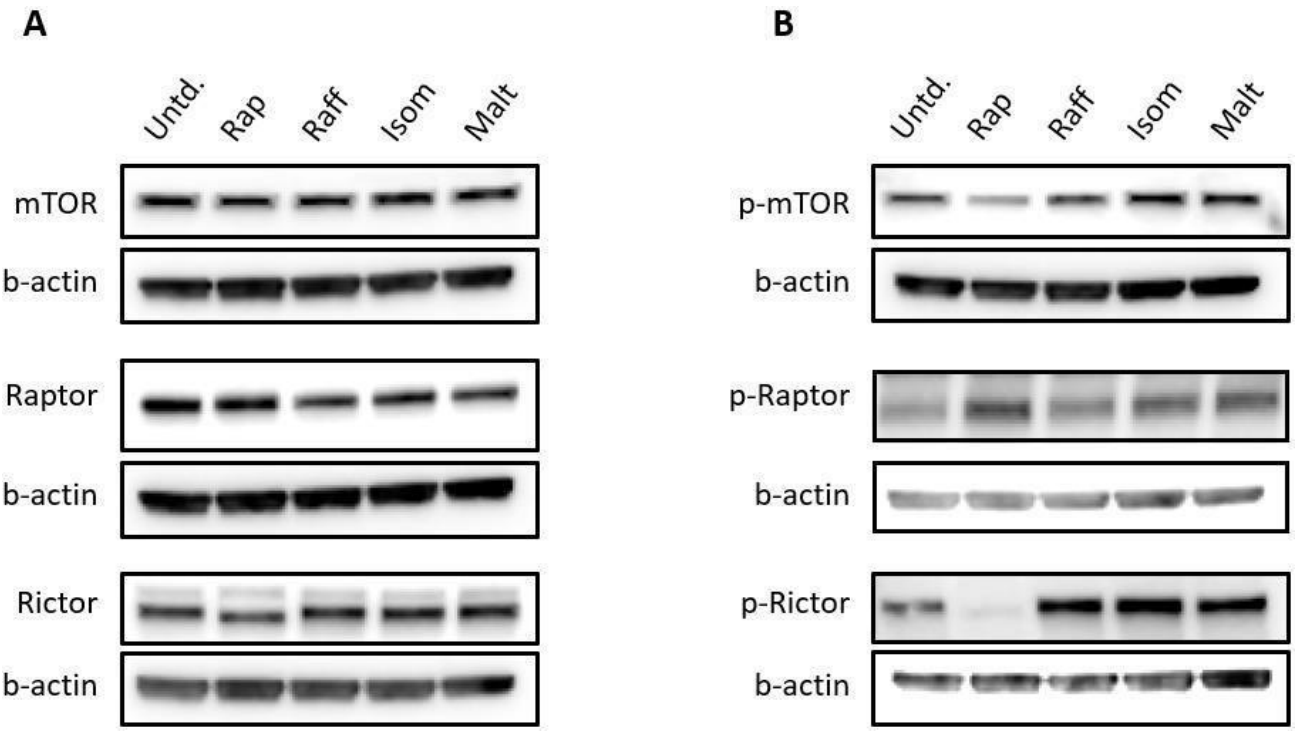

Figure 40: Western blot analysis of mTOR, p-mTOR, Raptor, p-Raptor, Rictor and p-Rictor in WS1 fibroblasts treated with raffinose, isomaltulose and maltose. Cells were either left untreated or treated with 100 mM sugars for 24 hours. (**A**) expression of mTOR, Raptor and Rictor. (**B**) expression of phosphorylated forms. 15 µg cell lysate were loaded. β-actin served as loading control. Representative figure of 2 biological replicates.

5.10. APOL2, CES2, PTTG1IP and MGARP proteins are upregulated in senescent NHDF

Specificsenescence markersarelackingforthetargetedeliminationofsenescentcells. Based ontheupregulated-proteins gene set enrichment analysis [Section 5.3], 4 biological processes were further selected for their potential role in senescent cell viability. For each BPs, 1 protein was chosen based on MS/MS-related criteria (number of unique peptides, protein coverage, number of PSMs and expression fold-change) and its novelty in the field of senescence.

Expression of each protein in senescent NHDF was validated by Western blot analysis and its role in senescent NHDF viability assessed by siRNA-mediated gene knockdown.

5.10.1. Identification and selection of Apolipoprotein L2

Apolipoprotein L2 (APOL2) is a member of the apolipoprotein L gene family. Mainly localized in nucleoplasm and cytosol, it may affect the movement of lipids or allow their binding to organelles.

Identification of APOL2 by 2D-LC-MS/MS analysis

Expression of Apolipoprotein L2 (APOL2) was significantly 2.45-fold higher in senescent NHDF compared to its expressionin proliferating NHDF(adj. *p*-value: 3.08E-2). Identificationof APOL2 was based onthe detection of 4 unique peptides, covering 12.17% of the protein [Fig. 41]. Corresponding Peptide-Spectrum Matches (PSMs) are shown in appendix [Appendix 6a].

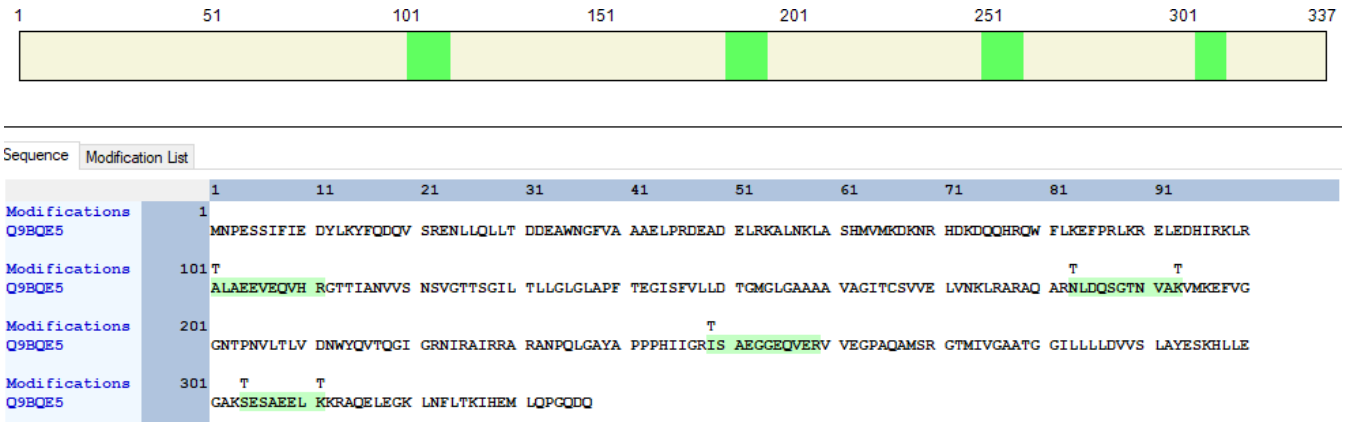

Figure 41: Details of APOL2 identification by 2D-LC-MS/MS. APOL2 was detected by 2D-LC-MS/MS based on the detection of 4 unique peptides, covering 12.17% of the protein.

To further investigate the impact of APOL2 overexpression in senescent NHDF, biological processes and pathways involving APOL2 have been highlighted in the upregulated proteins GSEA map. Based on the GSEA, APOL2 was shown to be involved in five biological processes [Fig. 42].

A

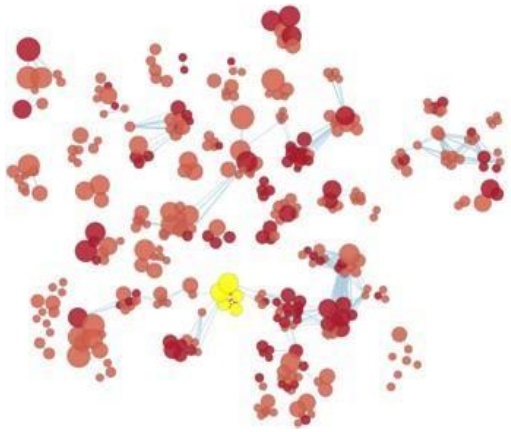

B

Name	EM name	FDR q-value
Alcohol metabolic process	GO:0006066	2.57E-02
Steroid metabolic process	GO:0008202	8.18E-03
Cholesterol metabolic process	GO:0008203	7.83E-03
Sterol metabolic process	GO:0016125	1.55E-03
Secondary alcohol metabolic process	GO:1902652	8.48E-03

Figure 42: **APOL2-related biological processes.** (A) Gene set enrichment analysis of all upregulated proteins in senescent NHDF. Yellow gene sets indicate biological processes where APOL2 is involved. (B) Enriched biological processes involving APOL2 with corresponding FDR q-values.

Validation of APOL2 overexpression in senescent NHDF

Expression of APOL2 was confirmed by Western blot analysis. NHDF from 3 different donors were induced senescent using doxorubicin. Expression of APOL2 was assessed 1-, 10- and 20 days after Dox-treatment, and compared to its expression in untreated cells [Fig. 43].

Expression of APOL2 increased overtime in NHDF from donor 1, and was 1.3-fold higher at day 20 compared to untreated cells. Expression of APOL2 in untreated NHDF from donor 1 was 3.5-fold lower compared to untreated NHDF donors 2 and 3. In NHDF from donors 2 and 3, APOL2 expression decreased overtime and was approximatively 2-fold decreased at day 20.

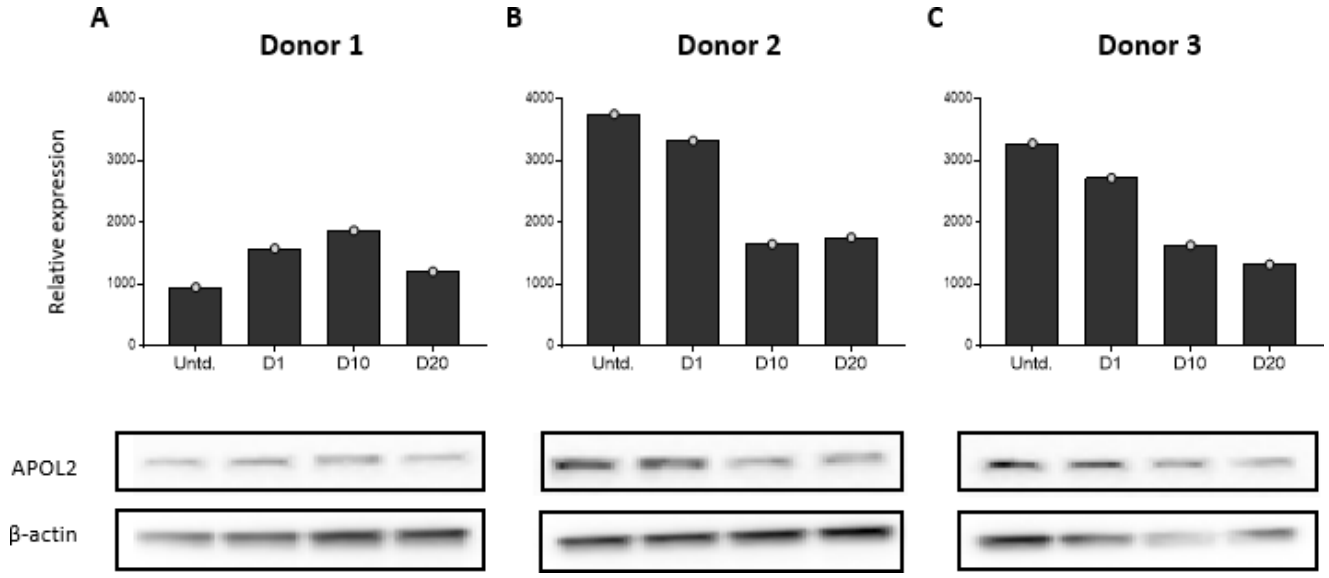

Figure 43: APOL2 expression in NHDF. NHDF were induced senescent using Dox. After 1-, 10- and 20 days, expression of APOL2 was compared with expression in untreated cells in 3 different donors. (**A**) Relative expression of APOL2 in donor 1, (**B**) in donor 2 and (**C**) in donor 3. Western blot analysis performed using 10 µg lysate at different time points. β-actin served as loading control.

5.10.2. Identification and selection of cocaine esterase 2

Cocaine esterase 2 (CES2) is a member of the carboxylesterase large family. These proteins are responsible for the hydrolysis or transesterification of various xenobiotics and endogenous substrates with ester, thioester or amid bonds. CES2 may participate in fatty acyl and cholesterol metabolism.

Identification of CES2 by 2D-LC-MS/MS analysis

Expression of CES2 was significantly 4.3-fold higher in senescent NHDF compared to its expression in proliferating NHDF (adj. *p*-value: 4-76E-2). Identification of CES2 was based on the detection of 3 unique peptides, covering 6% of the protein [Fig. 44]. Corresponding Peptide-Spectrum Matches (PSMs) are shown in appendix [Appendix 6b].

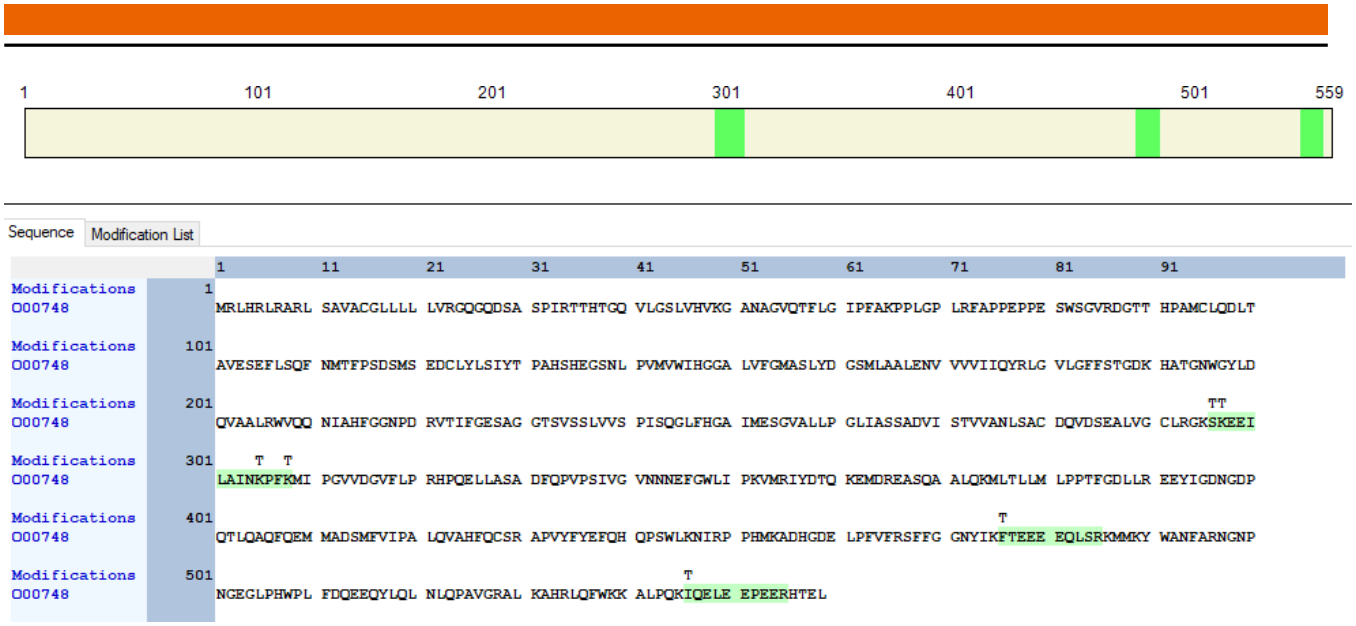

Figure 44: Details of CES2 identification by 2D-LC-MS/MS. CES2 was detected by 2D-LC-MS/MS based on the detection of 3 unique peptides, covering 6% of the protein.

To further investigate the impact of CES2 overexpression in senescent NHDF, biological processes and pathways involving CES2 have been highlighted in the upregulated proteins GSEA map. Based on the GSEA, CES2 was shown to be involved in five biological processes [Fig. 45].

A

B

Name	EM name	FDR q-value
Icosanoid metabolic process	GO:0006690	4.71E-03
Prostanoid metabolic process	GO:0006692	4.71E-03
Prostaglandin metabolic process	GO:0006693	1.61E-02
Fatty acid metabolic process	GO:0016125	1.29E-02
Fatty acid derivative metabolic process	GO:1901568	2.16E-03
Response to xenobiotic stimulus	GO:0009410	8.84E-04
Cellular response to xenobiotic stimulus	GO:0071466	1.51E-03
Xenobiotic metabolic process	GO:0006805	3.37E-05

Figure 45: **CES2-related biological processes.** (**A**) Gene set enrichment analysis of all upregulated proteins in senescent NHDF. Yellow gene sets indicate biological processes where CES2 is involved. (**B**) Enriched biological processes involving CES2 with corresponding FDR q-values.

Validation of CES2 overexpression in senescent NHDF

Expression of CES2 was confirmed by Western blot analysis. NHDF from 3 different donors were induced senescent using doxorubicin. Expression of CES2 was assessed 1-, 10- and 20 days after Dox-treatment, and compared to its expression in untreated cells [Fig. 46].

Expression of CES2 was barely detected in untreated NHDF from all donors and was 25-fold increased 1 day Dox-treatment. CES expression decreased overtime in all donors and was 18-fold, 14-fold and 21-fold increased compared to untreated cells in donor 1, 2 and 3, respectively.

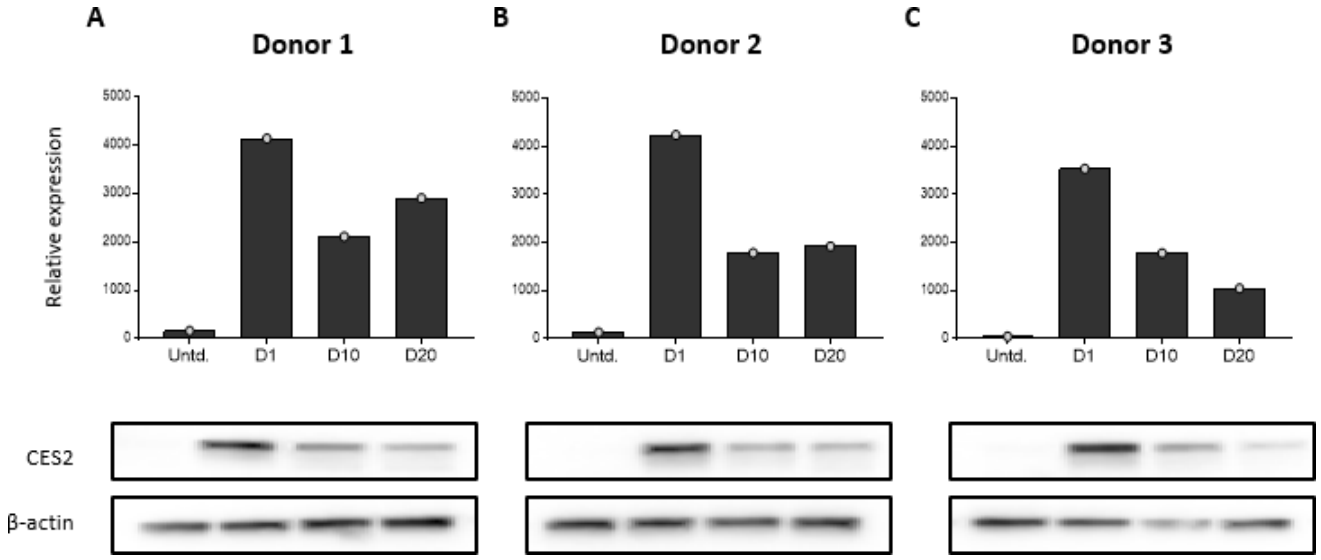

Figure 46: CES2 expression in NHDF. NHDF were induced senescent using Dox. After 1-, 10- and 20 days, expression of CES2 was compared with expression in untreated cells in 3 different donors. (**A**) Relative expression of CES2 in donor 1, (**B**) in donor 2 and (**C**) in donor 3. Western blot analysis performed using 10 µg lysate at different time points. β-actin served as loading control.

5.10.3.Identification and selection of Pituitary Tumor-Transforming Gene 1 Protein-interacting protein

Pituitary tumor-transforming gene 1 protein-interacting protein (PTTG1IP) is a poorly characterized protein though to facilitate PTTG1 nuclear translocation.

Identification of PTTG1IP by 2D-LC-MS/MS analysis

Expression of PTTG1IP was significantly 2.5-fold higher in senescent NHDF compared to its expression in proliferating NHDF (adj. *p*-value: 1.4E-4). Identification of PTTG1IP was based on the detection of 1 unique peptide, covering 10% of the protein [Fig. 47]. Corresponding Peptide-Spectrum Matches (PSMs) are shown in appendix [Appendix 6c]. Based on the GSEA, PTTG1IP was shown to be involved in 2 biological processes [Fig. 48].

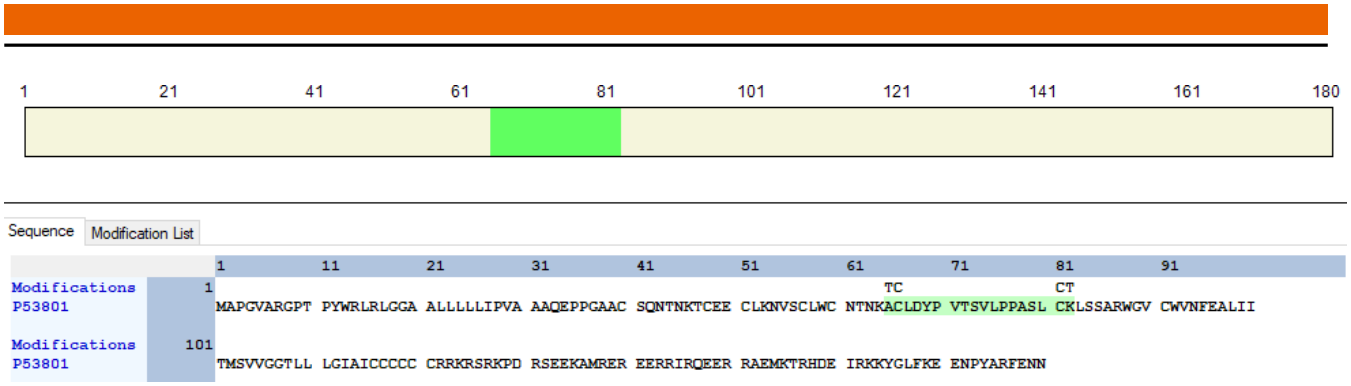

Figure 47: Details of PTTG1IP identification by 2D-LC-MS/MS. CES2 was detected by 2D-LC-MS/MS based on the detection of 1 unique peptide, covering 10% of the protein.

To further investigate the impact of PTTG1IP overexpression in senescent NHDF, biological processes and pathways involving PTTG1IP have been highlighted in the upregulated proteins GSEA map. Based on the GSEA, PTTG1IP was shown to be involved in five biological processes [Fig. 48].

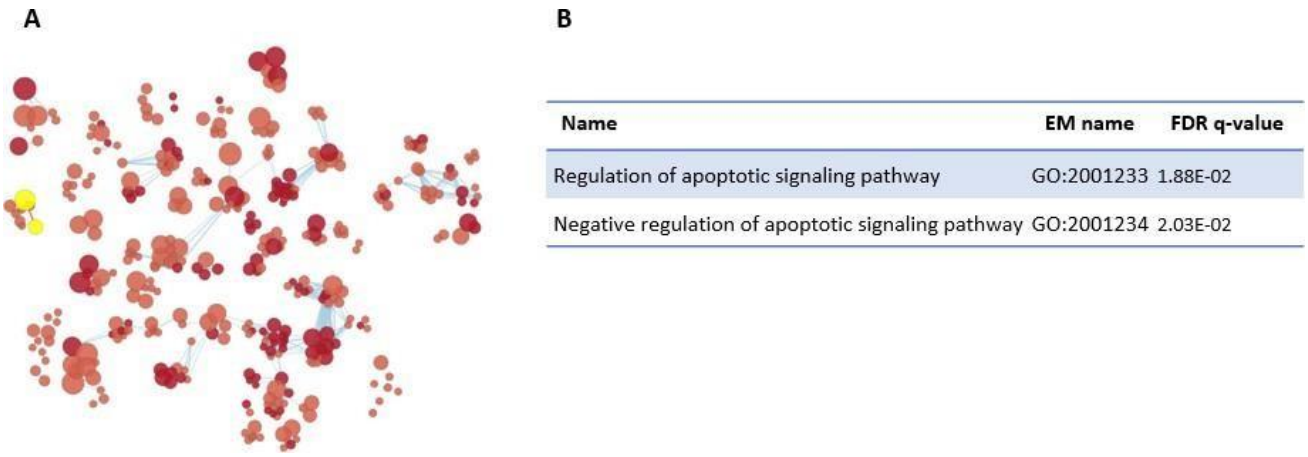

Figure 48: **PTTG1IP-related biological processes.** (**A**) Gene set enrichment analysis of all upregulated proteins in senescent NHDF. Yellow gene sets indicate biological processes where PTTG1IP is involved. (**B**) Enriched biological processes involving PTTG1IP with corresponding FDR q-values.

Validation of PTTG1IP overexpression in senescent NHDF

Expression of PTTG1IP was confirmed by Western blot analysis. NHDF from 3 different donors were induced senescent using doxorubicin. Expression of PTTG1IP was assessed 1-, 10- and 20 days after Dox-treatment, and compared to its expression in untreated cells [Fig. 49].

Western blot analysis showed basal expression of PTTG1IP, which increased over time following Dox- treatment in all donors. Following Dox-treatment, expression of PTTG1IP increased over time and was 11- fold, 2.8-fold and 3-fold increased compared to untreated cells in donor 1, 2 and 3, respectively.

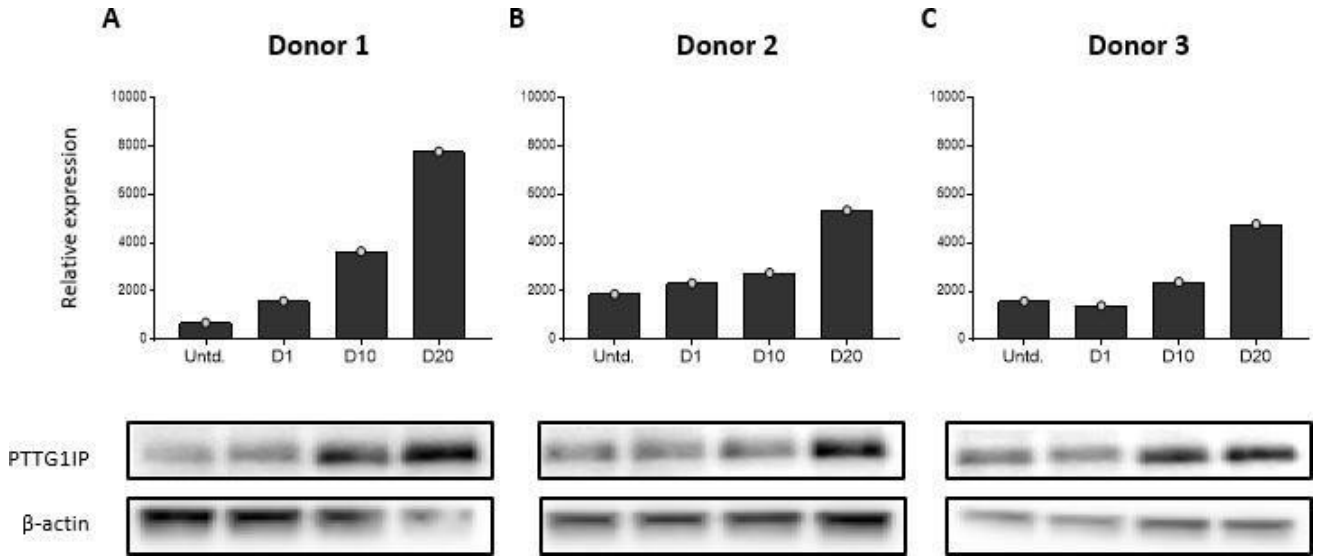

Figure 49: PTTG1IP expression in NHDF. NHDF were induced senescent using Dox. After 1-, 10- and 20 days, expression of PTTG1IP was compared with expression in untreated cells in 3 different donors. (**A**)Relative expression of PTTG1IP in donor 1, (**B**) in donor 2 and (**C**) in donor 3. Western blot analysis performed using 10 µg lysate at different time points. β-actin served as loading control.

5.10.4. Identification and selection of MGARP protein

Protein MGARP (MGARP) plays a role in the trafficking of mitochondria and is also involved in mitochondria abundance and morphology.

Identification of MGARP by 2D-LC-MS/MS analysis

Expression of MGARP was significantly 2.2-fold higher in senescent NHDF compared to its expression in proliferating NHDF (adj. *p*-value: 2.25E-2). Identification of MGARP was based on the detection of 6 unique peptides, covering 47% of the protein [Fig. 50]. Corresponding Peptide-Spectrum Matches (PSMs) are shown in appendix [Appendix 6d]. Based on the GSEA, MGARP was shown to beinvolved in nine biological processes [Fig. 51].

MGARP was not detected by Western blot analysis, neither in proliferating nor senescent NHDF.

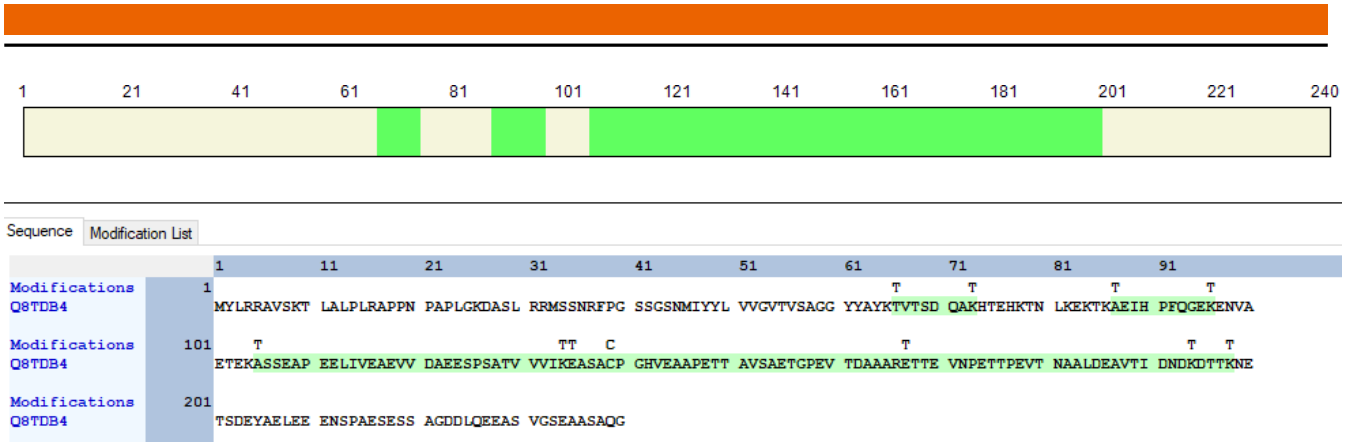

Figure 50: Details of MGARP identification by 2D-LC-MS/MS. CES2 was detected by 2D-LC-MS/MS based on the detection of 6 unique peptides, covering 47% of the protein.

To further investigate the impact of MGARP overexpression in senescent NHDF, biological processes and pathways involving PTT MGARP G1IP have been highlighted in the upregulated proteins GSEA map. Based on the GSEA, MGARP was shown to be involved in five biological processes [Fig. 51].

A

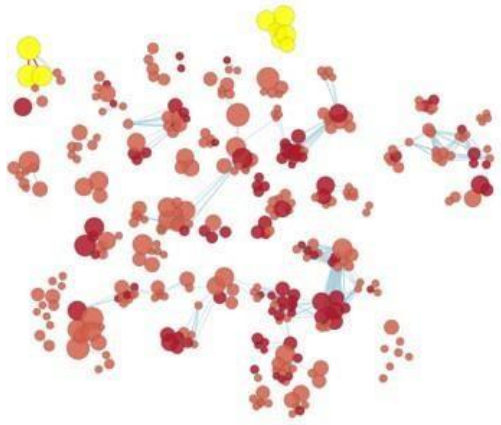

B

Name	EM name	FDR q-value
Response to peptide	GO:1901652	3.75E-03
Response to peptide hormone	GO:0043434	2.68E-02
Cellular response to peptide	GO:1901653	1.10E-02
Response to decreased oxygen levels	GO:0036293	1.57E-03
Response to oxygen levels	GO:0070482	5.90E-04
Cellular response to oxygen levels	GO:0071453	5.38E-03
Response to hypoxia	GO:0001666	1.47E-03
Cellular response to hypoxia	GO:0071456	1.27E-02
Cellular response to decreased oxygen levels	GO:0036294	1.35E-02

Figure 51: **MGARP-related biological processes.** (**A**) Gene set enrichment analysis of all upregulated proteins in senescent NHDF. Yellow gene sets indicate biological processes where MGARP is involved. (**B**) Enriched biological processes involving MGARP with corresponding FDR q-values.

Possible role of MGARP in mitochondria structure and abundance

Although MGARP was not detected by Western blot analysis, its detection by 2D-LC-MS/MS suggest an impairment of mitochondria abundance and structure in senescent NHDF. To validate this hypothesis, electron microscopy was performed on proliferating and senescent NHDF.

Mitochondria of proliferating NHDF had an oval shape, whereas mitochondria from senescent NHDF were enlarged and branched [Fig. 52]. Mitochondria number was decreased in senescent compared to proliferating NHDF (visual observation, data not shown).

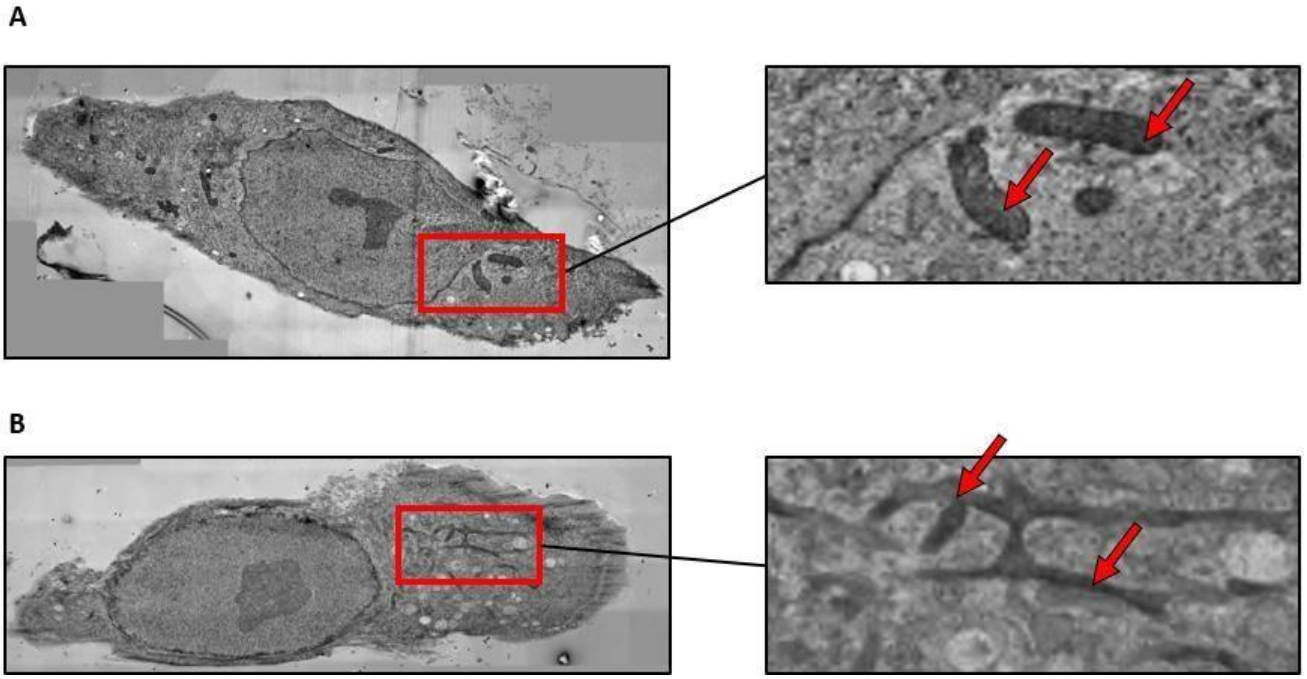

Figure 52: **Electron microscopy of NHDF.** NHDF were induced senescent using Dox. After 14 days, proliferating (control) and senescent NHDF were cryo-fixed, embedded and sectioned for electron microscopy (See section 4.15). (**A**) proliferating NHDF, with a focus on mitochondria (red square). (**B**) Senescent NHDF with a focus on mitochondria (red square).

5.11. APOL2, CES2, PTTG1IP and MGARP play a role in senescent NHDF viability

NHDF were induced senescent using Dox and allowed to recover for 14 days. At day 14, cells were treated with siRNA against APOL2, CES2, PTTG1IP and MGARP for 3 days. Lysis buffer, transfection reagent only (Transf), siRNA targeting GAPDH and scrambling siRNA served as control. After three days treatment, cell viability was assessed by ATP assay [Fig. 53].

After three days treatment, cell viability was significantly decreased for all four protein knockdowns. Viability of cells treated with siRNA targeting GAPDH was also significantly decreased compared to untreated cells.

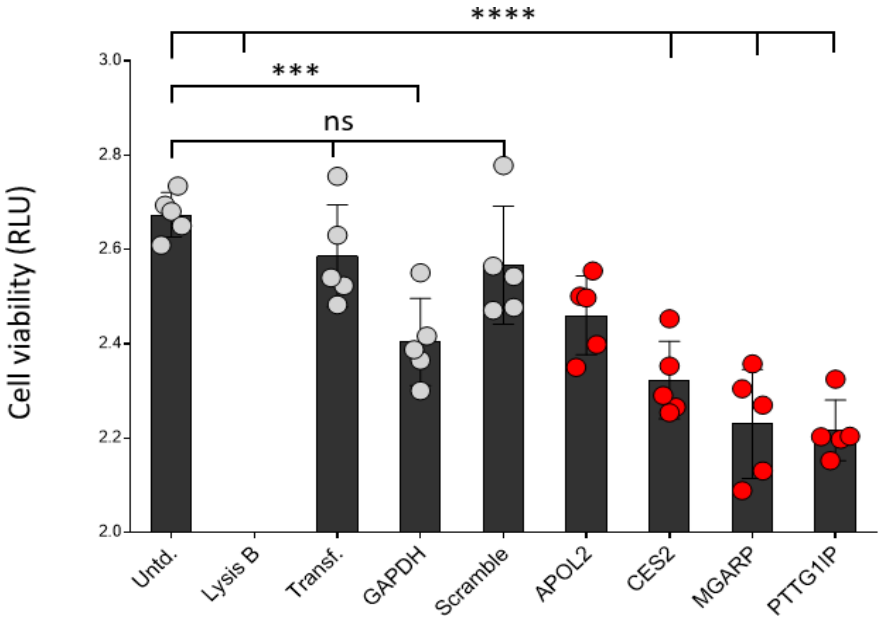

Figure 53: NHDF viability following APOL2, CES2, PTTG1IP and MGARP knock down. Senescent NHDF were treated for 3 days with siRNA targeting APOL2, CES2, PTTG1IP and MGARP. Lysis buffer, transfection reagent, scramble siRNA and siRNA targeting GAPDH served as control.

6. Discussion and outlook

6.1. Proteome analysis of senescent Normal Human Dermal Fibroblasts

To understand mechanisms of aging and age-related diseases, numerous studies in transcriptomics, metabolomics and proteomics have been conducted. For the past decade, research in senescence proteomics has been carried out using different methods as two-dimensional gel electrophoresis (2D-GE)[151,152] and two- dimensional differential gel electrophoresis (2D-DIGE)[153], providing limited efficiency for protein identificationand quantification. Recent advances in liquid chromatography-tandem mass spectrometry (LC-MS/MS) made this technology an excellent tool for large proteomics analysis and allowed for the identification of several senescence markers[154,155].

6.1.1. Differentially expressed proteins in senescent normal human dermal fibroblasts

Whole proteome analysisofnormal human dermal fibroblasts(NHDF) was conducted by 2-Dimensional Liquid Chromatography-tandem Mass Spectrometry. To detect low abundance peptides, often masked by highly abundant peptide peaks, NHDF protein samples were first fractionated by strong cation exchange chromatography, as previously described[156,157]. Further analysis of sample fractions by conventional LC- MS/MS allowed the identification of 4147 proteins [section 5.2], significantly contributing to previous studies[158-161].

Senescence-specific biomarkers are lacking[162]. Among the 4147 proteins previously identified, 20 and 19 proteins were specifically expressed in proliferating and senescent NHDF, respectively (Table 1a and 1b, p. 36 and 37). These proteins could be of interest for the identification and elimination of senescent cells and add knowledge to similar studies[151,163]. Nevertheless, extensive studies are required to confirm their overexpression in senescent NHDF, as well as in other cell types and with different senescence-inducers.

Proteomics technologies allow high throughput but are of limited use for the identification of novel drug targets due to difficult detection of low abundance proteins in complex protein mixes. The entire human genome codes for 21´000 canonical proteins and although fibroblasts-specific proteome is not fully characterized, the 4147 proteins identified by 2D-LC-MS/MS [section 5.2] might be a small part of it.

Cellular signaling and mechanisms often rely on reversible post-translational modifications (PTMs)[164], consisting, among other, of reversible addition of alkyl and acyl chains, sugars and phosphate groups to the protein[165]. Phosphorylation is a protein activator/deactivator and has been shown to affect 13000 proteins of the whole proteome (2/3). Around 90% of proteins are predicted to undergo phosphorylation and dephosphorylation cycles, underlying the importance of this PTM in cellular mechanisms[166].

A recent study on fibroblasts phospho-proteome identified 494 unique peptides with single or multiple phosphorylation sites undergoing phosphorylation cycles under irradiation, highlighting the importance of this post-translational modification in signal transduction[167] . Interestingly, corresponding proteins are involved in cell cycle checkpoint control, DNA damage response and apoptosis, which are also impaired processes in senescence.

Because cellular processes and signal transduction are mostly regulated *via* PTMs-mediated activation/inactivation of proteins, further PTMs-omics studies are required to provide more knowledge about cellular senescence mechanisms. Finally, lipid- and sugar-, as well as protein secretion-related biological processes (BPs) were impaired in senescent NHDF [Fig. 16, p. 41], suggesting that lipidomics, glycomics and secretomics should also be considered for senescence studies.

6.1.2. Gene Set Enrichment Analysis

Gene set enrichment analysis (GSEA) is a bioinformatic tool helping to identify biological pathways that are enriched in a gene list generated from -omics experiments[150,168]. To gain mechanistic insight into senescent NHDF down- and up-regulated proteins, GSEA was conducted using g:Profiler web tool and mapped using Cytoscape and EnrichmentMap software.

Downregulated proteins enrichment analysis

Along with BPs expected to be enriched in senescence downregulated proteins list [Table 2, p. 40], viral defense related mechanisms accounted for a significant portion of all enriched BPs [Appendix 1a and 1b, p. 103], indicating a correlation with senescence. This link was further strengthened by the identification of similar mechanisms in upregulated proteins enrichment analysis (data not shown). Proinflammatory-related BPs were also found enriched in GSEA of upregulated proteins, certainly reflecting the Senescence-Associated Secretory Phenotype (SASP); Senescent cells are metabolically active and secrete different factors to the extracellular environment. Made of chemokines, cytokines and matrix metalloproteases, the SASP is known to have proinflammatory properties[84,169].

Along with the ability of some viruses to inhibit cellular senescence, it has been hypothesized that senescence has evolved as a protective mechanism against viral infections[170].

Mounting evidences show that many viruses also hijack the autophagy machinery for their replication cycle[171-173]. The recent coronavirus outbreak (COVID-19) urges the scientific community to rapidly find therapeutic options, and the repurposing of drugs that are already approved and on the market makes for a good first step in fighting the virus. In this context, chloroquine (approved by the Food & Drug Administration (FDA) in 1949 for the treatment of malaria) is currently being tested in clinical trials for its potential ability to interfere with COVID-19 life cycle.

When entering the cell, the non-protonated portion of chloroquine becomes protonated and concentrates in organelles such as endosomes and lysosomes, where it increases the pH[174]. Fifteen years ago, Vincent *et al.* showed that the effect of chloroquine on coronavirus infection is also explained by the effect of the drug on the glycosylation of a cellular receptor involved in the virus entry[175].

Although preliminary tests suggest benefic effects on COVID-19 infection[176-178], whether chloroquine impacts virus life cycle through basification of vesicles, cellular receptor modification orautophagy-related inhibition of senescence remains to be clarified. Nevertheless, this support the hypothesis that senescence, autophagy and viral defenses are interconnected mechanisms.

The data show that viral defense mechanisms are impaired during senescence, possibly rending senescent cells more sensitive. Whether these findings can be exploited to modulate cellular senescence remains unexplored and might lead to innovative approaches for the elimination of senescent cells.

Upregulated proteins enrichment analysis

Aging is accompanied with a decrease in autophagic activity. In the context of senescence, it has been shown to be increased in order to support metabolic needs and survival of senescent cells.

Upregulated proteins enrichment analysis identified autophagy as a major cluster of biological processes in senescent NHDF, accounting for approximately 8% of all biological processes [Fig. 17, p. 42]. However, the exact role of autophagy in the context of senescence remains unclear.

6.2. Relevance of autophagy in the context of cellular senescence

Bothsenescence and autophagy have been describedas cytoprotectivemechanisms, suggestingsimilarorshared molecular regulation[137]. Reports where the role of autophagy in the context of senescence was assessed are conflicting.

To better understand the role of autophagy in the context of stress-induced premature senescence in skin fibroblasts, autophagy was modulated in three different experimental setups. Autophagic flux was either stimulated or inhibited (**1**) *before* the induction of senescence, (**2**) *during* the development of senescence and (**3**) *in* senescent normal human dermal fibroblasts [Fig. 19, 24 and 30, p. 44, 49 and 55, respectively]. SA-β-gal activity and autophagic activity were monitored at different time points, as previously described.

6.2.1. Stimulation of autophagy delays the onset of senescence in skin fibroblasts

Autophagy has been shown to *promote* cellular senescence, as functional autophagy accelerates the onset of cellular senescence[179,180]. Slobodnyuk *et al*. recently reported that induction of autophagy by p38α promotes cellular senescence[181].

The results obtained in the scope of this work show that Rap-mediated *stimulation* of autophagy *before* the induction of senescence delays its onset, as shown by an average decrease in the SA-β-gal activity of 7% compared to untreated WS1 [Fig. 22b *vs* 22a, p. 47]. Similarly, Rap-mediated *stimulation* of autophagy *during* the development of senescence delays its onset, as shown by an average decrease in the SA-β-gal activity of 12% compared to untreated WS1 [Fig. 27b *vs* 27a, p. 52]. Although autophagy stimulation delays the onset of senescence, it cannot prevent it, as no difference in SA-β-gal activity or staining were observed at day 13 compared to untreated WS1 [Fig. 22b *vs* 22a and Fig. 27b vs 27a, p. 47 and 52, respectively].

These observations were further validated by SA-β-gal staining of Rap-treated WS1, which show fewer senescent positive cells (blue staining) compared to untreated [Fig. 23, page 48 and Fig. 29, p. 54]. Nevertheless,SA-β-gal staining intensity in senescent cells has been reported to be decreased upon Rap treatment without affectingthecellcycle[182,183], whichcould explainwhy SA-β-galstainingof Rap-treated WS1 appears less intense compared to untreated cells [Fig. 23, p. 48]. The stimulation of autophagy in Dox-treated WS1 keeps a spindle-

like morphology in opposition to untreated cells [Fig. 29, p. 54], indicating a likely influence of Rap on the cellular metabolism with beneficial effects on senescent cells survival. If this is due to an increased autophagic activity or mTOR inhibition related mechanisms remains to be determined, as single rapamycin treatment has been shown to persistently change the proteome and metabolome of cells[184].

Rap-mediated stimulation of autophagy *in* senescent WS1 has no effect on SA-β-gal activity compared to untreated cells [Fig. 32b *vs* 32a, p. 57], highlighting the irreversible character of cellular senescence.

Together, these observations are consistent with previous studies which showed that autophagy prevents the onset of senescence[185,186]. This takes place in a larger context describing autophagy as a protective mechanism increasing organism and cellular lifespan by decreasing the rate at which cellular damages accumulate[187-189].

These results also correlate with the observations of Han *et al*., reporting a preventive effect of Rap treatment on replicative senescence in human dermal fibroblasts[185]. Nevertheless, they did not provide clear evidence that Rap-mediated increase of autophagic flux is sufficient for this protective mechanism, as Rap was also shown to have multiple beneficial effects on serially passaged human skin fibroblasts, including notably protection against telomere shortening, DNA methylation and increased stress resistance[190].

Lerner *et al*. provided compelling evidences that autophagy-mediated clearance of dysfunctional mitochondria (mitophagy) is one aspect contributing to the prevention of replicative senescence in human dermal fibroblasts[186]. Contradictorily, Young *et al*. reported that autophagy contributes to, and accelerates the onset of oncogene-induced senescence (OIS) in human fibroblasts[180]. The mechanisms involved in replicative senescenceand OIS differ from Dox-induced senescence, emphasizing the need to distinguish between different types of senescence and autophagy.

6.2.2. Inhibition of autophagy *after* induction of premature senescence leads to cell death in skin fibroblasts

It has been reported autophagy impairment triggers premature senescence[191-193].

The results obtained in this work show that inhibition of the autophagic flux in WS1 through Cq treatment*before* the induction of senescence *decreases* SA-β-gal activity, as shown by an average drop of ~40% comparedto untreated cells (D-1). After Dox-mediated induction of senescence (D1 – D13), SA-β-gal activity was on average 3% higher compared to untreated cells [Fig. 22a *vs* 22b and 23, p. 47], suggesting that autophagy impairment positively impact the development of senescence. This is in concordance with the observation of Fujii *et al*., who showed that insufficient autophagy promotes senescence[194].

In counterpart, inhibition of autophagy *during* the development of senescence *prima facie* decreased the SA-β-gal activity until 9 days after Dox-treatment [Fig. 27c, p. 52]. This decrease by 33% in SA-β-gal activity was further correlated with viability of senescent WS1 treated with Cq [Fig. 29 and 33c, p. 54 and 58, respectively], indicating that blocking autophagic flux during the development of senescence changes the cell fate from senescence to cell death.

These findings are supported by multiple reports, indicating that autophagy inhibition change the cell fate from senescence development to apoptosis[195-196]. Cavinato *et al*. provided evidences that autophagy inhibition is

sufficient to switch cell fate from senescence to apoptosis[179]. Consistently, Singh *et al.* showed that autophagy-mediatedremovalofp18-CycE(afragmentofcyclin E) favorizessenescenceuponapoptosisandthatimpairment of autophagy reverts the cell fate to apoptosis in epithelial carcinoma cells[195].

The cytotoxic effect of Cq seems to be specific to senescent cells, as the SA-β-gal activity increased again from day 9 [Fig. 27c, p. 52]. This could be explained by time-differential adoption of the senescence phenotype following Dox-treatment, resulting in a mixed population of proliferating (slowly turning senescent) and (already) senescent WS1. Until day 6, senescent cells die upon Cq treatment, which decreases the overall SA-β- gal activity. From day 9, previous proliferating WS1 turned senescent, increasing the SA-β-gal activity. The mixed population hypothesis, as well as the ability of Cq to specifically induced cell death in senescent WS1 wasconfirmed by SA-β-gal staining: after 13 days of autophagy inhibition (Cq), cell density was decreased by approximatively 84% compared to untreated WS1. Furthermore, the absence of SA-β-gal positive cell (blue staining) upon CQ treatment strengthens the hypothesis of the "senescence-apoptosis switch" described above [Fig. 29, p. 54].

Similarly, the apparent decrease in SA-β-gal activity observed upon Cq treatment *in* senescent WS1 [Fig. 32a *vs* 32c, p. 57] is correlated with cell death, as shown by a decrease of 42% (6d) and 75% (9d) of senescent WS1 viability.

As both Rap and Cq do not affect autophagy specifically, but also other cellular processes, results gathered from these experiments need to be carefully revised. In this context, Mizushima *et al.* shows how challenging it is to draw conclusions on the function of autophagy in a biological context where autophagy was pharmacologically inhibited[197]. Therefore, these results need to be further confirmed by genetic knock out of essentials genes involved in autophagy. Similarly, Rap is not a specific inducer of autophagy, as inhibition of its target (mTORC1)affects multiple cellular processes, including overall proteome and metabolome[198].

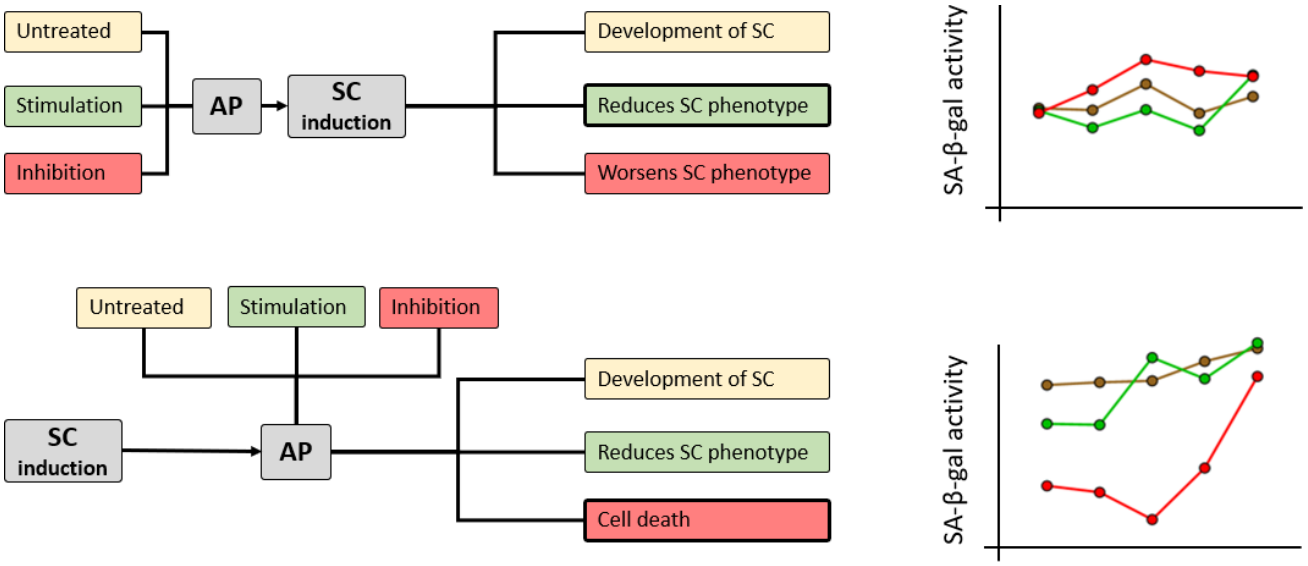

Figure 54: Role of autophagy in the context of cellular senescence (graphical summary). (**A**) Autophagy was modulated ***before*** Dox-mediated induction of senescence in WS1. Following Dox treatment, SA-β-activity

increased over time (UT). When autophagy is stimulated (Rap), the SA-β-activity is lower during the development of senescence compared to untreated (UT) and autophagy inhibited WS1 (Cq). When autophagy is inhibited (Cq), SA-β-activity is higher compared to the other groups. Neither stimulation nor inhibition of autophagy prior to senescence induction could avoid its establishment. (**B**) Autophagy was modulated ***during*** the development of senescence. Together, these data show that early stimulation of autophagy delays the onset of senescence, while its inhibition worthens the activity of the SA-β-activity. When autophagy is modulated ***after*** the induction of senescence, its stimulation results in lower SA-β-activity compared to untreated WS1, whereas its inhibition induce cell death.

6.2.3. Autophagy inhibition *per se* is responsible for senescent fibroblasts death, and not CQ treatment

Chloroquine is a potent autophagy inhibitor and has been shown to block the fusion autophagosome-lysosome[199]. To exclude that cell death observed upon Cq treatment is the result of an accumulation of vesicles in the cytoplasm, autophagy was inhibited by blocking phagosome formation and maturation in senescent NHDF. After 3 days of inhibition, senescent NHDF viability decreased by more than 50% for all autophagy inhibitors, except Wort (26%). After 6 days, viability decreased by more than 80% (Wort 60%) and after 9 days by more than 90% (Wort 50%) [Fig. 34, p. 59]. Together, this reinforces the hypothesis that decreased viability of senescent NHDF is a consequence of autophagy-inhibition and not a of the Cq treatment.

Potent and irreversible inhibitor of phosphatidylinositol 3-kinase (PI3K), an enzyme required for autophagy[200-201], Wortmannin (Wort) induced significant decrease in senescent NHDF viability [Fig. 34a to 34c, p. 59]. PI3K is known to be involved in Toll-like receptor (TLR) signaling, mediating the glycolytic reprogramming of cells[202]. Because glycolysis has been shown to be increased in senescent human fibroblasts[203], whether Wort- induced cell death observed in senescent NHDF is due to autophagy inhibition *or* glycolysis impairment needs to be further explored.

Autophagy related proteins 5 and 7 (Atg5 and Atg7) are essential proteins involved in autophagosomes maturation, and their depletion have been extensively used as a tool to inhibit autophagy[204,205]. Atg proteins have recently been shown to regulate many cellular processes, as depletion of Atg5 impacts 15% of the total proteome[206]. This could explain the decrease in senescent NHDF viability following Atg5/7 depletion [Fig. 34a to 34c, p. 59]. This is supported by a recent publication, highlighting an Atg5/ Atg7-independent alternative autophagy occurring under certain stresses[207]. Thus, whether Atg depletion-mediated cell death observed in senescent NHDF is a consequence of autophagy inhibition or of changes in the proteome needs to be further investigated.

Acting as a receptor for ubiquitinated proteins during selective (basal) autophagy, p62 increases when autophagy is inhibited[208]. High levels of p62 have been shown to delay the clearance of tagged-cargo by the ubiquitin-proteasome system[209]. Thus, Cq-mediated inhibition of autophagy could also result in a decrease activity of the proteasome, leading to the accumulation of damaged proteins and organelles.

Senescent fibroblasts exhibit elongated mitochondria [Fig. 52, p. 75]. Under normal conditions, these mitochondria are removed by a specific ubiquitin/p62 dependent selective autophagy, called “mitophagy”.

Weather Cq-mediated inhibition of autophagy impairs the removal of dysfunctional mitochondria, thus increasing cellular damages, needs to be validated.

Accumulation of p62 plays a role in cell survival. Organized in "speckles", p62 interact with both TRAF6 and caspase 8. The binding of p62 with TRAF6 activated the NK-κB signaling and promotes cell survival. The binding of p62 with caspase 8, in counterpart, triggers apoptosis. The exact mechanism deciding which pathway should be activated remains unclear, but Cq-mediated inhibition of autophagy might increase p62 levels and triggers the apoptotic pathway through caspase-8 activation in senescent skin fibroblasts.

6.2.4. Is autophagy sufficient for senescence induction in WS1?

To assess whether the modulation of autophagy is sufficient to trigger senescence in Dox-treated WS1, autophagic activity was measured during the development of senescence [Fig. 19, 24 and 30, p. 44, 49 and 55, respectively]. Autophagy was monitored in two different set-ups, (**1**) by staining autophagosomes and (**2**) by calculating the ratio LC3i/LC3ii. Autophagy works as a *flux*, a measure of autophagic degradation activity[210]. Rap-mediated stimulation of autophagy increases the rate at which autophagosomes are produced and matured, *and also* at which they are degraded by fusing with lysosomes. This increased turnover explains why stimulation of autophagy does not return a different signal compared to untreated cells [Fig. 18a and 18c, p. 43]. Similarly, blocking the fusion autophagosome-lysosome through Cq treatment leads to an accumulation of autophagosomes, responsible for the increase in autophagic vesicles [Fig. 18a, p. 43] and LC3 ratio observed [Fig. 18c, p. 43]. The autophagic activity can be evaluated by the LC3i (cytosolic) and LC3ii (membrane-bound)expressions, separately [Fig. 18b, p. 43]. When WS1 are left untreated, 76% of LC3 protein is under its cytosolicform (LC3i) and 24% is membrane-bound, indicating a basal autophagic activity. Upon Rap treatment, LC3i expression is 30% lower compared to untreated, indicating an increased turnover in the production/degradation of autophagosomes. Upon Cq treatment, LC3ii expression is 214% higher compared to untreated and is explained by the accumulation of autophagosomes.

Directly after Dox treatment (D0), autophagic activity is increased in WS1 fibroblasts, as expression of LC3ii is higher compared to untreated cells (D-1) [Fig. 20 and 25, p. 45 and 50, respectively].

This is in opposition with recent studies showing that Dox treatment induces dysfunction and impairment of autophagic flux[211,212].

One day after Dox treatment (D1), expression of LC3ii was decreased compared to untreated cells (D-1) and compared to cells directly after Dox treatment (D0) [Fig. 20a-20c and Fig. 26a, 26b, p. 45 and p. 51, respectively].

Two day after Dox treatment (D2), expressions of LC3i and LC3ii were the same as compared to untreated cells, suggesting the recovery of a basal autophagic activity.

During the development of SIPS (D2-D13), abundance of LC3i remains unchanged, whereas LC3ii expression gradually increases overtime in untreated cells [Fig. 20a and 26a, p. 45 and 51, respectively] as well as in cells treated with a single dose of Rap [Fig. 20b, p. 45]. These observations suggest that development of SIPS is accompanied with increase autophagic activity.

The decrease in both LC3 abundances observed at day 1 (D1) rises two hypotheses. First, the low detection signal could be the result of a decrease in autophagic activity, as the abundance of both cytosolic and membrane-bound forms of LC3 is decreased. This would mean that, following Dox-treatment, WS1 engage the senescence program because of an impaired autophagic activity. This is supported by different reports, showing that impairment of autophagy induces premature senescence[213,214].

Second, the low LC3 abundances could be explained by an extreme increase in autophagic activity, where the acceleration of theturnover production/elimination ofautophagic vesicles diminishes the detection of LC3. This would mean that, following Dox-treatment, WS1 engage the senescence program because of an increased extreme increase in the autophagic flux. This hypothesis is supported by the work of Slobodnyuk *et al*, which recently highlighted the role of p38α-mediated increased of autophagy in the development of senescence[181].

The data suggest that an extreme stimulation of autophagy is involved in the development of senescence in WS1 fibroblasts. This is supported by the fact that inhibition of autophagy through several inhibitors (Cq, Wort and siRNA Atg5/7) does not trigger senescence, but induces cell death *during* the development of SIPS and *in* senescent WS1 [Fig. 29, Fig. 33 and Fig. 34, p. 54, 58 and 59, respectively].

Whether this extreme autophagic activity is sufficient to trigger senescence in WS1 needs to be further investigated. For example, an experimental setup where autophagy is stimulated inthe absence of Dox-mediated induction of SIPS could answer this question.

These data suggest a switch in the autophagic flux occurring between day 0 and day 2 [D0-D2, Fig. 20 and Fig. 25, p. 45 and 50, respectively], changing the cell fate from basal autophagy to autophagy-mediated induction of senescence. Differential proteomics, aiming to compare the proteome of WS1 where autophagy was modulated, could potentially identify modulators of this switch.

6.3. Carbohydrates-mediated modulation of autophagy in WS1

From a broader perspective, these data show the effect of autophagy in the context of senescence; Early stimulation of autophagy delays its onset, whereas inhibition of autophagy in senescent skin fibroblasts leads to cell death. The identification of autophagy modulators is a promising therapeutic approach to counter cellular senescence. For their safety of use, sugars are extensively evaluated for their ability to modulate autophagy, which led to the recent identification of trehalose, raffinose and sucrose as mTOR-independent activator of autophagy in keratinocytes[136]. 10 sugars or sugars-derivatives were tested for their ability to modulate autophagy in WS1 fibroblasts [Fig. 35 p. 60].

All non-reducing sugars, as well as isomaltulose and sorbitol (sugars derivatives), increased in a dose-dependent manner the number of autophagic vesicles in WS1 fibroblasts [Fig. 36a – 36d, Fig. 37c and Fig. 38a, p. 62, 63 and 64, respectively]. Maltose and glucose (reducing sugars), as well as gluconic acid and meglumine (sugars derivatives) had no effect [Fig. 37a and 37b, Fig. 38b and 38c, p. 63 and 64, respectively].

The number of autophagic vesicles detected upon trehalose treatment in a combination with Cq was not different from Cq alone [Fig. 36a p. 62], suggesting an inhibitory effect. All other sugars and sugar derivatives tested showed an increased number of autophagic vesicles when used in combination with Cq compared to Cq alone, suggesting an increased autophagic flux. The sugars alone increased the number of autophagic vesicles, while Rap treatment did not. This indicates that the signal is a result from impaired autophagosome degradation.

To further validate these data [Fig. 36 to 38, p. 62, 63 and 64, respectively], LC3 abundance following raffinose, isomaltulose and maltose treatments where assessed by Western blot [Fig. 39a, p. 65]. Upon raffinose treatment, previously shown to increase autophagic vesicles [Fig. 36c, p. 62], expression of LC3ii was higher compared to untreated cells. For the reason explained above, this indicates an increase in autophagic activity. For the same reason, LC3 ratio was not different from Rap [Fig. 39b, p. 65]. In counterpart, isomaltulose and maltose did not impact LC3ii expression, suggesting that they did not stimulate autophagy. The increase in autophagic vesicles observed upon isomaltulose treatment [Fig. 37c, p. 63] need to be further investigated, as it is not clear whether it activates or inhibits autophagy.

Whether trehalose is an autophagy activator or inhibitor is debated. Whereas Yoon et al. described it as potent autophagic flux inhibitor[215], recent work of Chen et al. suggests an activator effect in keratinocytes[136]. To adjudicate on the role of trehalose, 3 weeks-old senescent NHDF were treated with 50, 100 and 200 mM trehalose for 3-, 6- and 12 days, and cell viability assessed using ATP assay [Appendix 7, p. 118]. Due to repeated medium change, the viability of old senescent NHDF decreases *in vitro* over time [Appendix 7, p. 118].Trehalose treatment led to an increase in old senescent NHDF viability, which was systematically higher compared to untreated cells at day 3, 6 and 12. As data generated in the frame of this work indicate that inhibitionof autophagy in senescent NHDF leads to cell death, trehalose might be considered as an activator of autophagy in senescent NHDF. Trehalose plays a role in energy metabolism in yeast[216-218], as inhibitor of hexokinases (glycolytic enzymes responsible for the transformation of glucose into glucose-6-phophate). Whether increased viability of old senescent NHDF treated with trehalose is due to increased autophagic activity or changes in glucose metabolism needs to be further investigated.

Exact mechanisms underlying sugars-mediated modulation of autophagy remain poorly understood. It is thought that, by opposition to Rap, sugars modulate autophagy in an mTOR-independent fashion[136]. Western blot analysis of mTOR, Raptor and Rictor (key components of the mTOR-mediated autophagy) showed that neither raffinose, nor isomaltulose or maltose change the expression or activation of these proteins [Fig. 40a, p. 66]. Since mTOR activity is regulated *via* phosphorylation cycles, it was assessed whether key phosphorylation sites were modified upon Rap and sugars treatments [Fig. 40b, p. 66].

The phosphorylated form of mTOR (p-mTOR) was lower upon Rap treatment, as previously shown[136]. Upon raffinose, isomaltulose and maltose treatments, p-mTOR levels were similar as in untreated cells, suggesting that none of these sugars impact the mTOR-mediated autophagic machinery.

Upon starvation, autophagy is activated through both mTORC1 inhibition and AMPK activation, AMPK ensuring mTORC1 inhibition through phosphorylation of Raptor at Ser792[220]. Consequently, unchanged phosphorylation levels of Raptor-Ser792 upon any treatment compared to untreated cells assured that autophagy was not activated through starvation conditions.

Julien *et al.* reported that mTORC1-activated S6K1 mediated the phosphorylation of Rictor on Thr1135[221]. Western blot analysis following Rap treatment shows that phosphorylation levels of Rictor (Thr1135) are decreased compared to untreated cells. Thisindicatesthat Rap inhibited mTORC1 activity byinactivating S6K1, consequently decreasing phosphorylation levels of Rictor on Thr1135. Interestingly, treatment with raffinose,

sucrose and maltose increased the phosphorylation level of Rictor, indicating a mTOR-dependent modulation of autophagy [Fig. 40b, p. 66].

Whether phosphorylation of Rictor on Thr1135 affects Akt-Ser473 phosphorylation, a downstream target of mTORC2, remains debated[221]. Neither mTORC2 integrity nor its kinase activity are impaired upon Rictor-Thr1135 phosphorylation[222]. However, phosphorylation of Thr1135 was shown to inhibit the association of Rictor with cullin-1, forming a functional E3 ubiquitin ligase[223]. This indicates that the phosphorylation site on Thr1135 could play a role in mTORC2-independent functions of Rictor within the cell[221]. Together, this suggest that Rictor-Thr1135 might not be an optimal target to assess whether autophagy modulation appears to be mTOR independent. In future studies, evaluating the activity of downstream targets of mTORC1 such as ULK1 should provide more information about whether autophagy is activated in an mTOR-dependent or independent manner.

6.4. APOL2, CES2, PTTG1IP and MGARP are potential targets for the elimination of senescent skin fibroblasts

Identification of unique and specific markers allowing one to identify and quantify senescent cells *in vivo* and *in vitro* is challenging[224]. To find novels markers of skin fibroblasts senescence, 4 proteins (APOL2, CES2, PTTG1IP and MGARP) were selected from 2D-LC-MS/MS analysis [Fig. 12, p. 37]. Upregulated in senescent NHDF, their potential role in senescent fibroblasts viability was assessed by gene knockdown.

6.4.1. Apolipoprotein L2 (APOL2)

APOL2 is thought to affect lipids metabolism, movement and their binding to organelles[225]. This was confirmed by upregulated proteins enrichment analysis [Fig. 42a, p. 68]. Further expression validation by Western blotting showed variation among the 3 different fibroblasts donors, where only donor 1 had increased APOL2 expression 20 days after SIPS induction [Fig. 43, p. 69]. Nevertheless, siRNA-mediated knockdown of APOL2 in donor 3 resulted in a decreased cell viability after 3 days treatment, suggesting that APOL2 could be used as therapeutic target for the specific elimination of senescent skin fibroblasts [Fig. 53, p. 76].

Role of APOL2 in the context of senescence remains unexplored. Recently, Luo *et al*. showed that cytosolic APOL2 is widely expressed in different cell type, and is induced by interferon-gamma during aging[226]. As interferon-gamma signaling was found enriched in GSEA, further studies need to be conducted to assess whether decreased viability of senescent NHDF observed following knockdown of APOL2 is the result of an impairment in the interferon-gamma signaling, or if inhibition of APOL2 is sufficient.

6.4.2. Cocaine esterase 2 (CES2)

CES2 plays a role in detoxification of xenobiotics[227] and lipid metabolism[228]. This was confirmed by upregulated proteins enrichment analysis, as well as a potential role in fatty acid metabolism [Fig. 45, p. 70]. Further expression validation by Western blotting showed an increased expression of APOL2 in all 3 fibroblasts donors directly after Dox treatment (D1), whereas CES2 was barely detected in untreated cells (Untd.) [Fig. 46, p. 71].

The decreased expression of CES2 during the development of SIPS shows that CES2 expression is due to Dox treatment. Nevertheless, siRNA-mediated knockdown of CES2 decreases senescent NHDF viability, suggesting a role in lipid or fatty acid metabolism. The role of CES2 in the context of senescence is unexplored. Nevertheless, further studies are required to assess whether CES2 is also increased when senescence is triggeredusing other induction methods, such as UV-B.

6.4.3. Pituitary tumor-transforming gen 1 protein-interacting proteins (PTTG1IP)

PTTG1IP is known to be involved in regulation of DNA Damage Response (DDR), important feature of SIPS[229] and is also involved in the regulation of protein ubiquitination and import into nucleus [229,230]. Moreover, PTTG1IP is a p53 binding protein[229], which was confirmed by the upregulated protein enrichment analysis [Fig. 48, p. 72].

Expression validation by Western blotting confirmed that expression of PTTG1IP increases over time during the development of SIPS, and this among all donors [Fig. 49, p. 73]. Binding to p53, PTTG1IP might block its translocation into the nucleus, thus inhibiting apoptosis. M. P. Baar *et al*., recently described a similar mechanism, showing that the interaction of p53 with FOXO4 avoid apoptosis in senescent cells[99]. Further studies need to validate the interaction of PTTG1IP with p53, which could be a potential target for the elimination of senescent skin fibroblasts.

6.4.4. MGARP protein (MGARP)

MGARP is a mitochondrial-localized glutamic acid rich protein, hypostatized to play a role in protein targeting to mitochondrion and response to hypoxia, as well as in mitochondrial abundance and morphology. Upregulated proteins enrichment analysis confirmed its role in hypoxia, but not its implication in mitochondrial structurenor transport [Fig. 51, p. 74].

Data supporting its expression in senescent NHDF are conflictual; while 2D-LC-MS/MS identified MGARP on the basis of 6 unique peptides covering 47% of the protein, it was not detected by Western blotting in 3 different donors of NHDF (data not shown). Moreover, MGARP was not identified in skin cells (The Human Protein Atlas, 2020).

Electron microscopy of proliferating and senescent NHDF revealed decreased number and impaired structure of mitochondria in senescent NHDF [Fig. 52, p. 75].

The role of mitochondria in the context of senescence, autophagy and apoptosis is extensively studied[55, 231-233]. Wang *et al*. reported that mitochondrial membranes are depolarized in Dox-induced senescence[234]. Whether MGARP overexpression is sufficient to induce these changes, or if mitophagy is also involved remains to be determined.

The relationship autophagy - senescence remains misunderstood, and seems to depend on the type of autophagy (selective VS basal), on the timing (*when* autophagy occurs) and on the location (*where* autophagy occurs). The graphical summary below shows what is already known about this relation, as well as the findings of this work [Fig. 55].

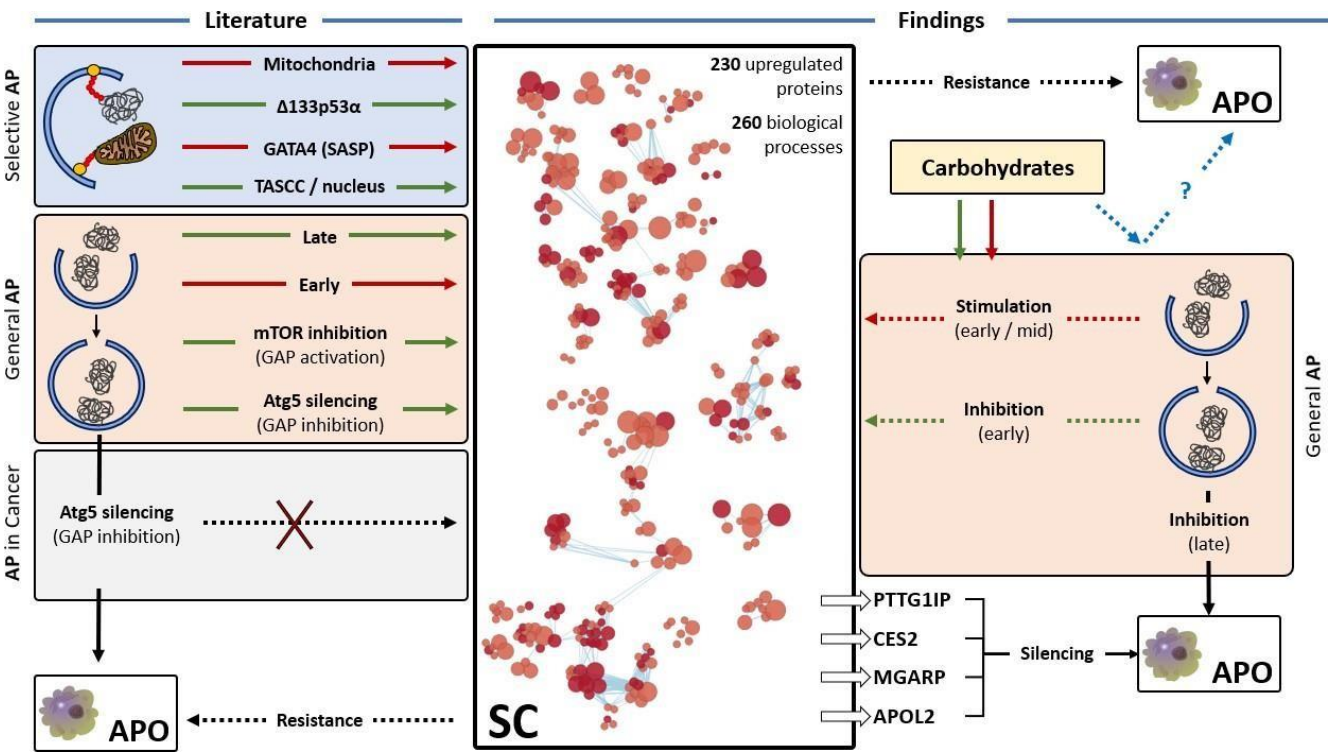

Figure 55: Graphical summary. (**Literature-left side**): Although extensively studied in the context of senescence, the role of autophagy remains poorly understood. **Selective autophagy (blue box)** describes the specific recognition and elimination of cargos, mediated by ubiquitination and cargo receptors (such as p62, lamin B1 and NBR1). In competition with the proteasome system, selective autophagy can be pro-senescence (target degradation of Δ133p53α and nucleus portions) or anti-senescence (target degradation of GATA4 and dysfunctional mitochondria). **General autophagy (pink box)** refers to the non-specific breakdown of cellular components. General autophagy is an important actor of longevity. In this context, it can be anti-senescence (degrading cellular damages delays the onset of senescence) or pro-senescence (limiting accumulation of damages in senescence cells and helping for the production of the SASP). Interestingly, prolonged *activation* of general autophagy has been shown to trigger the senescence program. Contradictorily, silencing of key genes involved in autophagosome maturation (Atg5) also triggers senescence. **Autophagy in cancer (grey box)** has different outcome, as Atg5 inhibition changes the cell fate from senescence to apoptosis (**APO, white box**). Together, these observations suggest that the role of autophagy depends on the timing (early vs late role of autophagy), on the type of autophagy (specific vs general), on the cell type, on the location (TASCC vs nucleus vs cytoplasm) and on the context (normal vs cancer cells).
(Findings-middle and right): Using 2D-LC-MS/MS analysis, we identified 230 upregulated protein in senescent skin fibroblasts. Subsequent analysis of these proteins led us to identify 260 enriched biological processes. Both upregulated proteins and enriched biological pathways are of interest for the identification of novel targets and elimination of senescent cells. In this context, we selected 4 upregulated proteins (APOL2, CES2, PTTG1IP and MGARP), involved in 4 different biological processes (respectively lipids metabolism, fatty acid metabolism, apoptosis and mitochondria biogenesis). Silencing of these genes in senescent skin fibroblasts engaged the apoptotic program (**APO**) in senescent NHDF (**Bottom right**).
Autophagy-related biological processes accounted for approximatively 8% of the total identified by gene set enrichment analysis. When autophagy was stimulated prior to senescence induction, or during the development of stress-induced premature senescence, the onset of senescence was delayed, whereas its inhibition prior to senescence induction worthened the senescence phenotype. Interestingly, inhibition of autophagy during the

development of in senescence NHDF significantly decreased cell viability (**right, pink box**). Together, these data show that autophagy can be targeted for the specific elimination of senescent skin fibroblasts.
Finally, we tested the ability of carbohydrate to modulate autophagy (**upper right, yellow box**). Depending on their nature, carbohydrate can either stimulate or inhibit autophagy. The exact mechanism by which this is regulated remains poorly understood. Weather carbohydrates-mediated modulation of autophagy, in the context of senescence, can trigger the apoptotic program remains to be determined and could be used for the elimination of senescent skin fibroblasts.

7. References

1. Elias P. M. (2007). The skin barrier as an innate immune element. *Seminars in immunopathology*, *29*(1), 3–14.
2. Pedersen, L., & Jemec, G. B. (2006). Mechanical properties and barrier function of healthy human skin. *Acta dermato-venereologica*, *86*(4), 308–311.
3. Wei, J., Meng, L., Hou, X., Qu, C., Wang, B., Xin, Y., & Jiang, X. (2018). Radiation-induced skin reactions: mechanism and treatment. *Cancer management and research*, *11*, 167–177.
4. Agner, T. (2016). Skin barrier function (Karger).
5. Sparr, E., Millecamps, D., Isoir, M., Burnier, V., Larsson, Å., & Cabane, B. (2012). Controlling the hydration of the skin though the application of occluding barrier creams. *Journal of the Royal Society, Interface*, *10*(80), 20120788.
6. Romanovsky A. A. (2014). Skin temperature: its role in thermoregulation. *Acta physiologica (Oxford, England)*, *210*(3), 498–507.
7. Holick M. F. (1988). Skin: site of the synthesis of vitamin D and a target tissue for the active form, 1,25-dihydroxyvitamin D3. *Annals of the New York Academy of Sciences*, *548*, 14–26.
8. Owens, D. M., & Lumpkin, E. A. (2014). Diversification and specialization of touch receptors in skin. *Cold Spring Harbor perspectives in medicine*, *4*(6), a013656.
9. Kuhtz-Buschbeck, J. P., Andresen, W., Göbel, S., Gilster, R., & Stick, C. (2010). Thermoreception and nociception of the skin: a classic paper of Bessou and Perl and analyses of thermal sensitivity during a student laboratory exercise. *Advances in physiology education*, *34*(2), 25–34.
10. Kanitakis J. (2002). Anatomy, histology and immunohistochemistry of normal human skin. *European journal of dermatology : EJD*, *12*(4), 390–401.
11. Baroni, A., Buommino, E., De Gregorio, V., Ruocco, E., Ruocco, V., & Wolf, R. (2012). Structure and function of the epidermis related to barrier properties. *Clinics in dermatology*, *30*(3), 257–262.
12. Pfalzgraff, A., Brandenburg, K., & Weindl, G. (2018). Antimicrobial Peptides and Their Therapeutic Potential for Bacterial Skin Infections and Wounds. *Frontiers in pharmacology*, *9*, 281.
13. Brown, T. M., & Krishnamurthy, K. (2020). Histology, Dermis. In *StatPearls*. StatPearls Publishing.
14. Rippa, A. L., Kalabusheva, E. P., & Vorotelyak, E. A. (2019). Regeneration of Dermis: Scarring and Cells Involved. *Cells*, *8*(6), 607.
15. Ruggiero, F., Roulet, M., & Bonod-Bidaud, C. (2005). Les collagènes du derme: au-delà de leurs propriétés structurales [Dermis collagens: beyond their structural properties]. *Journal de la Societe de biologie*, *199*(4), 301–311.
16. el Sayed, S. O., & Dyson, M. (1993). Responses of dermal mast cells to injury. *Journal of anatomy*, *182 (Pt 3)*(Pt 3), 369–376.
17. van Dongen, J. A., Harmsen, M. C., van der Lei, B., & Stevens, H. P. (2018). Augmentation of Dermal Wound Healing by Adipose Tissue-Derived Stromal Cells (ASC). *Bioengineering (Basel, Switzerland)*, *5*(4), 91.
18. Driskell, R. R., Jahoda, C. A., Chuong, C. M., Watt, F. M., & Horsley, V. (2014). Defining dermal adipose tissue. *Experimental dermatology*, *23*(9), 629–631.
19. Farage, M. A., Miller, K. W., Elsner, P., & Maibach, H. I. (2008). Intrinsic and extrinsic factors in skin ageing: a review. *International journal of cosmetic science*, *30*(2), 87–95.
20. Flament, F., Bazin, R., Laquieze, S., Rubert, V., Simonpietri, E., & Piot, B. (2013). Effect of the sun on visibleclinical signsofaging in Caucasian skin. *Clinical, cosmeticandinvestigationaldermatology*, *6*, 221–232.
21. Gems, D., & Partridge, L. (2013). Genetics of longevity in model organisms: debates and paradigm shifts. *Annual review of physiology*, *75*, 621–644.
22. Kirkwood T. B. (2005). Understanding the odd science of aging. *Cell*, *120*(4), 437–447.

23. Vijg, J., & Campisi, J. (2008). Puzzles, promises and a cure for ageing. *Nature*, *454*(7208), 1065–1071.
24. López-Otín, C., Blasco, M. A., Partridge, L., Serrano, M., & Kroemer, G. (2013). The hallmarks of aging. *Cell*, *153*(6), 1194–1217.
25. Moskalev, A. A., Shaposhnikov, M. V., Plyusnina, E. N., Zhavoronkov, A., Budovsky, A., Yanai, H., & Fraifeld, V. E. (2013). The role of DNA damage and repair in aging through the prism of Koch-like criteria. *Ageing research reviews*, *12*(2), 661–684.
26. Hoeijmakers J. H. (2009). DNA damage, aging, and cancer. *The New England journal of medicine*, *361*(15), 1475–1485.
27. Faggioli, F., Wang, T., Vijg, J., & Montagna, C. (2012). Chromosome-specific accumulation of aneuploidy in the aging mouse brain. *Human molecular genetics*, *21*(24), 5246–5253.
28. Wallace D. C. (2010). Mitochondrial DNA mutations in disease and aging. *Environmental and molecular mutagenesis*, *51*(5), 440–450.
29. Blackburn, E. H., Greider, C. W., & Szostak, J. W. (2006). Telomeres and telomerase: the path from maize, Tetrahymena and yeast to human cancer and aging. *Nature medicine*, *12*(10),1133–1138.
30. Maynard, S., Fang, E. F., Scheibye-Knudsen, M., Croteau, D. L., & Bohr, V. A. (2015). DNA Damage, DNA Repair, Aging, and Neurodegeneration. *Cold Spring Harbor perspectives in medicine*, *5*(10), a025130.
31. Greer, E. L., Maures, T. J., Hauswirth, A. G., Green, E. M., Leeman, D. S., Maro, G. S., Han, S., Banko, M. R., Gozani, O., & Brunet, A. (2010). Members of the H3K4 trimethylation complex regulate lifespan in a germline-dependent manner in C. elegans. *Nature*, *466*(7304), 383–387.
32. Maegawa, S., Hinkal, G., Kim, H. S., Shen, L., Zhang, L., Zhang, J., Zhang, N., Liang, S., Donehower, L. A., & Issa, J. P. (2010). Widespread and tissue specific age-related DNA methylation changes in mice. *Genome research*, *20*(3), 332–340.
33. Cakouros, D., & Gronthos, S. (2019). Epigenetic Regulation of Bone Marrow Stem Cell Aging: Revealing Epigenetic Signatures associated with Hematopoietic and Mesenchymal Stem Cell Aging. *Aging and disease*, *10*(1), 174–189.
34. Powers, E. T., Morimoto, R. I., Dillin, A., Kelly, J. W., & Balch, W. E. (2009). Biological and chemical approaches to diseases of proteostasis deficiency. *Annual review of biochemistry*, *78*, 959–991.
35. Tutar, L., & Tutar, Y. (2010). Heat shock proteins; an overview. *Current pharmaceutical biotechnology*, *11*(2), 216–222.
36. Kim, Y. E., Hipp, M. S., Bracher, A., Hayer-Hartl, M., & Hartl, F. U. (2013). Molecular chaperone functions in protein folding and proteostasis. *Annual review of biochemistry*, *82*, 323–355.
37. Mizushima, N., Levine, B., Cuervo, A. M., & Klionsky, D. J. (2008). Autophagy fights disease through cellular self-digestion. *Nature*, *451*(7182), 1069–1075.
38. Fontana, L., Partridge, L., & Longo, V. D. (2010). Extending healthy life span--from yeast to humans. *Science (New York, N.Y.)*, *328*(5976), 321–326.
39. Barzilai, N., Huffman, D. M., Muzumdar, R. H., & Bartke, A. (2012). The critical role of metabolic pathways in aging. *Diabetes*, *61*(6), 1315–1322.
40. Barbosa, M. C., Grosso, R. A., & Fader, C. M. (2019). Hallmarks of Aging: An Autophagic Perspective. *Frontiers in endocrinology*, *9*, 790.
41. Perls, T., Kunkel, L., & Puca, A. (2002). The genetics of aging. *Current opinion in genetics & development*, *12*(3), 362–369.
42. Green, D. R., Galluzzi, L., & Kroemer, G. (2011). Mitochondria and the autophagy-inflammation-cell death axis in organismal aging. *Science (New York, N.Y.)*, *333*(6046), 1109–1112.
43. Hayflick, L., Moorhead, P. S. (1961). The serial cultivation of human diploid cell strains. *Experimental cell research*, *25*, 585–621.
44. Hayflick, L. (1965). The limited in vitro lifetime of human diploid cell strains. *Experimental cell research*, *37*, 614–636.

45. Sedivy J. M. (1998). Can ends justify the means?: telomeres and the mechanisms of replicative senescenceand immortalization in mammaliancells. *Proceedingsofthe National Academyof Sciences of the United States of America*, *95*(16), 9078–9081.
46. Harley, C. B., Futcher, A. B., & Greider, C. W. (1990). Telomeres shorten during ageing of human fibroblasts. *Nature*, *345*(6274), 458–460.
47. Bodnar, A. G., Ouellette, M., Frolkis, M., Holt, S. E., Chiu, C. P., Morin, G. B., Harley, C. B., Shay, J. W., Lichtsteiner, S., & Wright, W. E. (1998). Extension of life-span by introduction of telomerase into normal human cells. *Science (New York, N.Y.)*, *279*(5349), 349–352.
48. Liu, X. L., Ding, J., & Meng, L. H. (2018). Oncogene-induced senescence: a double edged sword in cancer. *Acta pharmacologica Sinica*, *39*(10), 1553–1558.
49. Courtois-Cox, S., Jones, S. L., & Cichowski, K. (2008). Many roads lead to oncogene-induced senescence. *Oncogene*, *27*(20), 2801–2809.
50. Serrano, M., Lin, A. W., McCurrach, M. E., Beach, D., & Lowe, S. W. (1997). Oncogenic ras provokes premature cell senescence associated with accumulation of p53 and p16INK4a. *Cell*, *88*(5), 593–602.
51. Patil, P., Falabella, M., Saeed, A., Lee, D., Kaufman, B., Shiva, S., Croix, C. S., Van Houten, B., Niedernhofer, L. J., Robbins, P. D., Lee, J., Gwendolyn, S., & Vo, N. V. (2019). Oxidative stress-induced senescence markedly increases disc cell bioenergetics. *Mechanisms of ageing and development*, *180*, 97–106.
52. Dimozi, A., Mavrogonatou, E., Sklirou, A., & Kletsas, D. (2015). Oxidative stress inhibits the proliferation, induces premature senescence and promotes a catabolic phenotype in human nucleus pulposus intervertebral disc cells. *European cells & materials*,*30*, 89–103.
53. Coluzzi, E., Leone, S., & Sgura, A. (2019). Oxidative Stress Induces Telomere Dysfunction and Senescence by Replication Fork Arrest. *Cells*, *8*(1), 19.
54. Wiley, C. D., Velarde, M. C., Lecot, P., Liu, S., Sarnoski, E. A., Freund, A., Shirakawa, K., Lim, H. W., Davis, S. S., Ramanathan, A., Gerencser, A. A., Verdin, E., & Campisi, J. (2016). Mitochondrial Dysfunction Induces Senescence with a Distinct Secretory Phenotype. *Cell metabolism*, *23*(2), 303–314.
55. Chapman, J., Fielder, E., & Passos, J. F. (2019). Mitochondrial dysfunction and cell senescence: deciphering a complex relationship. *FEBS letters*, *593*(13), 1566–1579.
56. Qian, Y., & Chen, X. (2010). Tumor suppression by p53: making cells senescent. *Histology and histopathology*, *25*(4), 515–526.
57. Campisi J. (2001). Cellular senescence as a tumor-suppressor mechanism. *Trends in cell biology*, *11*(11), S27–S31.
58. Rentschler, M., Chen, Y., Pahl, J., Soria-Martinez, L., Braumüller, H., Brenner, E., Bischof, O., Röcken, M., & Wieder, T. (2018). Nuclear Translocation of Argonaute 2 in Cytokine-Induced Senescence. *Cellular physiology and biochemistry : international journal of experimental cellular physiology, biochemistry, and pharmacology*, *51*(3), 1103–1118.
59. Ortiz-Montero, P., Londoño-Vallejo, A., & Vernot, J. P. (2017). Senescence-associated IL-6 and IL-8 cytokines induce a self- and cross-reinforced senescence/inflammatory milieu strengthening tumorigenic capabilities in the MCF-7 breast cancer cell line. *Cell communication and signaling : CCS*, *15*(1), 17.
60. Lewis, D. A., Yi, Q., Travers, J. B., & Spandau, D. F. (2008). UVB-induced senescence in human keratinocytes requires a functional insulin-like growth factor-1 receptor and p53. *Molecular biology of the cell*, *19*(4), 1346–1353.
61. Li, M., You, L., Xue, J., & Lu, Y. (2018). Ionizing Radiation-Induced Cellular Senescence in Normal, Non-transformed Cells and the Involved DNA Damage Response: A Mini Review. *Frontiers in pharmacology*, *9*, 522.
62. Ewald, J. A., Desotelle, J. A., Wilding, G., & Jarrard, D. F. (2010). Therapy-induced senescence in cancer. *Journal of the National Cancer Institute*, *102*(20), 1536–1546.

63. Achuthan, S., Santhoshkumar, T. R., Prabhakar, J., Nair, S. A., & Pillai, M. R. (2011). Drug-induced senescence generates chemoresistant stemlike cells with low reactive oxygen species. *The Journal of biological chemistry*, *286*(43), 37813–37829.
64. Mao, Z., Ke, Z., Gorbunova, V., & Seluanov, A. (2012). Replicatively senescent cells are arrested in G1 and G2 phases. *Aging*, *4*(6), 431–435.
65. Gire, V., & Dulic, V. (2015). Senescence from G2 arrest, revisited. *Cell cycle (Georgetown, Tex.)*, *14*(3), 297–304.
66. Haferkamp, S., Tran, S. L., Becker, T. M., Scurr, L. L., Kefford, R. F., & Rizos, H. (2009). The relative contributions of the p53 and pRb pathways in oncogene-induced melanocyte senescence. *Aging*, *1*(6), 542–556
67. Lujambio A. (2016). To clear, or not to clear (senescent cells)? That is the question. *BioEssays : news and reviews in molecular, cellular and developmental biology*, *38 Suppl 1*, S56–S64.
68. hilds, B. G., Durik, M., Baker, D. J., & van Deursen, J. M. (2015). Cellular senescence in aging and age-related disease: from mechanisms to therapy. *Nature medicine*, *21*(12), 1424–1435.
69. Fumagalli, M., Rossiello, F., Clerici, M., Barozzi, S., Cittaro, D., Kaplunov, J. M., Bucci, G., Dobreva, M., Matti, V., Beausejour, C. M., Herbig, U., Longhese, M. P., & d'Adda di Fagagna, F. (2012). Telomeric DNA damage is irreparable and causes persistent DNA-damage-response activation. *Nature cell biology*, *14*(4), 355–365.
70. d'Adda di Fagagna F. (2008). Living on a break: cellular senescence as a DNA-damage response. *Nature reviews. Cancer*, *8*(7), 512–522.
71. Lowe, S. W., Cepero, E., & Evan, G. (2004). Intrinsic tumour suppression. *Nature*, *432*(7015), 307–315.
72. Kastenhuber, E. R., & Lowe, S. W. (2017). Putting p53 in Context. *Cell*, *170*(6), 1062–1078.
73. Endo-Munoz, L., Dahler, A., Teakle, N., Rickwood, D., Hazar-Rethinam, M., Abdul-Jabbar, I., Sommerville, S., Dickinson, I., Kaur, P., Paquet-Fifield, S., & Saunders, N. (2009). E2F7 can regulate proliferation, differentiation, and apoptotic responses in human keratinocytes: implications for cutaneous squamous cell carcinoma formation. *Cancer research*, *69*(5), 1800–1808.
74. Shay, J. W., Pereira-Smith, O. M., & Wright, W. E. (1991). A role for both RB and p53 in the regulation of human cellular senescence. *Experimental cell research*, *196*(1), 33–39.
75. Beauséjour, C. M., Krtolica, A., Galimi, F., Narita, M., Lowe, S. W., Yaswen, P., & Campisi, J. (2003). Reversal of human cellular senescence: roles of the p53 and p16 pathways. *The EMBO journal*, *22*(16), 4212–4222.
76. Sharpless, N. E., & Depinho, R. A. (2006). The mighty mouse: genetically engineered mouse models in cancer drug development. *Nature reviews. Drug discovery*, *5*(9),741–754.
77. Kim, W. Y., & Sharpless, N. E. (2006). The regulation of INK4/ARF in cancer and aging. *Cell*, *127*(2), 265–275.
78. Chen, J., Huang, X., Halicka, D., Brodsky, S., Avram, A., Eskander, J., Bloomgarden, N. A., Darzynkiewicz, Z., & Goligorsky, M. S. (2006). Contribution of p16INK4a and p21CIP1 pathways to induction of premature senescence of human endothelial cells: permissive role of p53. *American journal of physiology. Heart and circulatory physiology*, *290*(4), H1575–H1586.
79. Gil, J., & Peters, G. (2006). Regulation of the INK4b-ARF-INK4a tumour suppressor locus: all for one or one for all. *Nature reviews. Molecular cell biology*, *7*(9), 667–677.
80. Ritschka, B., Storer, M., Mas, A., Heinzmann, F., Ortells, M. C., Morton, J. P., Sansom, O. J., Zender, L., & Keyes, W. M. (2017). The senescence-associated secretory phenotype induces cellular plasticity and tissue regeneration. *Genes & development*, *31*(2), 172–183.
81. Tu, Q., Hao, J., Zhou, X., Yan, L., Dai, H., Sun, B., Yang, D., An, S., Lv, L., Jiao, B., Chen, C., Lai, R., Shi, P., & Zhao, X. (2018). CDKN2B deletion is essential for pancreatic cancer development instead of unmeaningful co-deletion due to juxtaposition to CDKN2A. *Oncogene*, *37*(1), 128–138.
82. Sharpless, N. E., & Sherr, C. J. (2015). Forging a signature of in vivo senescence. *Nature reviews. Cancer*, *15*(7), 397–408.

83. Kuilman, T., & Peeper, D. S. (2009). Senescence-messaging secretome: SMS-ing cellular stress. *Nature reviews. Cancer*, *9*(2), 81–94.
84. Coppé, J. P., Desprez, P. Y., Krtolica, A., & Campisi, J. (2010). The senescence-associated secretory phenotype: the dark side of tumor suppression. *Annual review of pathology*, *5*, 99–118.
85. Lujambio A. (2016). To clear, or not to clear (senescent cells)? That is the question. *BioEssays : news and reviews in molecular, cellular and developmental biology*, *38 Suppl 1*, S56–S64.
86. Muñoz-Espín, D., & Serrano, M. (2014). Cellular senescence: from physiology to pathology. *Nature reviews. Molecular cell biology*, *15*(7), 482–496.
87. Ohtani N. (2019). Deciphering the mechanism for induction of senescence-associated secretory phenotype (SASP) and its role in aging and cancer development. *Journal of biochemistry*, mvz055. Advance online publication.
88. Herranz, N., & Gil, J. (2018). Mechanisms and functions of cellular senescence. *The Journal of clinical investigation*, *128*(4), 1238–1246.
89. Crescenzi, E., De Palma, R., & Leonardi, A. (2012). Senescence and NFκB: A trojan horse in tumors?. *Oncoimmunology*, *1*(9), 1594–1597.
90. Acosta, J. C., Banito, A., Wuestefeld, T., Georgilis, A., Janich, P., Morton, J. P., Athineos, D., Kang, T. W., Lasitschka, F., Andrulis, M., Pascual, G., Morris, K. J., Khan, S., Jin, H., Dharmalingam, G., Snijders, A. P., Carroll, T., Capper, D., Pritchard, C., Inman, G. J., … Gil, J. (2013). A complex secretory program orchestrated by the inflammasome controls paracrine senescence. *Nature cell biology*, *15*(8), 978–990.
91. Nelson, G., Wordsworth, J., Wang, C., Jurk, D., Lawless, C., Martin-Ruiz, C., & von Zglinicki, T. (2012). A senescent cell bystander effect: senescence-induced senescence. *Aging cell*, *11*(2), 345–349.
92. Krtolica, A., Parrinello, S., Lockett, S., Desprez, P. Y., & Campisi, J. (2001). Senescent fibroblasts promote epithelial cell growth and tumorigenesis: a link between cancer and aging. *Proceedings of the National Academy of Sciences of the United States of America*, *98*(21), 12072–12077.
93. Coppé, J. P., Kauser, K., Campisi, J., & Beauséjour, C. M. (2006). Secretion of vascular endothelial growth factor by primary human fibroblasts at senescence. *The Journal of biological chemistry*, *281*(40), 29568–29574.
94. Kang, T. W., Yevsa, T., Woller, N., Hoenicke, L., Wuestefeld, T., Dauch, D., Hohmeyer, A., Gereke, M., Rudalska, R., Potapova, A., Iken, M., Vucur, M., Weiss, S., Heikenwalder, M., Khan, S., Gil, J., Bruder, D., Manns, M., Schirmacher, P., Tacke, F., … Zender, L. (2011). Senescence surveillance of pre-malignant hepatocytes limits liver cancer development. *Nature*, *479*(7374), 547–551.
95. Eggert, T., Wolter, K., Ji, J., Ma, C., Yevsa, T., Klotz, S., Medina-Echeverz, J., Longerich, T., Forgues, M., Reisinger, F., Heikenwalder, M., Wang, X. W., Zender, L., & Greten, T. F. (2016). Distinct Functions of Senescence-Associated Immune Responses in Liver Tumor Surveillance and Tumor Progression. *Cancer cell*, *30*(4), 533–547.
96. Franceschi, C., & Campisi, J. (2014). Chronic inflammation (inflammaging) and its potential contribution to age-associated diseases. *The journals of gerontology. Series A, Biological sciences and medical sciences*, *69 Suppl 1*, S4–S9.
97. Baker, D. J., Wijshake, T., Tchkonia, T., LeBrasseur, N. K., Childs, B. G., van de Sluis, B., Kirkland, J. L., & van Deursen, J. M. (2011). Clearance of p16Ink4a-positive senescent cells delays ageing-associated disorders. *Nature*, *479*(7372), 232–236.
98. Rodier, F., Muñoz, D. P., Teachenor, R., Chu, V., Le, O., Bhaumik, D., Coppé, J. P., Campeau, E., Beauséjour, C. M., Kim, S. H., Davalos, A. R., & Campisi, J. (2011). DNA-SCARS: distinct nuclear structures that sustain damage-induced senescence growth arrest and inflammatory cytokine secretion. *Journal of cell science*, *124*(Pt 1), 68–81.
99. Baar, M. P., Brandt, R., Putavet, D. A., Klein, J., Derks, K., Bourgeois, B., Stryeck, S., Rijksen, Y., van Willigenburg, H., Feijtel, D. A., van der Pluijm, I., Essers, J., van Cappellen, W. A., van IJcken, W. F., Houtsmuller, A. B., Pothof, J., de Bruin, R., Madl, T., Hoeijmakers, J., Campisi, J., … de Keizer, P.

(2017). Targeted Apoptosis of Senescent Cells Restores Tissue Homeostasis in Response to Chemotoxicity and Aging. *Cell*, *169*(1), 132–147.e16.

100. Dimri, G. P., Lee, X., Basile, G., Acosta, M., Scott, G., Roskelley, C., Medrano, E. E., Linskens, M., Rubelj, I., & Pereira-Smith, O. (1995). A biomarker that identifies senescent human cells in culture and in aging skin in vivo. *Proceedings of the National Academy of Sciences of the United States of America*, *92*(20), 9363–9367.
101. Ressler, S., Bartkova, J., Niederegger, H., Bartek, J., Scharffetter-Kochanek, K., Jansen-Dürr, P., & Wlaschek, M. (2006). p16INK4A is a robust in vivo biomarker of cellular aging in human skin. *Aging cell*, *5*(5), 379–389.
102. Pereira, B. I., Devine, O. P., Vukmanovic-Stejic, M., Chambers, E. S., Subramanian, P., Patel, N., Virasami, A., Sebire, N. J., Kinsler, V., Valdovinos, A., LeSaux, C. J., Passos, J. F., Antoniou, A., Rustin, M., Campisi, J., & Akbar, A. N. (2019). Senescent cells evade immune clearance via HLA-E-mediated NK and CD8^{+} T cell inhibition. *Nature communications*, *10*(1), 2387.
103. Narita, M., Nũnez, S., Heard, E., Narita, M., Lin, A. W., Hearn, S. A., Spector, D. L., Hannon, G. J., & Lowe, S. W. (2003). Rb-mediated heterochromatin formation and silencing of E2F target genes during cellular senescence. *Cell*, *113*(6), 703–716.
104. Funayama, R., & Ishikawa, F. (2007). Cellular senescence and chromatin structure. *Chromosoma*, *116*(5), 431–440.
105. Collado, M., Gil, J., Efeyan, A., Guerra, C., Schuhmacher, A. J., Barradas, M., Benguría, A., Zaballos, A., Flores, J. M., Barbacid, M., Beach, D., & Serrano, M. (2005). Tumour biology: senescence in premalignant tumours. *Nature*, *436*(7051), 642.
106. Chen, Z., Trotman, L. C., Shaffer, D., Lin, H. K., Dotan, Z. A., Niki, M., Koutcher, J. A., Scher, H. I., Ludwig, T., Gerald, W., Cordon-Cardo, C., & Pandolfi, P. P. (2005). Crucial role of p53-dependent cellular senescence in suppression of Pten-deficient tumorigenesis. *Nature*, *436*(7051), 725–730.
107. Lazzerini Denchi, E., Attwooll, C., Pasini, D., & Helin, K. (2005). Deregulated E2F activity induces hyperplasia and senescence-like features in the mouse pituitary gland. *Molecular and cellular biology*, *25*(7), 2660–2672.
108. Coppé, J. P., Patil, C. K., Rodier, F., Sun, Y., Muñoz, D. P., Goldstein, J., Nelson, P. S., Desprez, P. Y., & Campisi, J. (2008). Senescence-associated secretory phenotypes reveal cell-nonautonomous functions of oncogenic RAS and the p53 tumor suppressor. *PLoS biology*, *6*(12), 2853–2868.
109. Sedelnikova, O. A., Horikawa, I., Redon, C., Nakamura, A., Zimonjic, D. B., Popescu, N. C., & Bonner, W. M. (2008). Delayed kinetics of DNA double-strand break processing in normal and pathological aging. *Aging cell*, *7*(1), 89–100.
110. Debacq-Chainiaux, F., Erusalimsky, J. D., Campisi, J., & Toussaint, O. (2009). Protocols to detect senescence-associated beta-galactosidase (SA-betagal) activity, a biomarker of senescent cells in culture and in vivo. *Nature protocols*, *4*(12), 1798–1806.
111. Lee, B. Y., Han, J. A., Im, J. S., Morrone, A., Johung, K., Goodwin, E. C., Kleijer, W. J., DiMaio, D., & Hwang, E. S. (2006). Senescence-associated beta-galactosidase is lysosomal beta-galactosidase. *Aging cell*, *5*(2), 187–195.
112. Yang, N. C., & Hu, M. L. (2005). The limitations and validities of senescence associated-beta-galactosidase activity as an aging marker for human foreskin fibroblast Hs68 cells. *Experimental gerontology*, *40*(10), 813–819.
113. Barbosa, M. C., Grosso, R. A., & Fader, C. M. (2019). Hallmarks of Aging: An Autophagic Perspective. *Frontiers in endocrinology*, *9*, 790.
114. Tomaru, U., Takahashi, S., Ishizu, A., Miyatake, Y., Gohda, A., Suzuki, S., Ono, A., Ohara, J., Baba, T., Murata, S., Tanaka, K., & Kasahara, M. (2012). Decreased proteasomal activity causes age-

related phenotypes and promotes the development of metabolic abnormalities. *The American journal of pathology*, *180*(3), 963–972.
115. Lim, K. L., & Zhang, C. W. (2013). Molecular events underlying Parkinson's disease - an interwoven tapestry. *Frontiers in neurology*, *4*, 33.
116. Ohsumi, Y., & Mizushima, N. (2004). Two ubiquitin-like conjugation systems essential for autophagy. *Seminars in cell & developmental biology*, *15*(2), 231–236.
117. Kaushik, S., & Cuervo, A. M. (2018). The coming of age of chaperone-mediated autophagy. *Nature reviews. Molecular cell biology*, *19*(6), 365–381.
118. Deretic, V., Saitoh, T., & Akira, S. (2013). Autophagy in infection, inflammation and immunity. *Nature reviews. Immunology*, *13*(10), 722–737.
119. Mizushima, N., Levine, B., Cuervo, A. M., & Klionsky, D. J. (2008). Autophagy fights disease through cellular self-digestion. *Nature*, *451*(7182), 1069–1075.
120. Condello, M., Pellegrini, E., Caraglia, M., & Meschini, S. (2019). Targeting Autophagy to Overcome Human Diseases. *International journal of molecular sciences*, *20*(3), 725.
121. Mukhopadhyay, D., & Riezman, H. (2007). Proteasome-independent functions of ubiquitin in endocytosis and signaling. *Science (New York, N.Y.)*, *315*(5809), 201–205.
122. Ikeda, F., & Dikic, I. (2008). Atypical ubiquitin chains: new molecular signals. 'Protein Modifications: Beyond the Usual Suspects' review series. *EMBO reports*, *9*(6), 536–542.
123. Liu, W. J., Ye, L., Huang, W. F., Guo, L. J., Xu, Z. G., Wu, H. L., Yang, C., & Liu, H. F. (2016). p62 links the autophagy pathway and the ubiqutin-proteasome system upon ubiquitinated protein degradation. *Cellular & molecular biology letters*, *21*, 29.
124. Demishtein, A., Fraiberg, M., Berko, D., Tirosh, B., Elazar, Z., & Navon, A. (2017). SQSTM1/p62-mediated autophagy compensates for loss of proteasome polyubiquitin recruiting capacity. *Autophagy*, *13*(10), 1697–1708.
125. Hansen, M., Rubinsztein, D. C., & Walker, D. W. (2018). Autophagy as a promoter of longevity: insights from model organisms. *Naturereviews. Molecularcellbiology*, *19*(9), 579–593.
126. Papadopoli, D., Boulay, K., Kazak, L., Pollak, M., Mallette, F., Topisirovic, I., & Hulea, L. (2019). mTOR as a central regulator of lifespan and aging. *F1000Research*, *8*, F1000 Faculty Rev-998.
127. Mizushima N. (2010). The role of the Atg1/ULK1 complex in autophagy regulation. *Current opinion in cell biology*, *22*(2), 132–139.
128. Dunlop, E. A., & Tee, A. R. (2009). Mammalian target of rapamycin complex 1: signalling inputs, substrates and feedback mechanisms. *Cellular signalling*, *21*(6), 827–835.
129. Dunlop, E. A., & Tee, A. R. (2014). mTOR and autophagy: a dynamic relationship governed by nutrients and energy. *Seminars in cell & developmental biology*, *36*, 121–129.
130. Jung, C. H., Ro, S. H., Cao, J., Otto, N. M., & Kim, D. H. (2010). mTOR regulation of autophagy. *FEBS letters*, *584*(7), 1287–1295.
131. Mammucari, C., Milan, G., Romanello, V., Masiero, E., Rudolf, R., Del Piccolo, P., Burden, S. J., Di Lisi, R., Sandri, C., Zhao, J., Goldberg, A. L., Schiaffino, S., & Sandri, M. (2007). FoxO3 controls autophagy in skeletal muscle in vivo. *Cell metabolism*, *6*(6), 458–471.
132. Rubinsztein, D. C., Mariño, G., & Kroemer, G. (2011). Autophagy and aging. *Cell*, *146*(5), 682–695.
133. Maiuri, M. C., & Kroemer, G. (2019). Therapeutic modulation of autophagy: which disease comes first?. *Cell death and differentiation*, *26*(4),680–689.
134. Sarkar, S., Davies, J. E., Huang, Z., Tunnacliffe, A., & Rubinsztein, D. C. (2007). Trehalose, a novel mTOR-independent autophagy enhancer, accelerates the clearance of mutant huntingtin and alpha-synuclein. *The Journal of biological chemistry*, *282*(8), 5641–5652.
135. Aguib, Y., Heiseke, A., Gilch, S., Riemer, C., Baier, M., Schätzl, H. M., & Ertmer, A. (2009). Autophagy induction by trehalose counteracts cellular prion infection. *Autophagy*, *5*(3), 361–369.

136. Chen, X., Li, M., Li, L., Xu, S., Huang, D., Ju, M., Huang, J., Chen, K., & Gu, H. (2016). Trehalose, sucrose and raffinose are novel activators of autophagy in human keratinocytes through an mTOR-independent pathway. *Scientific reports*, *6*, 28423.
137. Gewirtz D. A. (2013). Autophagy and senescence: a partnership in search of definition. *Autophagy*, *9*(5), 808–812.
138. Kang, C., & Elledge, S. J. (2016). How autophagy both activates and inhibits cellular senescence. *Autophagy*, *12*(5), 898–899.
139. Tompkins, K. D., & Thorburn, A. (2019). Regulation of Apoptosis by Autophagy to Enhance Cancer Therapy. *The Yale journal of biology and medicine*, *92*(4), 707–718.
140. Schosserer, M., Grillari, J., & Breitenbach, M. (2017). The Dual Role of Cellular Senescence in Developing Tumors and Their Response to Cancer Therapy. *Frontiers in oncology*, *7*, 278.
141. Kwon, Y., Kim, J. W., Jeoung, J. A., Kim, M. S., & Kang, C. (2017). Autophagy Is Pro-Senescence When Seen in Close-Up, but Anti-Senescence in Long-Shot. *Molecules and cells*, *40*(9), 607–612.
142. Kravic, B., Behrends, C., & Meyer, H. (2020). Regulation of lysosome integrity andlysophagy by the ubiquitin-conjugating enzyme UBE2QL1. *Autophagy*, *16*(1), 179–180.
143. Kang, C., Xu, Q., Martin, T. D., Li, M. Z., Demaria, M., Aron, L., Lu, T., Yankner, B. A., Campisi, J., & Elledge, S. J. (2015). The DNA damage response induces inflammation and senescence by inhibiting autophagy of GATA4. *Science (New York, N.Y.)*, *349*(6255), aaa5612.
144. Wang, Y., Wang, X. D., Lapi, E., Sullivan, A., Jia, W., He, Y. W., Ratnayaka, I., Zhong, S., Goldin, R. D., Goemans, C. G., Tolkovsky, A. M., & Lu, X. (2012). Autophagic activity dictates the cellularresponsetooncogenic RAS. *Proceedings of the National Academyof Sciencesofthe United Statesof America*, *109*(33), 13325–13330.
145. Narita, M., Young, A. R., Arakawa, S., Samarajiwa, S. A., Nakashima, T., Yoshida, S., Hong, S., Berry, L. S., Reichelt, S., Ferreira, M., Tavaré, S., Inoki, K., Shimizu, S., & Narita, M. (2011). Spatial coupling of mTOR and autophagy augments secretory phenotypes. *Science (New York, N.Y.)*, *332*(6032), 966–970.
146. Horikawa, I., Fujita, K., Jenkins, L. M., Hiyoshi, Y., Mondal, A. M., Vojtesek, B., Lane, D. P., Appella, E., & Harris, C. C. (2014). Autophagic degradation of the inhibitory p53 isoform Δ133p53α as a regulatory mechanism for p53-mediated senescence. *Nature communications*, *5*, 4706.
147. Lenain, C., Gusyatiner, O., Douma, S., van den Broek, B., & Peeper, D. S. (2015). Autophagy-mediated degradation of nuclear envelope proteins during oncogene-induced senescence. *Carcinogenesis*, *36*(11), 1263–1274.
148. Capparelli, C., Chiavarina, B., Whitaker-Menezes, D., Pestell, T. G., Pestell, R. G., Hulit, J., Andò, S., Howell, A., Martinez-Outschoorn, U. E., Sotgia, F., & Lisanti, M. P. (2012). CDK inhibitors (p16/p19/p21) induce senescence and autophagy in cancer-associated fibroblasts, "fueling" tumor growth via paracrine interactions, without an increase in neo-angiogenesis. *Cell cycle (Georgetown, Tex.)*, *11*(19), 3599–3610.
149. Hu, X., & Zhang, H. (2019). Doxorubicin-Induced Cancer Cell Senescence Shows a Time Delay Effect and Is Inhibited by Epithelial-Mesenchymal Transition (EMT). *Medical science monitor : international medical journal of experimental and clinical research*, *25*, 3617–3623.
150. Reimand, J., Isserlin, R., Voisin, V., Kucera, M., Tannus-Lopes, C., Rostamianfar, A., Wadi, L., Meyer, M., Wong, J., Xu, C., Merico, D., & Bader, G. D. (2019). Pathway enrichment analysis and visualization of omics data using g:Profiler, GSEA, Cytoscape and EnrichmentMap. *Nature protocols*, *14*(2), 482–517.
151. Goon, JA. (2011). Differential protein expression in senescent human skin fibroblasts and stress induced premature senescence (SIPS) fibroblasts. *Sains Malaysiana*.; 40(11):1247–1253

152. Trougakos, I. P., Saridaki, A., Panayotou, G., & Gonos, E. S. (2006). Identification of differentially expressed proteins in senescent human embryonic fibroblasts. *Mechanisms of ageing and development*, *127*(1), 88–92.
153. Hammad, G., Legrain, Y., Touat-Hamici, Z., Duhieu, S., Cornu, D., Bulteau, A. L., & Chavatte, L. (2018). Interplay between Selenium Levels and Replicative Senescence in WI-38 Human Fibroblasts: A Proteomic Approach. *Antioxidants (Basel, Switzerland)*, *7*(1), 19.
154. Cong, Y. S., Fan, E., & Wang, E. (2006). Simultaneous proteomic profiling of four different growth states of human fibroblasts, using amine-reactive isobaric tagging reagents and tandem mass spectrometry. *Mechanisms of ageing and development*, *127*(4), 332–343.
155. Wiley, C. D., Davis, S., & Ramanathan, A. (2019). Measurement of Metabolite Changes in Senescent Cells by Mass Spectrometry. *Methodsin molecular biology (Clifton, N.J.)*, *1896*, 139–147.
156. Raijmakers, R., Heck, A. J., & Mohammed, S. (2009). Assessing biological variation and protein processing in primary human leukocytes by automated multiplex stable isotope labeling coupled to 2 dimensional peptide separation. *Molecular bioSystems*, *5*(9), 992–1003.
157. Delahunty, C., & Yates, J. R., 3rd (2005). Protein identification using 2D-LC-MS/MS. *Methods (San Diego, Calif.)*, *35*(3), 248–255.
158. Tan, J. K., Jaafar, F., & Makpol, S. (2018). Proteomic profiling of senescent human diploid fibroblasts treated with gamma-tocotrienol. *BMCcomplementaryandalternativemedicine*, *18*(1), 314.
159. Meng, Q., Gao, J., Zhu, H., He, H., Lu, Z., Hong, M., & Zhou, H. (2018). The proteomic study of serially passaged human skin fibroblast cells uncovers down-regulation of the chromosome condensin complex proteins involved in replicative senescence. *Biochemical and biophysical research communications*, *505*(4), 1112–1120.
160. Yang, K. E., Jang, H. J., Hwang, I. H., Hong, E. M., Lee, M. G., Lee, S., Jang, I. S., & Choi, J. S. (2020). Stereoisomer-specific ginsenoside 20(*S*)-Rg3 reverses replicative senescence of human diploid fibroblasts via Akt-mTOR-Sirtuin signaling. *Journal of ginseng research*, *44*(2), 341–349.
161. Benvenuti, S., Cramer, R., Quinn, C. C., Bruce, J., Zvelebil, M., Corless, S., Bond, J., Yang, A., Hockfield, S., Burlingame, A. L., Waterfield, M. D., & Jat, P. S. (2002). Differential proteome analysis of replicative senescence in rat embryo fibroblasts. *Molecular & cellular proteomics : MCP*, *1*(4), 280–292.
162. Kritsilis, M., V Rizou, S., Koutsoudaki, P. N., Evangelou, K., Gorgoulis, V. G., & Papadopoulos, D. (2018). Ageing, Cellular Senescence and Neurodegenerative Disease. *International journal of molecular sciences*, *19*(10), 2937.
163. Nagano, T., Nakano, M., Nakashima, A., Onishi, K., Yamao, S., Enari, M., Kikkawa, U., & Kamada, S. (2016). Identification of cellular senescence-specific genes by comparative transcriptomics. *Scientific reports*, *6*, 31758.
164. Walsh, C. T., Garneau-Tsodikova, S., & Gatto, G. J., Jr (2005). Protein posttranslational modifications: the chemistry of proteome diversifications. *Angewandte Chemie (International ed. in English)*, *44*(45), 7342–7372.
165. Khoury, G. A., Baliban, R. C., & Floudas, C. A. (2011). Proteome-wide post-translational modification statistics: frequency analysis and curation of the swiss-prot database. *Scientific reports*, *1*, 90.
166. Vlastaridis, P., Kyriakidou, P., Chaliotis, A., Van de Peer, Y., Oliver, S. G., & Amoutzias, G. D. (2017). Estimating the total number of phosphoproteins and phosphorylation sites in eukaryotic proteomes. *GigaScience*, *6*(2), 1–11.
167. Yang, F., Stenoien, D. L., Strittmatter, E. F., Wang, J., Ding, L., Lipton, M. S., Monroe, M. E., Nicora, C. D., Gristenko, M. A., Tang, K., Fang, R., Adkins, J. N., Camp, D. G., 2nd, Chen, D. J., & Smith, R. D. (2006). Phosphoproteome profiling of human skin fibroblast cells in response to low- and high-dose irradiation. *Journal of proteome research*, *5*(5), 1252–1260.
168. Subramanian, A., Tamayo, P., Mootha, V. K., Mukherjee, S., Ebert, B. L., Gillette, M. A., Paulovich, A., Pomeroy, S. L., Golub, T. R., Lander, E. S., & Mesirov, J. P. (2005). Gene set

enrichment analysis: a knowledge-based approach for interpreting genome-wide expression profiles. *Proceedings of the National Academy of Sciences of the United States of America*, *102*(43), 15545–15550.

169. Young, A. R., & Narita, M. (2009). SASP reflects senescence. *EMBO reports*, *10*(3), 228–230.
170. Reddel R. R. (2010). Senescence: an antiviral defense that is tumor suppressive?. *Carcinogenesis*, *31*(1), 19–26.
171. Zhang, S., Yi, C., Li, C., Zhang, F., Peng, J., Wang, Q., Liu, X., Ye, X., Li, P., Wu, M., Yan, Q., Guo, W., Niu, X., Feng, L., Pan, W., Chen, L., & Qu, L. (2019). Chloroquine inhibits endosomal viral RNA release and autophagy-dependent viral replication and effectively prevents maternal to fetal transmission of Zika virus. *Antiviral research*, *169*, 104547.
172. Lennemann, N. J., & Coyne, C. B. (2015). Catch me if you can: the link between autophagy and viruses. *PLoS pathogens*, *11*(3), e1004685.
173. Wang, R., Zhu, Y., Zhao, J., Ren, C., Li, P., Chen, H., Jin, M., & Zhou, H. (2019). Autophagy Promotes Replication of Influenza A Virus *In Vitro*. *Journal of virology*, *93*(4), e01984-18.
174. Lu, S., Sung, T., Lin, N., Abraham, R. T., & Jessen, B. A. (2017). Lysosomal adaptation: How cells respond to lysosomotropic compounds. *PloS one*, *12*(3), e0173771.
175. Vincent, M. J., Bergeron, E., Benjannet, S., Erickson, B. R., Rollin, P. E., Ksiazek, T. G., Seidah, N. G., & Nichol, S. T. (2005). Chloroquine is a potent inhibitor of SARS coronavirus infection and spread. *Virology journal*, *2*, 69.
176. Colson, P., Rolain, J. M., & Raoult, D. (2020). Chloroquine for the 2019 novel coronavirus SARS-CoV-2. *International journal of antimicrobial agents*, *55*(3), 105923.
177. Gao, J., Tian, Z., & Yang, X. (2020). Breakthrough: Chloroquine phosphate has shown apparent efficacy in treatment of COVID-19 associated pneumonia in clinical studies. *Bioscience trends*, *14*(1), 72–73.
178. Liu, J., Cao, R., Xu, M., Wang, X., Zhang, H., Hu, H., Li, Y., Hu, Z., Zhong, W., & Wang, M. (2020). Hydroxychloroquine, a less toxic derivative of chloroquine, is effective in inhibiting SARS-CoV-2 infection in vitro. *Cell discovery*, *6*, 16.
179. Cavinato, M., Koziel, R., Romani, N., Weinmüllner, R., Jenewein, B., Hermann, M., Dubrac, S., Ratzinger, G., Grillari, J., Schmuth, M., & Jansen-Dürr, P. (2017). UVB-Induced Senescence of Human Dermal Fibroblasts Involves Impairment of Proteasome and Enhanced Autophagic Activity. *The journals of gerontology. Series A, Biological sciences and medical sciences*, *72*(5), 632–639.
180. Young, A. R., Narita, M., Ferreira, M., Kirschner, K., Sadaie, M., Darot, J. F., Tavaré, S., Arakawa, S., Shimizu, S., Watt, F. M., & Narita, M. (2009). Autophagy mediates the mitotic senescence transition. *Genes & development*, *23*(7), 798–803.
181. Slobodnyuk, K., Radic, N., Ivanova, S., Llado, A., Trempolec, N., Zorzano, A., & Nebreda, A. R. (2019). Autophagy-induced senescence is regulated by p38α signaling. *Cell death & disease*, *10*(6), 376.
182. aberge, R. M., Sun, Y., Orjalo, A. V., Patil, C. K., Freund, A., Zhou, L., Curran, S. C., Davalos, A. R., Wilson-Edell, K. A., Liu, S., Limbad, C., Demaria, M., Li, P., Hubbard, G. B., Ikeno, Y., Javors, M., Desprez, P. Y., Benz, C. C., Kapahi, P., Nelson, P. S., … Campisi, J. (2015). MTOR regulates the pro-tumorigenic senescence-associated secretory phenotype by promoting IL1A translation. *Nature cell biology*, *17*(8), 1049–1061.
183. Demidenko, Z. N., Zubova, S. G., Bukreeva, E. I., Pospelov, V. A., Pospelova, T. V., & Blagosklonny, M. V. (2009). Rapamycin decelerates cellular senescence. *Cell cycle (Georgetown, Tex.)*, *8*(12), 1888–1895.
184. Quarles, E., Basisty, N., Chiao, Y. A., Merrihew, G., Gu, H., Sweetwyne, M. T., Fredrickson, J., Nguyen, N. H., Razumova, M., Kooiker, K., Moussavi-Harami, F., Regnier, M., Quarles, C., MacCoss, M., & Rabinovitch, P. S. (2020). Rapamycin persistently improves cardiac function in aged, male and female mice, even following cessation of treatment. *Aging cell*, *19*(2), e13086.

185. Han, B. I., Hwang, S. H., & Lee, M. (2017). A progressive reduction in autophagic capacity contributes to induction of replicative senescence in Hs68 cells. *The international journal of biochemistry & cell biology*, *92*, 18–25.
186. Lerner, C., Bitto, A., Pulliam, D., Nacarelli, T., Konigsberg, M., Van Remmen, H., Torres, C., & Sell, C. (2013). Reduced mammalian target of rapamycin activity facilitates mitochondrial retrograde signaling and increases life span in normal human fibroblasts. *Aging cell*, *12*(6), 966–977.
187. Hansen, M., Rubinsztein, D. C., & Walker, D. W. (2018). Autophagy as a promoter of longevity: insightsfrommodel organisms. *Naturereviews. Molecularcellbiology*, *19*(9), 579–593.
188. Bareja, A., Lee, D. E., & White, J. P. (2019). Maximizing Longevity and Healthspan: Multiple Approaches All Converging on Autophagy. *Frontiers in cell and developmental biology*, *7*, 183.
189. Madeo, F., Zimmermann, A., Maiuri, M. C., & Kroemer, G. (2015). Essential role for autophagy in life span extension. *The Journal of clinical investigation*, *125*(1), 85–93.
190. Sodagam, L., Lewinska, A., Wnuk, M., & Rattan, S. (2017). Chronic exposure to rapamycinand episodic serum starvation modulate ageing of human fibroblasts in vitro. *Biogerontology*, *18*(5), 841–854.
191. Han, X., Tai, H., Wang, X., Wang, Z., Zhou, J., Wei, X., Ding, Y., Gong, H., Mo, C., Zhang, J., Qin, J., Ma, Y., Huang, N., Xiang, R., & Xiao, H. (2016). AMPK activation protects cells from oxidative stress-induced senescence via autophagic flux restoration and intracellular NAD(+) elevation. *Aging cell*, *15*(3), 416–427.
192. Chang, Y. C., Liu, H. W., Chen, Y. T., Chen, Y. A., Chen, Y. J., & Chang, S. J. (2018). Resveratrol protects muscle cells against palmitate-induced cellular senescence and insulin resistance through ameliorating autophagic flux. *Journal of food and drug analysis*, *26*(3), 1066–1074.
193. Tan, P., Wang, H., Zhan, J., Ma, X., Cui, X., Wang, Y., Wang, Y., Zhong, J., & Liu, Y. (2019). Rapamycin-induced miR-30a downregulation inhibits senescence of VSMCs by targeting Beclin1. *International journal of molecular medicine*, *43*(3), 1311–13
194. Fujii, S., Hara, H., Araya, J., Takasaka, N., Kojima, J., Ito, S., Minagawa, S., Yumino, Y., Ishikawa, T., Numata, T., Kawaishi, M., Hirano, J., Odaka, M., Morikawa, T., Nishimura, S., Nakayama, K., & Kuwano, K. (2012). Insufficient autophagy promotes bronchial epithelial cell senescence in chronic obstructive pulmonary disease. *Oncoimmunology*, *1*(5), 630–641.
195. Singh, K., Matsuyama, S., Drazba, J. A., & Almasan, A. (2012). Autophagy-dependent senescence in response to DNA damage and chronic apoptotic stress. *Autophagy*, *8*(2), 236–251.
196. Zhang, J. W., Zhang, S. S., Song, J. R., Sun, K., Zong, C., Zhao, Q. D., Liu, W. T., Li, R., Wu, M. C., & Wei, L. X. (2014). Autophagy inhibition switches low-dose camptothecin-induced premature senescence to apoptosis in human colorectal cancer cells. *Biochemical pharmacology*, *90*(3), 265–275.
197. Mizushima, N., Yoshimori, T., & Levine, B. (2010). Methods in mammalian autophagy research. *Cell*, *140*(3), 313–326.
198. Weichhart T. (2018). mTOR as Regulator of Lifespan, Aging, and Cellular Senescence: A Mini-Review. *Gerontology*, *64*(2), 127–134.
199. Mauthe, M., Orhon, I., Rocchi, C., Zhou, X., Luhr, M., Hijlkema, K. J., Coppes, R. P., Engedal, N., Mari, M., & Reggiori, F. (2018). Chloroquine inhibits autophagic flux by decreasing autophagosome-lysosome fusion. *Autophagy*, *14*(8), 1435–1455.
200. Elsemüller, A. K., Tomalla, V., Gärtner, U., Troidl, K., Jeratsch, S., Graumann, J., Baal, N., Hackstein, H., Lasch, M., Deindl, E., Preissner, K. T., & Fischer, S. (2019). Characterization of mast cell-derived rRNA-containing microvesicles and their inflammatory impact on endothelial cells. *FASEB journal : official publication of the Federation of American Societies for Experimental Biology*, *33*(4), 5457–5467.
201. Ren, B. J., Zhou, Z. W., Zhu, D. J., Ju, Y. L., Wu, J. H., Ouyang, M. Z., Chen, X. W., & Zhou, S. F. (2015). Alisertib Induces Cell Cycle Arrest, Apoptosis, Autophagy and Suppresses EMT in HT29 and Caco-2 Cells. *International journal of molecular sciences*, *17*(1), 41.

202. Hansen, I. S., Krabbendam, L., Bernink, J. H., Loayza-Puch, F., Hoepel, W., van Burgsteden, J. A., Kuijper, E. C., Buskens, C. J., Bemelman, W. A., Zaat, S., Agami, R., Vidarsson, G., van den Brink, G. R., de Jong, E. C., Wildenberg, M. E., Baeten, D., Everts, B., & den Dunnen, J. (2018). FcαRI co-stimulation converts human intestinal CD103+ dendritic cells into pro-inflammatory cells through glycolytic reprogramming. *Nature communications*, *9*(1), 863.
203. James, E. L., Michalek, R. D., Pitiyage, G. N., de Castro, A. M., Vignola, K. S., Jones, J., Mohney, R. P., Karoly, E. D., Prime, S. S., & Parkinson, E. K. (2015). Senescent human fibroblasts show increased glycolysis and redox homeostasis with extracellular metabolomes that overlap with those of irreparable DNA damage, aging, and disease. *Journal of proteome research*, *14*(4), 1854–1871.
204. Mizushima, N., Sugita, H., Yoshimori, T., & Ohsumi, Y. (1998). A new protein conjugation system in human. The counterpart of the yeast Apg12p conjugation system essential for autophagy. *The Journal of biological chemistry*, *273*(51), 33889–33892.
205. Klionsky, D. J., Cregg, J. M., Dunn, W. A., Jr, Emr, S. D., Sakai, Y., Sandoval, I. V., Sibirny, A., Subramani, S., Thumm, M., Veenhuis, M., & Ohsumi, Y. (2003). A unified nomenclature for yeast autophagy-related genes. *Developmental cell*, *5*(4), 539–545.
206. Sharma, K. B., Sharma, M., Aggarwal, S., Yadav, A. K., Bhatnagar, S., Vrati, S., & Kalia, M. (2019). Quantitative Proteome Analysis of *Atg5*-Deficient Mouse Embryonic Fibroblasts Reveals the Range of the Autophagy-Modulated Basal Cellular Proteome. *mSystems*, *4*(6), e00481-19.
207. Arakawa, S., Honda, S., Yamaguchi, H., & Shimizu, S. (2017). Molecular mechanisms and physiological roles of Atg5/Atg7-independent alternative autophagy. *Proceedings of the Japan Academy. Series B, Physical and biological sciences*, *93*(6), 378–385.
208. Korolchuk, V. I., Mansilla, A., Menzies, F. M., & Rubinsztein, D. C. (2009). Autophagy inhibition compromises degradation of ubiquitin-proteasome pathway substrates. *Molecular cell*, *33*(4), 517–527.
209. Komatsu, M., Waguri, S., Koike, M., Sou, Y. S., Ueno, T., Hara, T., Mizushima, N., Iwata, J., Ezaki, J., Murata, S., Hamazaki, J., Nishito, Y., Iemura, S., Natsume, T., Yanagawa, T., Uwayama, J., Warabi, E., Yoshida, H., Ishii, T., Kobayashi, A., … Tanaka, K. (2007). Homeostatic levels of p62 control cytoplasmic inclusion body formation in autophagy-deficient mice. *Cell*, *131*(6), 1149–1163.
210. Loos, B., du Toit, A., & Hofmeyr, J. H. (2014). Defining and measuring autophagosome flux-concept and reality. *Autophagy*, *10*(11), 2087–2096.
211. Shabalala, S., Muller, C., Louw, J., & Johnson, R. (2017). Polyphenols, autophagy and doxorubicin-induced cardiotoxicity. *Life sciences*, *180*, 160–170.
212. Xiao, B., Hong, L., Cai, X., Mei, S., Zhang, P., & Shao, L. (2019). The true colors of autophagy in doxorubicin-induced cardiotoxicity. *Oncology letters*, *18*(3), 2165–2172.
213. Kang, H. T., Lee, K. B., Kim, S. Y., Choi, H. R., & Park, S. C. (2011). Autophagy impairment induces premature senescence in primary human fibroblasts. *PloS one*, *6*(8), e23367.
214. Tai, H., Wang, Z., Gong, H., Han, X., Zhou, J., Wang, X., Wei, X., Ding, Y., Huang, N., Qin, J., Zhang, J., Wang, S., Gao, F., Chrzanowska-Lightowlers, Z. M., Xiang, R., & Xiao, H. (2017). Autophagy impairment with lysosomal and mitochondrial dysfunction is an important characteristic of oxidative stress-induced senescence. *Autophagy*, *13*(1), 99–113.
215. Yoon, Y. S., Cho, E. D., Jung Ahn, W., Won Lee, K., Lee, S. J., & Lee, H. J. (2017). Is trehalose an autophagic inducer? Unraveling the roles of non-reducing disaccharides on autophagic flux and alpha-synuclein aggregation. *Cell death & disease*, *8*(10), e3091.
216. Blázquez, M. A., Lagunas, R., Gancedo, C., & Gancedo, J. M. (1993). Trehalose-6-phosphate, a new regulator of yeast glycolysis that inhibits hexokinases. *FEBS letters*, *329*(1-2), 51–54.
217. Bonini, B. M., Van Dijck, P., & Thevelein, J. M. (2003). Uncoupling of the glucose growth defect and the deregulation of glycolysis in Saccharomyces cerevisiae Tps1 mutants expressing trehalose-6-phosphate-insensitive hexokinase from Schizosaccharomyces pombe. *Biochimica et biophysica acta*, *1606*(1-3), 83–93.

218. Thevelein, J. M., & Hohmann, S. (1995). Trehalose synthase: guard to the gate of glycolysis in yeast?. *Trends in biochemical sciences*, *20*(1), 3–10.
219. Gwinn, D. M., Shackelford, D. B., Egan, D. F., Mihaylova, M. M., Mery, A., Vasquez, D. S., Turk, B. E., & Shaw, R. J. (2008). AMPK phosphorylation of raptor mediates a metabolic checkpoint. *Molecular cell*, *30*(2), 214–226.
220. Gwinn, D. M., Shackelford, D. B., Egan, D. F., Mihaylova, M. M., Mery, A., Vasquez, D. S., Turk, B. E., & Shaw, R. J. (2008). AMPK phosphorylation of raptor mediates a metabolic checkpoint. *Molecular cell*, *30*(2), 214–226.
221. Oh, W. J., & Jacinto, E. (2011). mTOR complex 2 signaling and functions. *Cell cycle (Georgetown, Tex.)*, *10*(14), 2305–2316.
222. Xie, J., & Proud, C. G. (2014). Signaling crosstalk between the mTOR complexes. *Translation (Austin, Tex.)*, *2*(1), e28174.
223. Gao, D., Wan, L., & Wei, W. (2010). Phosphorylation of Rictor at Thr1135 impairs the Rictor/Cullin-1 complex to ubiquitinate SGK1. *Protein & cell*, *1*(10), 881–885.
224. Sharpless, N. E., & Sherr, C. J. (2015). Forging a signature of in vivo senescence. *Nature reviews. Cancer*, *15*(7), 397–408.
225. Page, N. M., Butlin, D. J., Lomthaisong, K., & Lowry, P. J. (2001). The human apolipoprotein L gene cluster: identification, classification, and sites of distribution. *Genomics*, *74*(1), 71–78.
226. Luo, A., Jung, J., Longley, M., Rosoff, D. B., Charlet, K., Muench, C., Lee, J., Hodgkinson, C. A., Goldman, D., Horvath, S., Kaminsky, Z. A., & Lohoff, F. W. (2020). Epigenetic aging is accelerated in alcohol use disorder and regulated by genetic variation in APOL2. *Neuropsychopharmacology : official publication of the American College of Neuropsychopharmacology*, *45*(2), 327–336.
227. Pindel, E. V., Kedishvili, N. Y., Abraham, T. L., Brzezinski, M. R., Zhang, J., Dean, R. A., & Bosron, W. F. (1997). Purification and cloning of a broad substrate specificity human liver carboxylesterase that catalyzes the hydrolysis of cocaine and heroin. *The Journal of biological chemistry*, *272*(23), 14769–14775.
228. Lian, J., Nelson, R., & Lehner, R. (2018). Carboxylesterases in lipid metabolism: from mouse to human. *Protein & cell*, *9*(2), 178–195.
229. Read, M. L., Seed, R. I., Fong, J. C., Modasia, B., Ryan, G. A., Watkins, R. J., Gagliano, T., Smith, V. E., Stratford, A. L., Kwan, P. K., Sharma, N., Dixon, O. M., Watkinson, J. C., Boelaert, K., Franklyn, J. A., Turnell, A. S., & McCabe, C. J. (2014). The PTTG1-binding factor (PBF/PTTG1IP) regulates p53 activity in thyroid cells. *Endocrinology*, *155*(4), 1222–1234.
230. Chien, W., & Pei, L. (2000). A novel binding factor facilitates nuclear translocation and transcriptional activation function of the pituitary tumor-transforming gene product. *The Journal of biological chemistry*, *275*(25), 19422–19427.
231. Vasileiou, P., Evangelou, K., Vlasis, K., Fildisis, G., Panayiotidis, M. I., Chronopoulos, E., Passias, P. G., Kouloukoussa, M., Gorgoulis, V. G., & Havaki, S. (2019). Mitochondrial Homeostasis and Cellular Senescence. *Cells*, *8*(7), 686.
232. Hubackova, S., Davidova, E., Rohlenova, K., Stursa, J., Werner, L., Andera, L., Dong, L., Terp, M. G., Hodny, Z., Ditzel, H. J., Rohlena, J., & Neuzil, J. (2019). Selective elimination of senescent cells by mitochondrial targeting is regulated by ANT2. *Cell death and differentiation*, *26*(2), 276–290.
233. Moiseeva, O., Bourdeau, V., Roux, A., Deschênes-Simard, X., & Ferbeyre, G. (2009). Mitochondrial dysfunction contributes to oncogene-induced senescence. *Molecular and cellular biology*, *29*(16), 4495–4507.
234. Wang, Y., & Hekimi, S. (2015). Mitochondrial dysfunction and longevity in animals: Untangling the knot. *Science (New York, N.Y.)*, *350*(6265), 1204–1207.

8. Appendix

8.1. Supplementary graphs and tables

Appendix 1 Downregulated proteins enrichment analysis

No	Description	FDR q-value
1	Defense response to virus	3.33E-10
2	Response to virus	4.24E-08
3	Negative regulation of viral process	6.64E-07
4	Negative regulation of multi-organism process	2.47E-06
5	Negative regulation of viral life cycle	3.93E-06
6	Negative regulation of viral genome replication	1.20E-05
7	Viral life cycle	6.92E-05
8	Regulation of viral process	7.21E-05
9	Regulation of viral life cycle	8.55E-05
10	Regulation of viral genome replication	9.76E-05
11	Viral genome replication	3.48E-04
12	Interaction with host	6.29E-04
13	Regulation by virus of viral protein levels in host cell	6.48E-04
14	Entry into host	7.94E-04
15	Entry into host cell	7.94E-04
16	Positive regulation of defense response to virus by host	2.32E-03
17	Viral entry into host cell	3.46E-03
18	Regulation of defense response to virus by host	4.82E-03
19	Hepatitis C	5.78E-03
20	Multi-organism intracellular transport	9.31E-03
21	Multi-organism cellular localization	9.31E-03
22	Measles	1.25E-02
23	Detection of virus	1.30E-02
24	Cellular response to dsRNA	1.73E-02
25	Negative regulation of viral entry into host cell	1.83E-02
26	Regulation of defense response to virus	2.07E-02
27	Influenza A	3.06E-02
28	Positive regulation of viral genome replication	3.14E-02
29	Response to exogenous dsRNA	3.37E-02
30	Response to dsRNA	3.56E-02
31	Positive regulation of viral life cycle	4.23E-02
32	Negative regulation of defense response	4.71E-02
33	Multi-organism localization	4.75E-02
34	Multi-organism transport	4.75E-02

Appendix 1a: List of BPs and pathways linked to viral defense enriched in senescent NHDF downregulated proteins set. Downregulated proteins were subjected to a gene set enrichment analysis. Mining GO:BP and REAC databases, a total of 681 biological processes were enriched, among which 34 were linked to viral defense. The table lists each BPs and its corresponding *p*-value (see section 4.8).

No	Description	FDR q-value
1	response to type I interferon	1.54E-11
2	type I interferon signaling pathway	2.14E-10
3	cellular response to type I interferon	2.14E-10
4	response to interferon-gamma	1.43E-05
5	interferon-gamma-mediated signaling pathway	1.20E-04
6	cellular response to interferon-gamma	3.48E-04
7	negative regulation of plasminogen activation	3.48E-04
8	response to interferon-beta	2.95E-03
9	platelet degranulation	3.13E-03
10	regulation of plasminogen activation	4.64E-03
11	regulation of response to cytokine stimulus	4.68E-03
12	positive regulation of response to cytokine stimulus	4.86E-03
13	regulation of T cell activation via T cell receptor contact with antigen bound to MHC molecule on antigen presenting cell	5.72E-03
14	regulation of interferon-gamma-mediated signaling pathway	9.31E-03
15	regulation of response to interferon-gamma	9.31E-03
16	T cell activation via T cell receptor contact with antigen bound to MHC molecule on antigen presenting cell	9.79E-03
17	natural killer cell degranulation	1.03E-02
18	regulation of cytokine-mediated signaling pathway	1.34E-02
19	plasminogen activation	1.50E-02
20	cellular response to interleukin-21	2.07E-02
21	interleukin-21-mediated signaling pathway	2.07E-02
22	response to interleukin-21	2.07E-02
23	positive regulation of interferon-alpha production	2.11E-02
24	positive regulation of cytokine-mediated signaling pathway	2.25E-02
25	response to interferon-alpha	2.34E-02
26	cellular response to interleukin-9	2.47E-02
27	interleukin-9-mediated signaling pathway	2.47E-02
28	cellular response to tumor necrosis factor	2.47E-02
29	regulation of T cell activation	2.77E-02
30	regulation of T cell receptor signaling pathway	2.79E-02
31	interferon-alpha production	2.81E-02
32	regulation of interferon-alpha production	2.81E-02
33	response to tumor necrosis factor	2.81E-02
34	response to interleukin-9	2.81E-02
35	T cell activation	2.88E-02
36	positive regulation of leukocyte mediated immunity	2.90E-02
37	interleukin-35-mediated signaling pathway	3.10E-02
38	interleukin-27-mediated signaling pathway	3.10E-02
39	negative regulation of coagulation	3.14E-02
40	astrocyte differentiation	3.24E-02
41	cellular response to interleukin-6	3.37E-02
42	interleukin-23-mediated signaling pathway	3.40E-02
43	cyclooxygenase pathway	3.47E-02
44	positive regulation of leukocyte degranulation	3.48E-02

45	antigen processing and presentation of peptide antigen via MHC class I	3.62E-02
46	negative regulation of cell activation	3.75E-02
47	response to interleukin-6	3.79E-02
48	lymphocyte activation involved in immune response	3.81E-02
49	negative regulation of innate immune response	3.92E-02
50	positive regulation of astrocyte differentiation	4.37E-02
51	negative regulation of defense response	4.71E-02
52	antigen processing and presentation of exogenous peptide antigen via MHC class I, TAP-dependent	4.92E-02
53	negative regulation of immune response	4.95E-02

Appendix 1b: List of BPs and pathways linked to immune response enriched in senescent NHDF downregulated proteins set. Downregulated proteins were subjected to a gene set enrichment analysis. Mining GO:BP and REAC databases, a total of 681 biological processes were enriched, among which 53 were linked to immune response. The table lists each BPs and its corresponding *p*-value (see section 4.8).

Appendix 2 Modulation of autophagy prior to senescence induction in WS1 fibroblasts

Autophagy-untreated WS1					
Tukey's multiple comparisons test	**Mean Diff.**	**95.00% CI of diff.**	**Significant?**	**Summary**	**Adjusted P Value**
D-1 vs. D0	-10050	-15055 to -5045	Yes	***	0.0001
D-1 vs. D1	-11823	-16828 to -6818	Yes	****	<0.0001
D-1 vs. D2	-11582	-16587 to -6577	Yes	****	<0.0001
D-1 vs. D5	-15225	-20230 to -10220	Yes	****	<0.0001
D-1 vs. D8	-11146	-16151 to -6142	Yes	****	<0.0001
D-1 vs. D13	-13472	-18477 to -8467	Yes	****	<0.0001
D0 vs. D1	-1773	-6778 to 3232	No	ns	0.8793
D0 vs. D2	-1532	-6537 to 3472	No	ns	0.934
D0 vs. D5	-5176	-10180 to -170.7	Yes	*	0.0406
D0 vs. D8	-1097	-6102 to 3908	No	ns	0.9865
D0 vs. D13	-3422	-8427 to 1583	No	ns	0.2937
D1 vs. D2	240.4	-4764 to 5245	No	ns	>0.9999
D1 vs. D5	-3403	-8408 to 1602	No	ns	0.2992
D1 vs. D8	676.2	-4329 to 5681	No	ns	0.999
D1 vs. D13	-1649	-6654 to 3356	No	ns	0.9099
D2 vs. D5	-3643	-8648 to 1362	No	ns	0.2356
D2 vs. D8	435.8	-4569 to 5441	No	ns	>0.9999
D2 vs. D13	-1889	-6894 to 3115	No	ns	0.8461
D5 vs. D8	4079	-926 to 9084	No	ns	0.1478
D5 vs. D13	1754	-3251 to 6759	No	ns	0.8844
D8 vs. D13	-2325	-7330 to 2680	No	ns	0.6925

Appendix 2a: Modulation of autophagy prior to senescence induction. Statistical comparisons of SA-β-gal activity among time points in autophagy-untreated cells. D-1: after autophagy modulation & before senescence induction. D1 – D13: number ofdays following senescence induction in WS1. Means comparisons calculated by One-Way ANOVA.

Rap-treated WS1					
Tukey's multiple comparisons test	**Mean Diff.**	**95.00% CI of diff.**	**Significant?**	**Summary**	**Adjusted P Value**
D-1 vs. D0	-2909	-9459 to 3640	No	ns	0.7315
D-1 vs. D1	-6763	-13312 to -213.3	Yes	*	0.041
D-1 vs. D2	-4413	-10962 to 2137	No	ns	0.3081
D-1 vs. D5	-6906	-13455 to -357	Yes	*	0.0358
D-1 vs. D8	-4037	-10586 to 2512	No	ns	0.4002
D-1 vs. D13	-11757	-18306 to -5208	Yes	***	0.0004
D 0 vs. D1	-3853	-10402 to 2696	No	ns	0.4504
D0 vs. D2	-1503	-8052 to 5046	No	ns	0.9829
D0 vs. D5	-3997	-10546 to 2552	No	ns	0.4109
D0 vs. D8	-1127	-7677 to 5422	No	ns	0.9962
D0 vs. D13	-8848	-15397 to -2299	Yes	**	0.0057
D1 vs. D2	2350	-4199 to 8899	No	ns	0.8731
D1 vs. D5	-143.7	-6693 to 6406	No	ns	>0.9999
D1 vs. D8	2726	-3824 to 9275	No	ns	0.7827
D1 vs. D13	-4995	-11544 to 1555	No	ns	0.1965
D2 vs. D5	-2494	-9043 to 4056	No	ns	0.8412
D2 vs. D8	375.8	-6173 to 6925	No	ns	>0.9999
D2 vs. D13	-7345	-13894 to -795.3	Yes	*	0.0237
D5 vs. D8	2869	-3680 to 9419	No	ns	0.7429
D5 vs. D13	-4851	-11400 to 1698	No	ns	0.2205
D8 vs. D13	-7720	-14270 to -1171	Yes	*	0.0166

Appendix 2b: Modulation of autophagy prior to senescence induction. Statistical comparisons of SA-β-gal activity among time points in autophagy-stimulated (Rap) cells. D-1: after autophagy modulation & before senescence induction. D1 – D13: number of days following senescence induction in WS1. Means comparisons calculated by One-Way ANOVA.

Cq-treated WS1					
Tukey's multiple comparisons test	**Mean Diff.**	**95.00% CI of diff.**	**Significant?**	**Summary**	**Adjusted P Value**
D-1 vs. D0	-11876	-18547 to -5205	Yes	***	0.0004
D-1 vs. D1	-19991	-26662 to -13320	Yes	****	<0.0001
D-1 vs. D2	-23230	-29901 to -16560	Yes	****	<0.0001
D-1 vs. D5	-27468	-34138 to -20797	Yes	****	<0.0001
D-1 vs. D8	-25863	-32534 to -19193	Yes	****	<0.0001
D-1 vs. D13	-25087	-31758 to -18417	Yes	****	<0.0001
D0 vs. D1	-8115	-14786 to -1444	Yes	*	0.0131
D0 vs. D2	-11354	-18025 to -4684	Yes	***	0.0007
D0 vs. D5	-15592	-22262 to -8921	Yes	****	<0.0001
D0 vs. D8	-13987	-20658 to -7317	Yes	****	<0.0001
D0 vs. D13	-13211	-19882 to -6541	Yes	***	0.0001
D1 vs. D2	-3239	-9910 to 3431	No	ns	0.6512
D1 vs. D5	-7477	-14147 to -806	Yes	*	0.0238

D1 vs. D8	-5872	-12543 to 798.1	No	ns	0.1019
D1 vs. D13	-5096	-11767 to 1574	No	ns	0.1951
D2 vs. D5	-4237	-10908 to 2433	No	ns	0.3683
D2 vs. D8	-2633	-9304 to 4037	No	ns	0.8189
D2 vs. D13	-1857	-8528 to 4813	No	ns	0.9568
D5 vs. D8	1604	-5066 to 8275	No	ns	0.9785
D5 vs. D13	2380	-4290 to 9051	No	ns	0.8758
D8 vs. D13	776	-5895 to 7447	No	ns	0.9996

Appendix 2c: Modulation of autophagy prior to senescence induction. Statistical comparisons of SA-β-gal activity among time points in autophagy-inhibited (Cq) cells. D-1: after autophagy modulation & before senescence induction. D1 – D13: number of days following senescence induction in WS1. Means comparisons calculated by One-Way ANOVA.

Appendix 3 Modulation of autophagy during the development of senescence in WS1

Autophagy-untreated WS1					
Tukey's multiple comparisons test	**Mean Diff.**	**95% CI of diff.**	**Significant?**	**Summary**	**Adjusted *p*-value**
D-1 vs. D0	-15311	-19322 to -11300	Yes	****	<0.0001
D-1 vs. D1	-12049	-16060 to -8038	Yes	****	<0.0001
D-1 vs. D2	-12442	-16453 to -8432	Yes	****	<0.0001
D-1 vs. D6	-12622	-16633 to -8612	Yes	****	<0.0001
D-1 vs. D9	-15358	-19369 to -11347	Yes	****	<0.0001
D-1 vs. D13	-17149	-21160 to -13138	Yes	****	<0.0001
D0 vs. D1	3262	-748.5 to 7273	No	ns	0.1491
D0 vs. D2	2869	-1142 to 6880	No	ns	0.2512
D0 vs. D6	2689	-1322 to 6700	No	ns	0.3131
D0 vs. D9	-46.89	-4058 to 3964	No	ns	>0.9999
D0 vs. D13	-1838	-5849 to 2173	No	ns	0.7048
D1 vs. D2	-393.6	-4404 to 3617	No	ns	0.9998
D1 vs. D6	-573.6	-4584 to 3437	No	ns	0.9986
D1 vs. D9	-3309	-7320 to 701.6	No	ns	0.1397
D1 vs. D13	-5100	-9111 to -1089	Yes	**	0.0093
D2 vs. D6	-180	-4191 to 3831	No	ns	>0.9999
D2 vs. D9	-2916	-6926 to 1095	No	ns	0.2367
D2 vs. D13	-4707	-8717 to -695.8	Yes	*	0.0171
D6 vs. D9	-2736	-6746 to 1275	No	ns	0.296
D6 vs. D13	-4527	-8537 to -515.8	Yes	*	0.0227
D9 vs. D13	-1791	-5802 to 2220	No	ns	0.7271

Appendix 3a: Modulation of autophagy during the development of senescence in WS1. Statistical comparisons of SA-β-gal activity among time points in autophagy-untreated cells. D-1: before autophagy modulation & before senescence induction. D1 – D13: number of days following senescence induction in WS1. Means comparisons calculated by One-Way ANOVA.

Rap-treated WS1					
Tukey's multiple comparisons test	**Mean Diff.**	**95.00% CI of diff.**	**Significant?**	**Summary**	**Adjusted P Value**
D-1 vs. D0	-5311	-11996 to 1374	No	ns	0.1655
D-1 vs. D1	-6671	-13356 to 14.33	No	ns	0.0507
D-1 vs. D2	-6500	-13185 to 185.3	No	ns	0.0591
D-1 vs. D6	-15877	-22563 to -9192	Yes	****	<0.0001
D-1 vs. D9	-12924	-19609 to -6238	Yes	***	0.0002
D-1 vs. D13	-17928	-24614 to -11243	Yes	****	<0.0001
D0 vs. D1	-1360	-8045 to 5325	No	ns	0.9908
D0 vs. D2	-1189	-7874 to 5496	No	ns	0.9955
D0 vs. D6	-10566	-17251 to -3881	Yes	**	0.0014
D0 vs. D9	-7613	-14298 to -927.3	Yes	*	0.0213
D0 vs. D13	-12617	-19303 to -5932	Yes	***	0.0002
D1 vs. D2	171	-6514 to 6856	No	ns	>0.9999

D1 vs. D6	-9206	-15892 to -2521	Yes	**	0.0048
D1 vs. D9	-6253	-12938 to 432.6	No	ns	0.0738
D1 vs. D13	-11257	-17943 to -4572	Yes	***	0.0008
D2 vs. D6	-9377	-16063 to -2692	Yes	**	0.0041
D2 vs. D9	-6424	-13109 to 261.6	No	ns	0.0633
D2 vs. D13	-11428	-18114 to -4743	Yes	***	0.0007
D6 vs. D9	2953	-3732 to 9639	No	ns	0.7361
D6 vs. D13	-2051	-8736 to 4634	No	ns	0.9334
D9 vs. D13	-5005	-11690 to 1681	No	ns	0.2116

Appendix 3b: Modulation of autophagy during the development of senescence in WS1. Statistical comparisonsof SA-β-galactivity amongtime pointsinautophagy-stimulated(Rap) cells. D-1: before autophagy modulation & before senescence induction. D1 – D13: number of days following senescence induction in WS1. Means comparisons calculated by One-Way ANOVA.

Cq-treated WS1					
Tukey's multiple comparisons test	**Mean Diff.**	**95.00% CI of diff.**	**Significant?**	**Summary**	**Adjusted P Value**
D-1 vs. D0	-5311	-9024 to -1599	Yes	**	0.0035
D-1 vs. D1	1982	-1730 to 5694	No	ns	0.555
D-1 vs. D2	2876	-836.4 to 6588	No	ns	0.1842
D-1 vs. D6	6666	2953 to 10378	Yes	***	0.0004
D-1 vs. D9	-488.3	-4201 to 3224	No	ns	0.9991
D-1 vs. D13	-13250	-16962 to -9537	Yes	****	<0.0001
D0 vs. D1	7293	3581 to 11005	Yes	***	0.0002
D0 vs. D2	8187	4475 to 11900	Yes	****	<0.0001
D0 vs. D6	11977	8265 to 15689	Yes	****	<0.0001
D0 vs. D9	4823	1110 to 8535	Yes	**	0.0078
D0 vs. D13	-7939	-11651 to -4226	Yes	****	<0.0001
D1 vs. D2	894.1	-2818 to 4607	No	ns	0.9783
D1 vs. D6	4684	971.5 to 8396	Yes	**	0.0099
D1 vs. D9	-2470	-6183 to 1242	No	ns	0.3205
D1 vs. D13	-15232	-18944 to -11519	Yes	****	<0.0001
D2 vs. D6	3790	77.39 to 7502	Yes	*	0.044
D2 vs. D9	-3364	-7077 to 348.1	No	ns	0.0876
D2 vs. D13	-16126	-19838 to -12413	Yes	****	<0.0001
D6 vs. D9	-7154	-10867 to -3442	Yes	***	0.0002
D6 vs. D13	-19915	-23628 to -16203	Yes	****	<0.0001
D9 vs. D13	-12761	-16474 to -9049	Yes	****	<0.0001

Appendix 3c: Modulation of autophagy during the development of senescence in WS1. Statistical comparisons of SA-β-gal activity among time points in autophagy-inhibited (Cq) cells. D-1: before autophagy modulation & before senescence induction. D1 – D13: number of days following senescence induction in WS1. Means comparisons calculated by One-Way ANOVA.

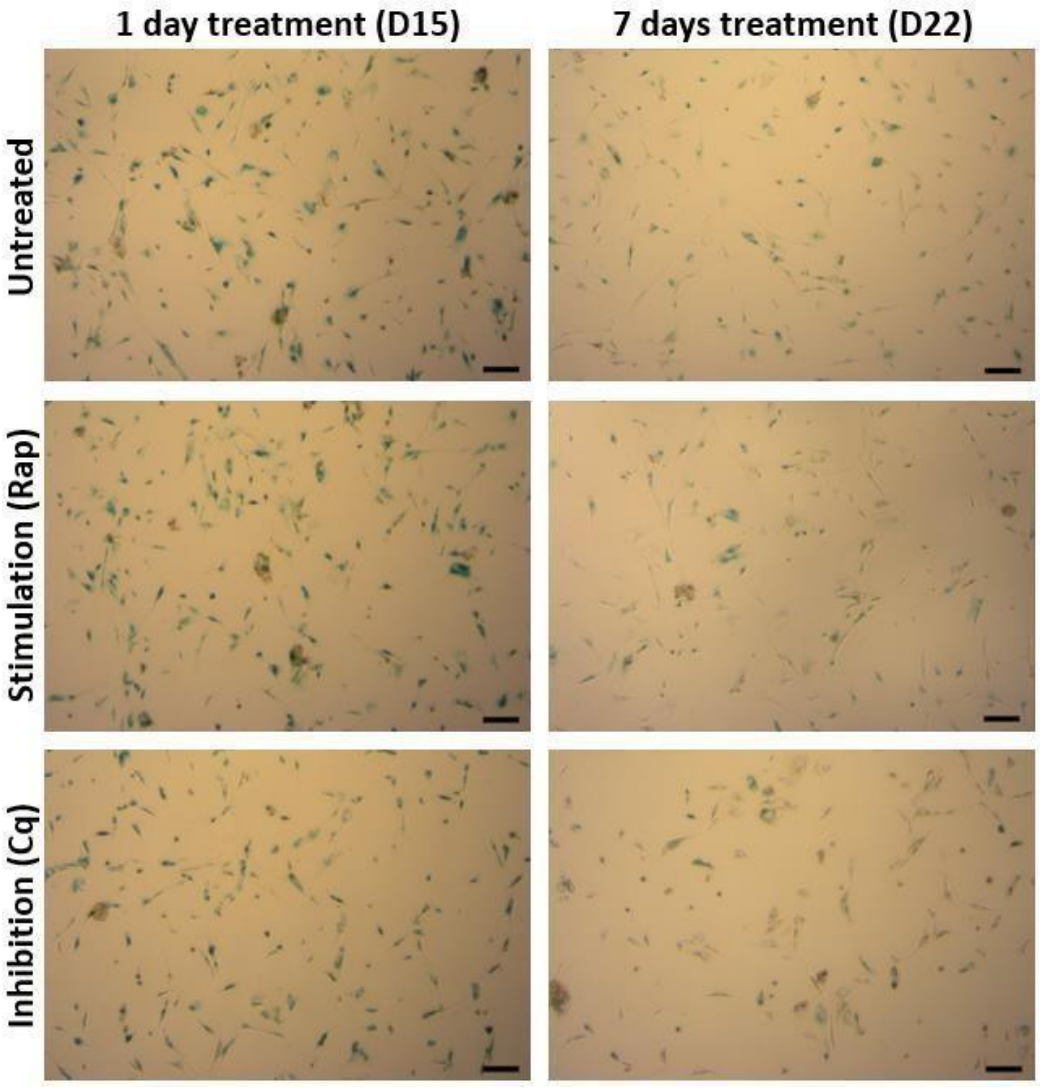

Appendix 4: SA-β-gal staining of senescent WS1 treated with Rap, Cq or left untreated for 1 day (D15) and 7 days (D22). Blue staining indicates senescent cells. Representative figures from three biological replicates are shown. Scalebar: 100 µM

3d inhibition of autophagy					
Tukey's multiple comparisons test	**Mean Diff.**	**95.00% CI of diff.**	**Significant?**	**Summary**	**Adjusted P Value**
Untd vs. Wort	18971	7752 to 30190	Yes	****	<0.0001
Untd vs. Cq	34489	23270 to 45708	Yes	****	<0.0001
Untd vs. Atg5	40116	28897 to 51335	Yes	****	<0.0001
Untd vs. Atg7	47187	35968 to 58406	Yes	****	<0.0001
Untd vs. Atg5+Cq	58197	46978 to 69416	Yes	****	<0.0001
Untd vs. Atg7+ Cq	60910	49690 to 72129	Yes	****	<0.0001
Wort vs. Cq	15518	4299 to 26737	Yes	**	0.0017
Wort vs. Atg5	21146	9926 to 32365	Yes	****	<0.0001
Wort vs. Atg7	28216	16997 to 39435	Yes	****	<0.0001
Wort vs. Atg5+ Cq	39226	28007 to 50445	Yes	****	<0.0001
Wort vs. Atg7+ Cq	41939	30720 to 53158	Yes	****	<0.0001
Cq vs. Atg5	5627	-5592 to 16846	No	ns	0.7186
Cq vs. Atg7	12698	1479 to 23917	Yes	*	0.0172
Cq vs. Atg5+ Cq	23708	12489 to 34927	Yes	****	<0.0001
Cq vs. Atg7+ Cq	26420	15201 to 37639	Yes	****	<0.0001
Atg5 vs. Atg7	7071	-4148 to 18290	No	ns	0.4665
Atg5 vs. Atg5+ Cq	18081	6862 to 29300	Yes	***	0.0002
Atg5 vs. Atg7+ Cq	20793	9574 to 32012	Yes	****	<0.0001
Atg7 vs. Atg5+ Cq	11010	-208.8 to 22229	No	ns	0.0576
Atg7 vs. Atg7+ Cq	13723	2504 to 24942	Yes	**	0.0077
Atg5+ Cq vs. Atg7+ Cq	2712	-8507 to 13931	No	ns	0.989

Appendix 5a: Viability of senescent NHDF following inhibition of autophagy. Autophagy was inhibited using Wortmannin (Wort), chloroquine (Cq) and siRNA targeting Atg5/7. Cell viability assessed by ATP assay after 3 days treatment. Mean comparisons calculated using One-Way ANOVA.

6d inhibition of autophagy					
Tukey's multiple comparisons test	**Mean Diff.**	**95.00% CI of diff.**	**Significant?**	**Summary**	**Adjusted P Value**
Untd vs. Wort	44534	37857 to 51210	Yes	****	<0.0001
Untd vs. Cq	59512	52835 to 66188	Yes	****	<0.0001
Untd vs. Atg5	60692	54015 to 67368	Yes	****	<0.0001
Untd vs. Atg7	66615	59939 to 73292	Yes	****	<0.0001
Untd vs. Atg5+Cq	69755	63078 to 76431	Yes	****	<0.0001
Untd vs. Atg7+ Cq	71159	64483 to 77836	Yes	****	<0.0001
Wort vs. Cq	14978	8301 to 21654	Yes	****	<0.0001
Wort vs. Atg5	16158	9481 to 22834	Yes	****	<0.0001
Wort vs. Atg7	22082	15405 to 28758	Yes	****	<0.0001
Wort vs. Atg5+ Cq	25221	18545 to 31897	Yes	****	<0.0001
Wort vs. Atg7+ Cq	26626	19949 to 33302	Yes	****	<0.0001
Cq vs. Atg5	1180	-5496 to 7857	No	ns	0.998
Cq vs. Atg7	7104	427.5 to 13780	Yes	*	0.0302
Cq vs. Atg5+ Cq	10243	3567 to 16920	Yes	***	0.0004

Cq vs. Atg7+ Cq	11648	4971 to 18324	Yes	****	<0.0001
Atg5 vs. Atg7	5924	-752.7 to 12600	No	ns	0.1129
Atg5 vs. Atg5+ Cq	9063	2387 to 15740	Yes	**	0.0022
Atg5 vs. Atg7+ Cq	10468	3791 to 17144	Yes	***	0.0003
Atg7 vs. Atg5+ Cq	3139	-3537 to 9816	No	ns	0.7745
Atg7 vs. Atg7+ Cq	4544	-2132 to 11220	No	ns	0.3733
Atg5+ Cq vs. Atg7+ Cq	1405	-5272 to 8081	No	ns	0.9948

Appendix 5b: Viability of senescent NHDF following inhibition of autophagy. Autophagy was inhibited using Wortmannin (Wort), chloroquine (Cq) and siRNA targeting Atg5/7. Cell viability assessed by ATP assay after 6 days treatment. Mean comparisons calculated using One-Way ANOVA.

9d inhibition of autophagy					
Tukey's multiple comparisons test	**Mean Diff.**	**95.00% CI of diff.**	**Significant?**	**Summary**	**Adjusted P Value**
Untd vs. Wort	38542	28059 to 49024	Yes	****	<0.0001
Untd vs. Cq	71009	60527 to 81492	Yes	****	<0.0001
Untd vs. Atg5	68837	58355 to 79320	Yes	****	<0.0001
Untd vs. Atg7	74814	64332 to 85297	Yes	****	<0.0001
Untd vs. Atg5+ Cq	74907	64424 to 85389	Yes	****	<0.0001
Untd vs. Atg7+ Cq	75109	64626 to 85591	Yes	****	<0.0001
Wort vs. Cq	32468	21985 to 42950	Yes	****	<0.0001
Wort vs. Atg5	30295	19813 to 40778	Yes	****	<0.0001
Wort vs. Atg7	36273	25790 to 46755	Yes	****	<0.0001
Wort vs. Atg5+ Cq	36365	25882 to 46847	Yes	****	<0.0001
Wort vs. Atg7+ Cq	36567	26085 to 47049	Yes	****	<0.0001
Cq vs. Atg5	-2172	-12655 to 8310	No	ns	0.9952
Cq vs. Atg7	3805	-6678 to 14287	No	ns	0.9202
Cq vs. Atg5+ Cq	3897	-6585 to 14380	No	ns	0.9114
Cq vs. Atg7+ Cq	4099	-6383 to 14582	No	ns	0.89
Atg5 vs. Atg7	5977	-4505 to 16460	No	ns	0.5851
Atg5 vs. Atg5+ Cq	6070	-4413 to 16552	No	ns	0.5675
Atg5 vs. Atg7+ Cq	6272	-4211 to 16754	No	ns	0.5291
Atg7 vs. Atg5+ Cq	92.38	-10390 to 10575	No	ns	>0.9999
Atg7 vs. Atg7+ Cq	294.5	-10188 to 10777	No	ns	>0.9999
Atg5+ Cq vs. Atg7+ Cq	202.1	-10280 to 10685	No	ns	>0.9999

Appendix 5c: Viability of senescent NHDF following inhibition of autophagy. Autophagy was inhibited using Wortmannin (Wort), chloroquine (Cq) and siRNA targeting Atg5/7. Cell viability assessed by ATP assay after 9 days treatment. Mean comparisons calculated using One-Way ANOVA.

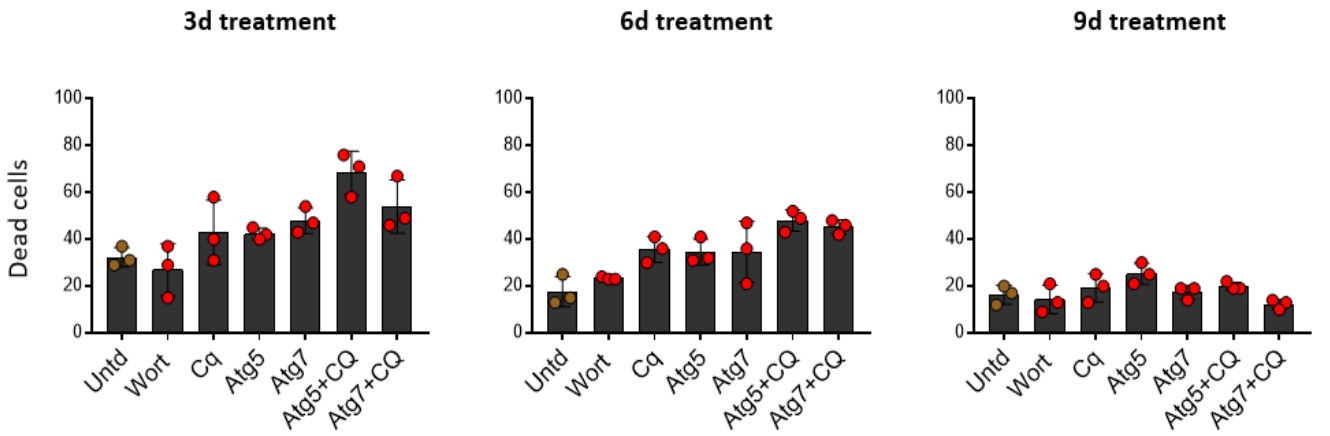

Appendix 5d: Viability of senescent NHDF following inhibition of autophagy. Autophagy was inhibited using Wortmannin (Wort), chloroquine (Cq) and siRNA targeting Atg5/7. Cell viability evaluated by counting the number of floating (dead) cells in culture medium after 3-, 6- and 9 days treatment.

Appendix 6 Identification of APOL2, CES2, PTTG1IP and MGARP by 2D-LC-MS/MS analysis

Conf	Sequence	Accession numbers	MC	II [%]	RT [min]
High	[R].aLAEEVEQVHR.[G]	Q9BQE5	0	8	151.42
High	[R].aLAEEVEQVHR.[G]	Q9BQE5	0	3	151.60
High	[R].nLDQSGTNVAk.[V]	Q9BQE5	0	0	86.66
High	[R].iSAEGGEQVER.[V]	Q9BQE5	0	0	82.93
High	[R].aLAEEVEQVHR.[G]	Q9BQE5	0	3	151.78
High	[R].aLAEEVEQVHR.[G]	Q9BQE5	0	16	151.97
High	[R].iSAEGGEQVER.[V]	Q9BQE5	0	0	35.30
High	[R].aLAEEVEQVHR.[G]	Q9BQE5	0	25	151.26
High	[K].sESAEELk.[K]	Q9BQE5	0	0	103.54
High	[K].sESAEELk.[K]	Q9BQE5	0	0	103.77
High	[K].sESAEELk.[K]	Q9BQE5	0	6	103.97
High	[K].sESAEELk.[K]	Q9BQE5	0	4	40.54
High	[K].sESAEELk.[K]	Q9BQE5	0	12	104.18

Appendix 6a: Peptide-spectrum matches from APOL2 identification by 2D-LC-MSMS. Conf: confidence, MC: miss cleavage, II: isolation interference and RT: retention time.

Conf	Sequence	Accession numbers	MC	II [%]	RT [min]
High	[K].skEEILAINkPFk.[M]	O00748	1	37	144.58
High	[K].fTEEEEQLSR.[K]	O00748	0	50	160.77
High	[K].iQELEEPEER.[H]	O00748	0	5	166.35
High	[K].fTEEEEQLSR.[K]	O00748	0	0	160.43
High	[K].iQELEEPEER.[H]	O00748	0	19	166.16
High	[K].iQELEEPEER.[H]	O00748	0	0	166.59
High	[K].fTEEEEQLSR.[K]	O00748	0	7	161.17
High	[K].fTEEEEQLSR.[K]	O00748	0	6	61.58
High	[K].iQELEEPEER.[H]	O00748	0	4	166.66
High	[K].iQELEEPEER.[H]	O00748	0	0	166.32
High	[K].fTEEEEQLSR.[K]	O00748	0	23	61.71

Appendix 6b: Peptide-spectrum matches from CES2 identification by 2D-LC-MSMS. Conf: confidence, MC: miss cleavage, II: isolation interference and RT: retention time.

Conf	Sequence	Accession numbers	MC	II [%]	RT [min]
High	ACLDYPVTSVLPPASLCK	P53801	0	12	180.4575
High	ACLDYPVTSVLPPASLCK	P53801	0	4	180.659
High	ACLDYPVTSVLPPASLCK	P53801	0	5	180.84
High	ACLDYPVTSVLPPASLCK	P53801	0	4	180.9427
High	ACLDYPVTSVLPPASLCK	P53801	0	8	181.023
High	ACLDYPVTSVLPPASLCK	P53801	0	3	181.1559
High	ACLDYPVTSVLPPASLCK	P53801	0	11	181.2019
High	ACLDYPVTSVLPPASLCK	P53801	0	11	181.3856
High	ACLDYPVTSVLPPASLCK	P53801	0	7	181.5712
High	ACLDYPVTSVLPPASLCK	P53801	0	0	180.9803
High	ACLDYPVTSVLPPASLCK	P53801	0	0	180.7116

Appendix 6c: Peptide-spectrum matches from PTTG1IP identification by 2D-LC-MSMS. Conf: confidence, MC: miss cleavage, II: isolation interference and RT: retention time.

Conf	Sequence	Accession numbers	MC	II [%]	RT [min]
High	EASACPGHVEAAPETTAVSAETGPEVTDAAAR	Q8TDB4	0	0	174.9751
High	EASACPGHVEAAPETTAVSAETGPEVTDAAAR	Q8TDB4	0	0	174.9979
High	EASACPGHVEAAPETTAVSAETGPEVTDAAAR	Q8TDB4	0	0	175.2095
High	EASACPGHVEAAPETTAVSAETGPEVTDAAAR	Q8TDB4	0	0	175.2121
High	EASACPGHVEAAPETTAVSAETGPEVTDAAAR	Q8TDB4	0	0	175.3998
High	EASACPGHVEAAPETTAVSAETGPEVTDAAAR	Q8TDB4	0	0	61.5678
High	ETTEVNPETTPEVTNAALDEAVTIDNDK	Q8TDB4	0	0	129.5852
High	ETTEVNPETTPEVTNAALDEAVTIDNDK	Q8TDB4	0	0	129.7975
High	ETTEVNPETTPEVTNAALDEAVTIDNDKDTTK	Q8TDB4	1	0	124.8301
High	ETTEVNPETTPEVTNAALDEAVTIDNDK	Q8TDB4	0	0	129.6554
High	ETTEVNPETTPEVTNAALDEAVTIDNDK	Q8TDB4	0	0	129.4861
High	EASACPGHVEAAPETTAVSAETGPEVTDAAAR	Q8TDB4	0	0	61.4524
High	ETTEVNPETTPEVTNAALDEAVTIDNDKDTTK	Q8TDB4	1	0	125.1581

High	ETTEVNPETTPEVTNAALDEAVTIDNDK	Q8TDB4	0	0	129.4397
High	ETTEVNPETTPEVTNAALDEAVTIDNDK	Q8TDB4	0	0	129.3991
High	ETTEVNPETTPEVTNAALDEAVTIDNDK	Q8TDB4	0	0	129.8562
High	ASSEAPEELIVEAEVVDAEESPSATVVVIK	Q8TDB4	0	17	177.1379
High	TVTSDQAK	Q8TDB4	0	35	64.4283
High	AEIHPFQGEK	Q8TDB4	0	51	99.1924

Appendix 6d: Peptide-spectrum matches from MGARP identification by 2D-LC-MSMS. Conf: confidence, MC: miss cleavage, II: isolation interference and RT: retention time.

Appendix 7 Trehalose-mediated stimulation of autophagy in senescent NHDF

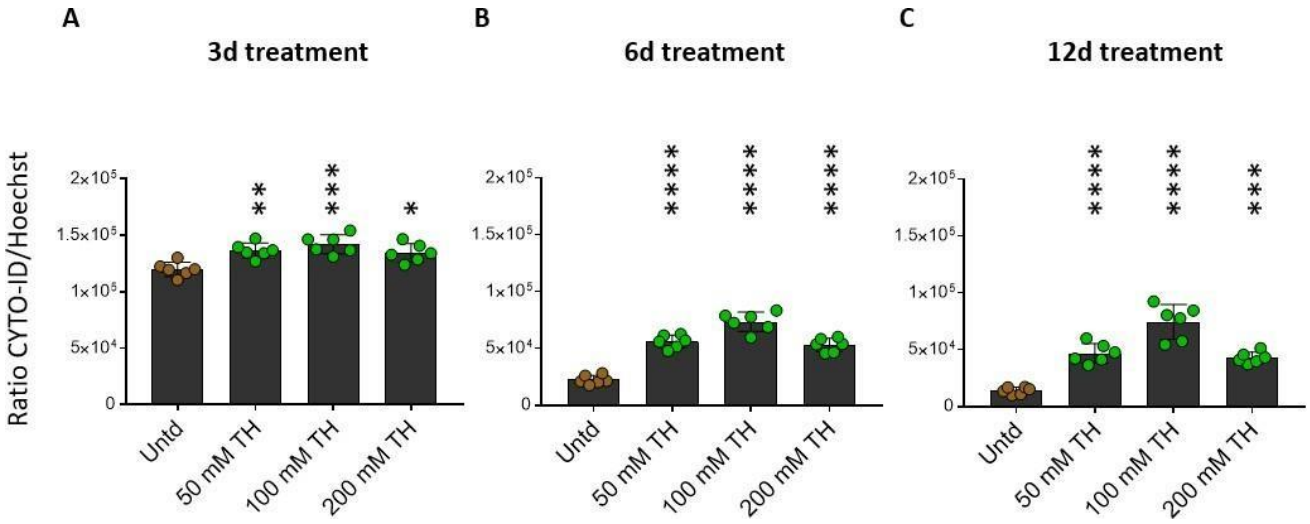

Appendix 7: 3 weeks old senescent NHDF viability following 3-, 6- and 12 days of trehalose treatment. 3 weeks old senescent NHDF were treated with 50, 100 and 200 mM trehalose for 3, 6 and 12 days. Cell viability was assessed by ATP assay. Values were obtained from n ≥ 6 biological replicates. Means ± SEM are shown. Adjusted p-values of Tukey's multiple comparison test: (****): < 0.0001, (**): < 0.01, (ns): not significant.

8.2. Abbreviations

Abbreviation	Definition
ATG12	Autophagy related protein 12
2D-DIGE	2-dimensional differential gel electrophoresis
2D-GE	2-dimensional gel electrophoresis
2D-LC-MS/MS	2-dimensional liquid chromatography tandem mass spectrometry
Akt	Protein Kinase B
AMPK	Adenosine monophosphate-activated kinase
ANOVA	Analysis of variance
AP	Autophagy
APOL2	Apolipoprotein 2
ATG5	Autophagy related protein 5
ATG7	Autophagy related protein 7
ATP	Adenosine triphosphate
AV	Autophagic vesicle
BCL-2	*B-cell lymphoma 2*
BPs	Biological processes
BSA	Bovine serum albumin
C/EBP	CCAAT/Enhancer-Binding-Protein
CDK	Cyclin-dependent kinase
CES2	Cocaine esterase 2
CMA	Chaperone-mediated autophagy
COVID-19	Coronavirus disease 2019
Cq	Chloroquine
DC	Dendritic cell
DDR	DNA damage response
DEPs	Differentially expressed proteins
DETC	Dendritic epidermal T cell
DMSO	Dimethyl sulfoxide
DNA	Deoxyribonucleic acid
Dox	Doxorubicin
E2F	Transcription factor E2F
ECM	Extracellular matrix
EM	Enrichment map
FDR	False discovery rate
FoxO3	Forkhead-box-protein O3

GATA4	Transcription factor GATA-4
GO:BP	Gene Ontology, Biological Processes database
GSEA	Gene set enrichment analysis
HMDM2	Human mouse double minute 2
HRP	Horseradish peroxidase
HSC70	Heat shock protein 70
HSP	Heat shock protein
IIS	Insulin and IGF-1 signaling
IL-6	Interleukin 6
IL-8	Interleukin 8
ILC	Innate lymphoid cell
K	Amino acid Lysin
LAMP2A	Lysosome-associated membrane protein 2
LC3	Microtubule-associated protein light chain 3
LC3i	Microtubule-associated protein light chain 3, cytosolic form
LC3ii	Microtubule-associated protein light chain 3, membrane-bound
LDH	Lactate dehydrogenase
MEM	Minimum essential medium
MGARP	MGARP protein
MMP	Matrix metal-protease
mTOR	Mechanistic target of rapamycin
mTORC1	Mechanistic target of rapamycin complex 1
mTORC2	Mechanistic target of rapamycin complex 2
MW	Molecular weight
NC	Non-senescent
NF-κB	Nuclear factor 'kappa-light-chain-enhancer' of activated B-cells
NHDF	Normal human dermal fibroblasts
NT	No treatment
OIS	Oncogene-induced senescence
p14ARF	ARF tumor suppressor
p16 INK4A	Cyclin-dependent kinase inhibitor 2A
p21	Cyclin-dependent kinase inhibitor 1 or CDK-interacting protein 1
p53	Cellular tumor antigen p53
p62	Sequestosome 1
pDC	Plasmacytoid dendritic cell
PE	Phosphatidlyethanolamine

PI3KIII	Class III PI 3-kinase
PSM	Peptide-spectrum match
PTTG1IP	Pituitary Tumor-Transforming Gene 1 Protein-Interacting Protein
pU	Poly-ubiquitination
PVDF	Polyvinylidene difluoride
Rap	Rapamycin
Raptor	Regulatory associated protein of mTOR
Rb	Retinoblastoma
REAC	Reactrome database
RFU	Relative fluorescent unit
Rictor	Rapamycin-insensitive companion of mTOR
ROS	Reactive oxygen species
RT	Room temperature
S6K1	p70 ribosomal protein S6 kinase 1
SA-b-gal	Senescence-associates beta galactosidase
SAHF	Senescence-associated heterochromatin foci
SASP	Senescence-associated secretory phenotype
SC	Senescent
SDS-PAGE	Sodium dodecyl sulfate - polyacrylamide gel electrophoresis
SEM	Standard error mean
SIPS	Stress induced premature senescence
siRNA	Small interfering RNA
TASCC	TOR-autophagy spatial coupling compartment
TBS	Tris-buffered saline
TIMP	Tissue inhibitor of metalloproteases
ULK1	Unc-51-like kinase 1
UPS	Ubiquitin-proteasome system
UT	Untreated
UV	Ultraviolet
Wort	Wortmannin
X-Gal	5-bromo-4-chloro-3-indoyl b-D-galactopyranoside
γH2AX	Phosphorylated form of the histone H2AX

8.3. List of figures

8.4. List of tables

8.5. Curriculum Vitae

GREG SOM

PhD Fellow at Merck KGaA

Darmstadt, Germany

PROFILE

PhD student with 3 years of international experience in the pharmaceutical industry. Enthusiastic team player equipped with excellent interpersonal skills, adept at connecting people and ideas in a multidisciplinary environment. Curious mind with strong interest in translating scientific projects into business.

ACADEMIC BACKGROUND

Ph.D. Biochemistry

Merck KGaA and TU Darmstadt, Germany | May 2017-2020

Under the supervision of Prof. Harald Kolmar (TU Darmstadt) and Prof. Jörg von Hagen (Merck KGaA)

Completing a doctoral dissertation on: "Identification of novel markers involved in skin aging"

- Defined and defended research´s scope with senior management
- Presented my intermediate results at 3 conferences
- Parallelly established a proteomic/bioinformatic platform allowing for the screening of chemical activities on age-related biological processes and wrote related protocols
- Enthusiastically supervised 2 master´s students by leading their projects, defining objectives and setting deadlines
- Adapted to multinational & multicultural working spaces

M.Sc Medical Biology (metabolism)

University of Lausanne (UNIL), Switzerland | 2015 - 2017

Under the supervision of Prof. Lee Ann Applegate, Regenerative Therapy Unit, Lausanne University Hospital (CHUV)

Completed a dissertation on: "Testosterone hormonotherapy influence on female ASC in vitro"

B.Sc Biology

University of Lausanne (UNIL), Switzerland | 2012 - 2015

Under the supervision of Prof. Stefan Kunz, Institute of Microbiology, Lausanne University Hospital (CHUV)

Completed a dissertation on: "CRELD1/CRELD2 interaction with Arenaviruses glycoproteins"

LANGUAGES

INFORMATICS SKILLS

- MSOffice
- R-Project
- GraphPad Prism

HOBBIES

CrossFit andweightlifting

- Training 5x/week
- Strict control on diet and lifestyle

An excellent way to strengthen my mind and body, optimize work-life balance

Literature

- Devouring books (mostly science-fiction)
- Writing a book

Travel

Fascinated by Japan and its culture

EXTRA-CURRICULAR ACTIVITIES

SCC delegate at Faculty of Biology and Medicine

University of Lausanne (UNIL), Switzerland | 2015 - 2017

The Student Consultative Committee aims to connect direction, students and professors of the faculty of biology and medicine in order to improve teaching quality

Mentor for exchange students

University of Lausanne (UNIL), Switzerland | 2015 - 2017

Social insertion and help with paper work and organization in Switzerland for foreigner master students of the faculty of Biology

Assistant in Physics

Ecole Polytechnique Fédérale de Lausanne(EPFL), Switzerland | 2015 - 2016

Lecture explanation and exercises supervision (Prof. Tran) for biology students

Volunteer at Foundation "Mère Sofia"

“Soupe Populaire”, Lausanne, Switzerland | 2014 - 2015

The foundation provides social help and services for immigrants, homeless and in-need people

WORK EXPERIENCES

Boarding school tutor

“Collège Champittet”, Pully, Switzerland | 2015 - 2017

Mentoring pupils and managing activities over the weekend in an international boarding school

Cashier in a supermarket

COOP Stores, St-Prex and Crissier, Switzerland | 2005 - 2015

Cashier and customer service to finance my studies and life expenses

8.6. Acknowledgments

I would like to express my deepest gratitude to **Prof. Dr. Dipl-Ing. Jörg von Hagen** and **Prof. Dr. Harald Kolmar**, for the chance to start the career I have always dreamed of. Without their constant support and advice, this work would not have been possible and both their vast knowledge and passion for science have been a source of inspiration.

I am especially thankful to **Dr. Andrew Salazar**, who supervised this work on a daily basis. His guidance and bounds of encouragement, both private and professional, were a priceless resource during the last three years.

Special thanks go to **Sebastian Holzner** and **Stefan Zens**, who enormously helped this project by working in the lab and bringing fresh ideas. Both did a really good job for their master thesis and I wish them all the best for the future.

I had the chance to work in a fantastic work environment. In this regard, I would like to thank all former and currentlab-mates: Nico Wettnerand Artem Dudkin, JuliaBleifuss, Lisa Eckelhöferand Alexander-Paul Schiller, as well as Julian Osthoff, Anita Jäger and Dr. Anja Krattenmacher. Thank you to the "skin penetration team": Markus Lubda, Inga Pelzer, Maximilian Zander and Yannik Hein. Each of you helped me many times, in a way or in another.

Merck KGaA is a pool of brilliant people always ready to help. I would like to thank Dr. Aline Zimmer and Dr. Maxime le Mignon, who helped with data analysis and provided useful advice. I also would like to thank Sara Kalman, Dr. Janis Roßkopf, Martina Zimmerman, Marie Quillmann, Natasha Csonge and Camille Albisser, as well as all the people I had the chance to meet at Merck.

Leaving his country, family, friends and his comfort zone is never easy. In this regard, I will never be thankful enough to **Alexander-Paul Schiller**, **Annika Käshammer** and **Markus Lubda**. You made my stay in Germany the best experience of my life, and I am glad to consider you as real friends.

I would like to thank my parents, **Marlyse** and **Jean-Claude**, who always supported and helped me. I would like to thank my siblings, Jeremy and Noemi, as well as my grandparents. Finally, my biggest thanks go to **Lea Bruno**, to whom I owe everything I am today.

9. Affirmations

Gregory Valentin Som

Neckarstr. 6

64283 Darmstadt

02.07.2020

(Datum)

Erklärung

Ich erkläre hiermit, dass ich meine Dissertation selbstständig

und nur mit den angegebenen Hilfsmitteln angefertigt habe.

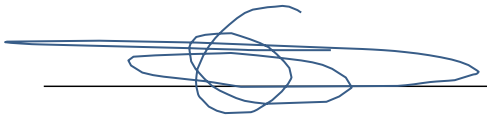

(Gregory Som)

Gregory Valentin Som
Neckarstr. 6
64283 Darmstadt

02.07.2020
(Datum)

Erklärung

Ich erkläre hiermit, noch keinen Promotionsversuch unternommen zu haben.

(Gregory Som)

Gregory Valentin Som
Neckarstr. 6
64283 Darmstadt

02.07.2020
(Datum)

Erklärung

Ich erkläre hiermit, dass die elektronische Version der Doktorarbeit mit der schriftlichen Version übereinstimmt. Die elektronische Version liegt dem Prüfungssekretariat vor.

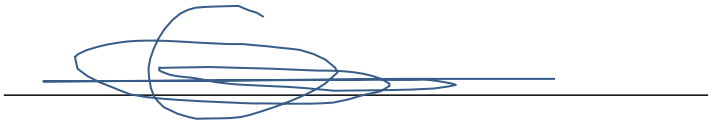

(Gregory Som)